No. 4/2018

HIDRAULICA

HYDRAULICS-PNEUMATICS-TRIBOLOGY-ECOLOGY-SENSORICS-MECHATRONICS

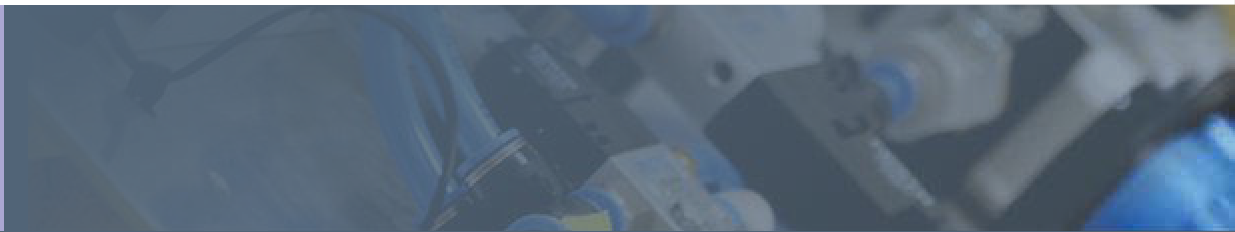

http://hidraulica.fluidas.ro

ISSN 1453 - 7303
ISSN-L 1453 - 7303

CONTENTS

BOARD

Published by:
Hydraulics and Pneumatics Research Institute, Bucharest-Romania
Address: 14 Cuţitul de Argint, district 4, Bucharest, 040558, Romania
Phone: +40 21 336 39 91; Fax: +40 21 337 30 40; e-Mail: ihp@fluidas.ro; Web: www.ihp.ro
with support from:
National Professional Association of Hydraulics and Pneumatics in Romania - FLUIDAS
e-Mail: fluidas@fluidas.ro; Web: www.fluidas.ro

HIDRAULICA Magazine is indexed by international databases

ISSN 1453 – 7303; ISSN – L 1453 – 7303

EDITORIAL

Inspectors, assessors, counselors, supervisors, etc.

Ph.D.Eng. Petrin DRUMEA
MANAGING EDITOR

For years, everyone has been complaining about the poor activity relative to attracting European funds in all areas. Comparisons with other countries are made, statistics by domains and subdomains are considered, random issues are being analyzed, but in the end, things hardly change, almost not at all. Since I am involved in implementation of European research projects, I thought I should state my opinion, too, even if some of my colleagues tell me it's a waste of time.

That's right, but rather than writing an editorial about winter holidays, which would also require some talent, it's better to talk as .. an intellectual about some of our daily troubles.

Early since launching this kind of programmes so many conditions are imposed and so many unnecessary things are required that you often give up projects even though you have the desire and the ability to implement them, and there is also a social need for them. When you go to writing the project proposal, you have to face insignificant requests, unnecessary details and many things that are repeated in other words, or sometimes in the same words, so that the project proposal gets extremely large in volume. In the assessment phase, there is a grid which often requires for things other than what was required in the guidelines according to which the project proposal has been elaborated.

When you get into the assessor's hands, there are great chances for you to come across someone who did not understand the meaning of that type of project and, for instance, he / she scores primarily the scientific papers to be delivered in a project with physical achievements and technology transfer. It is quite interesting that persons who have never implemented projects themselves have been appointed as counselors and supervisors; instead, they are full of knowledge, eagerness, and especially intransigency. Lacking better ideas to increase absorption of funds, the pays for these "specialists" have been raised, which made them even more intransigent and more aggressive, without improving their professional level in the field, and especially without actually supporting the process which they are part of.

If I take into account the complication of the system through which we are transmitted the idea that it does not matter the subject of the project but how wide and redundant the project proposal is, I would say that these moderators, counselors are victims themselves, but when I see how aggressive and often malicious they are, I think they actually have a problem understanding their part in this such important activity.

Why do we feel the need for unnecessary complications? Why do we wonder that interest in this kind of projects is diminishing? I'd say we shall think it over. At the root of all these troubles, I think there is the inability of those I am targeting here, coupled with non-liability, to which we must add a misunderstanding of the seriousness of action. It is good to meet the European requirements; it is good to promote serious, enforceable projects, but the EU's bureaucracy, already quite dense, must not be doubled or tenfold increased.

I still hope for a rethinking of the whole system. If we cannot do it by ourselves, we shall take over the ideas of those who are more active than us and just as good Europeans.

Happy New Year!

Simulation of an Electro-Hydraulic System for a P.E.T. Waste Baling Press

Lect.PhD.Eng. **Iulian-Claudiu DUȚU**[1], Prof.PhD.Eng. **Edmond MAICAN**, Prof.PhD.Eng. **Sorin-Ștefan BIRIȘ**, Lect.PhD.Eng. **Mihaela-Florentina DUȚU**, As.PhD.St.Eng. **Mariana-Gabriela MUNTEANU**

[1] University Politehnica of Bucharest, iulian_claudiu.dutu@upb.ro

Abstract: *Energy efficiency is nowadays a key factor in designing industrial machinery, where digital technologies, modeling and simulation software environments are beginning to have a deeper impact. Smart technologies have entered industrial field supporting machine design engineers to develop and optimize their technical solutions. In some cases, when energy efficiency of old machinery needs to be increased, retrofitting existing schematics is not always an easy task, instead of modifying the connections between components or replacing some of the existing components with new ones it is preferred to replace old and inefficient parts with new modular solutions. Hydraulics and pneumatics are still two types of industrial drives that are used widely, but their overall energy efficiency has not improved very much in the past years. There are conducted industrial researches having good laboratory results, but these solutions are not ready yet for the market – standardized equipment and modules being preferred. These researches are targeted not on the entire application itself but on specific functional phases or modules.*

In the particular case of an existing hydraulic P.E.T. waste baling press, functional cycle optimization and energy efficiency improvement can lead to entirely replacement of the hydraulic drive and control algorithm, where digital hydraulics might be taken into consideration as a modern technical solution. It must be paid attention not only to the engineering side of these improvements, but to the economical side as well because retrofitting costs depreciation is poor. In this paper, the authors propose a simple and energy efficient electro hydraulic driving system for an existing small capacity P.E.T. waste baling press that was modeled and simulated using FluidSIM Hydraulic software environment.

Keywords: *Modeling, simulation, electro-hydraulic, FluidSIM*

1. Introduction

Most of industrial applications and machinery are using electro-hydraulic or electro-pneumatic drives [1, 2], even if their drawbacks are very well known by design engineers: energy dissipation, high maintenance costs and their reliability [3].

Modern industrial design is now targeting optimization through energy efficiency and digital solutions along with the use of virtual tools for design, modeling and simulation [4, 5]. One of these virtual tools, a modeling and simulation software environment is FluidSIM Hydraulics. This software environment includes a schematic editor using configurable standardized hydraulic components and a real-time simulation module that include digital and analogic data acquisition using FESTO EasyPort DAQ board.

In this paper, the authors present the modeling and simulation of a simple and energy efficient electro-hydraulic driving system for an existing small capacity P.E.T. waste baling press [6] using FluidSIM Hydraulic software environment.

2. Hydraulics system

Diagram of the hydraulic circuit that the authors propose is considered to be simple and can be used as a development ground for other engineering applications including lifting systems or elevators. Diagram and components of the hydraulic system are given in figure 1, mainly consisting of a fixed-displacement pump, a pressure-relief valve, an electro-hydraulic directional valve and a double-acting hydraulic linear motor.

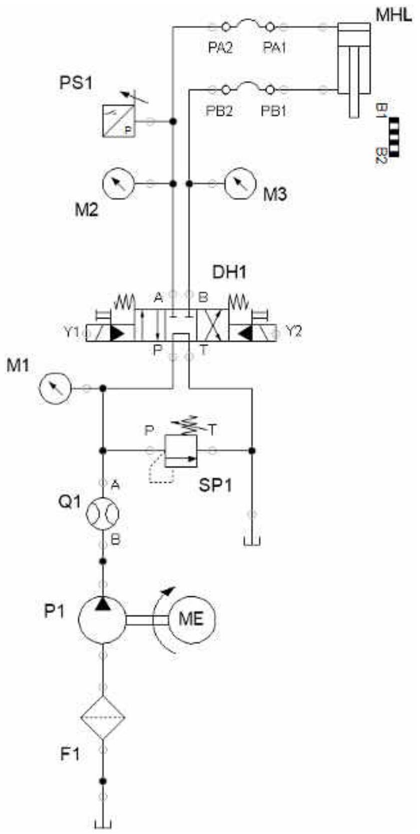

F1: hydraulic oil filter
P1: fixed-displacement pump
Q1: flowmeter
SP1: pressure-relief valve
M1 … *M3*: pressure gauges
DH1: electro-hydraulic directional valve
PS1: pressure switch
PA1/*PA2, PB1*/*PB2*: flexible pressure lines
MHL: double-acting hydraulic linear motor

Fig. 1. Hydraulics schematic of the driving system

In the hydraulic schematic in figure 1, there are shown three pressure gauges *M1*, *M2* and *M3*that are used in the simulation part to monitor pressure values in the hydraulic circuits. Also, *PS1* is a pressure activated switch used both in the simulation and the electrical automation schematic for signaling the end of pressing cycle and for controlling the press platter return movement in its initial position, unless P.E.T. bale must be evacuated.

3. Electrical schematic

Diagram of the electrical system that the authors propose here is given in figure 2. There was designed a relay logic automation schematic, modeled and simulated using *FluidSIM Hydraulics*. Functional phases of the P.E.T. waste press are given below in table 1, schematic symbols are in accordance with the electrical schematic in figure 2.
As can be seen from the hydraulics schematic in figure 1, directional valve *DH1* has two 24VDC electromagnets, *Y1* and *Y2*, which need to be energized according to functional phases of the pressing cycle.

Table 1: P.E.T. press operation logic

Functional phase	Schematic symbol									
	S0	**S1**	**S2**	**S3**	**Y1**	**Y2**	**B1**	**B2**	**PS1**	**MHL**
Emergency STOP (manual)	1	X	X	X	X	X	X	X	X	LK
Stand-by mode	0	0	0	0	0	0	1	0	0	0
START pressing (auto)	0	1	1	0	1	0	1	0	0	1
Press plate retract (auto)	0	1	0	0	0	1	0	X	1	0
Press plate retract (semi auto)	0	1	0	1	0	1	0	X	X	0
Bale out (auto-stop)	0	1	0	0	0	0	0	1	1	LK

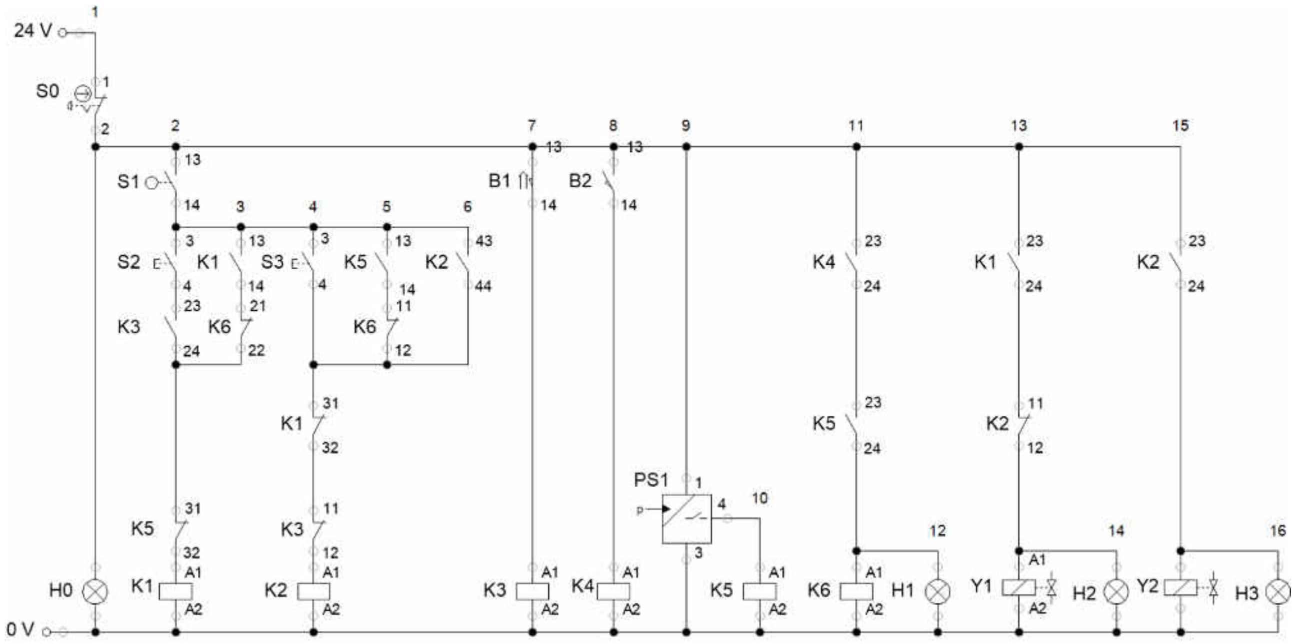

Fig. 2. Electrical schematic of the driving system

4. Simulation

The authors used for modeling and simulation the software environment FESTO FluidSIM having the *Hydraulics* module.

4.1 FluidSIM simulation environment

FluidSIM, having the Hydraulics extension module can be used for simulating hydraulics and electro-hydraulics schematics, in real time. Probably of the most important features of FluidSIM is its connection with CAD functionality and simulation. FluidSIM uses DIN-compliant drawing of electro-hydraulic circuit diagrams and can execute realistic simulations of circuits using physical models of electro-hydraulic components. FluidSIM is taking over a gap between the drawing of a hydraulic circuit diagram and its simulation.
All hydraulic components from FluidSIM's libraries have ISO symbols, functional and connection descriptions and some of them have short animations that depict the working principle. User interface is easy to use and intuitive. Main advantage is that both hydraulics and electric circuit diagrams can be modeled and simulated in the same time. As an example, if the user clicks an electrical button, the associated relay or valve electromagnet will be energized, in the same time it will be driving a valve or a hydraulic motor (shown by an intuitive animation).

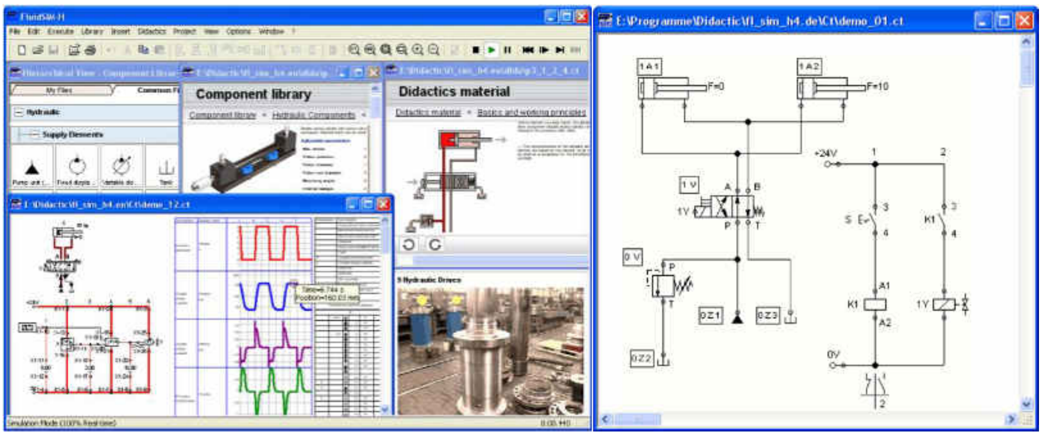

Fig. 3. FluidSIM Hydraulics modeling and simulation environment [7]

4.2 Simulation results

There are certain advantages using FluidSim Hydraulics, because of its modeling capabilities and connection of its virtual component libraries with real-life physical equipment. All virtual hydraulic components can be parameterized according to physical technical specifications given by the equipment’s manufacturer. The simulation extension of FluidSIM allows dynamic movement of virtual hydraulic system components.

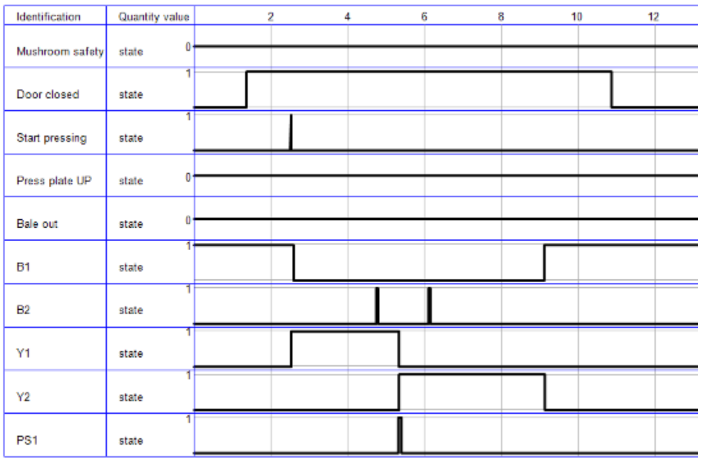

Fig. 4. State diagram showing normal start conditions on the electrical diagram

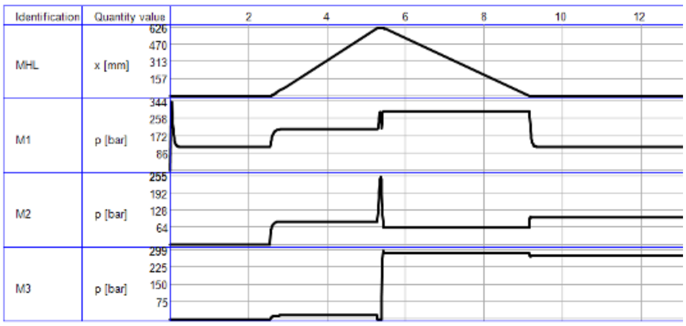

Fig. 5. State diagram showing normal start conditions on the hydraulic diagram

In figures 4 and 5 there are shown simulation results using *FluidSIM Hydraulics*, for normal start conditions, when button *S2 (Start pressing)* is pushed, press plate is in initial position and press chamber door is closed. From figure 5 it can be seen *MHL* hydraulic motor rod travel and pressure variations in all three measurement points – pressure gauges *M1*, *M2* and *M3*.

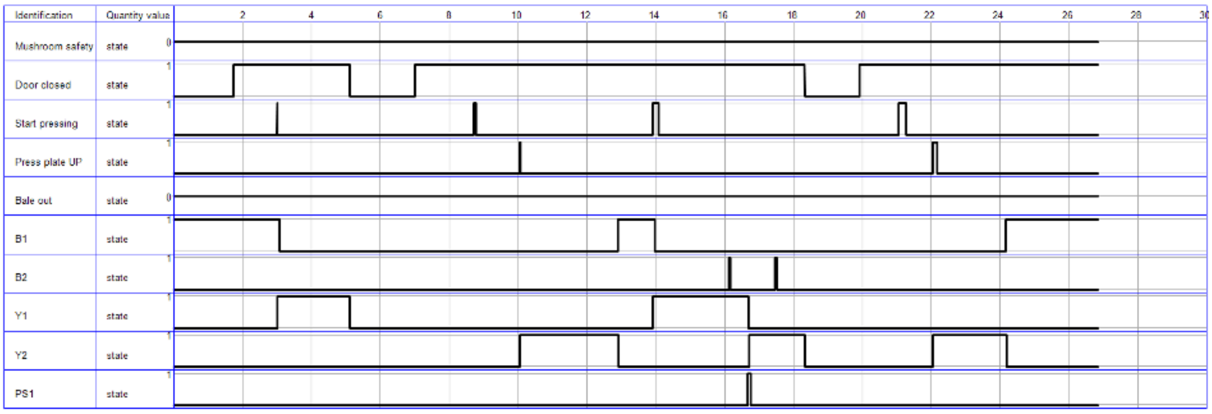

Fig. 6. State diagram showing abnormal condition,
when press door chamber is opened during pressing – electrical schematic

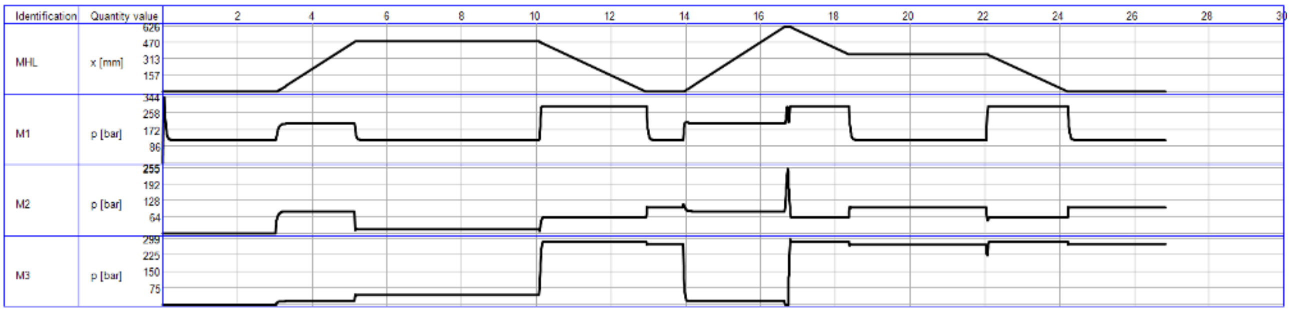

Fig. 7. State diagram showing abnormal condition,
when press door chamber is opened during pressing – hydraulic schematic

In figures 6 and 7 there is shown an abnormal functional condition, both on electrical and hydraulic state diagrams. After pressing the start button, pressing cycle takes place normally, until the pressing door chamber is opened (seconds 5 to 7 on electrical state diagram), causing *Y1* electromagnet to be no longer energized and locking the pressing plate into its current position. The *S3* button must be used now for retracting the press plate into its initial position, causing *Y2* electromagnet to be energized.

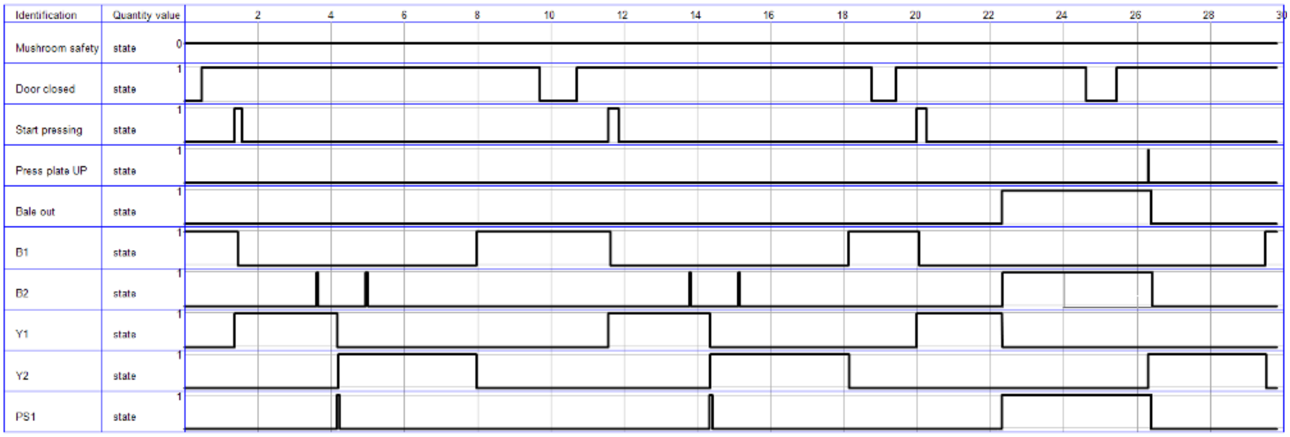

Fig. 8. State diagram showing two pressing cycles and bale evacuation – electrical schematic

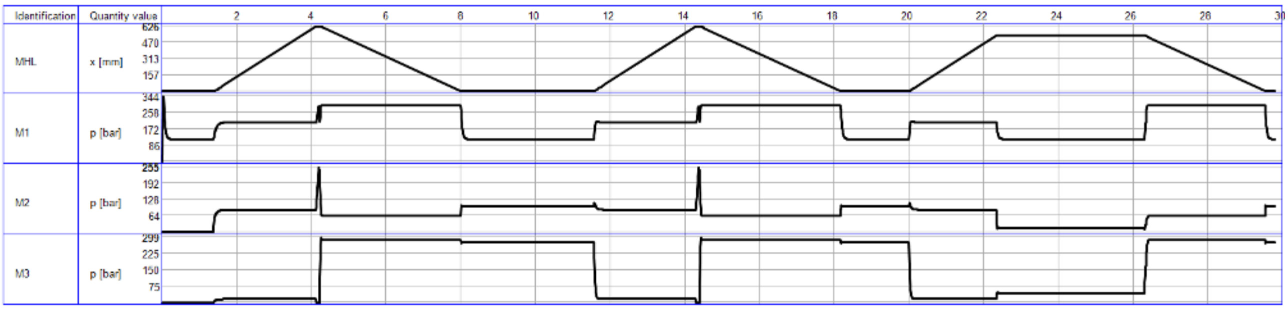

Fig. 9. State diagram showing two pressing cycles and bale evacuation – hydraulic schematic

In figures 8 and 9 there is shown two normal pressing cycles, the pressing plate starts from its initial (up) position, *B1* limit switch is pressed, and travels down until *B2* limit switch will be pressed (no pressure load) or *PS1* pressure switch electrical contact will be closed (with pressure load). The pressing plate will now return into its initial position.

The electro-hydraulic press will enter in bale evacuation functional state (*bale out* in figure 8) when both limit switch *B2* and pressure switch *PS1* are activated at the same time. Now, human operator can safely open the pressing chamber door and proceed binding the P.E.T. bale, while the pressing plate is locked into last position. After binding, the bale must be manually evacuated from the pressing chamber. Before evacuation, the human operator must press button *S3* in order to retract the pressing plate.

5. Conclusions

Electro-hydraulics field of engineering has developed largely past years, due to the benefit of using technological advances in materials science, electronics and informatics. Reliable and accurate hydraulics systems include digital or analog electronic control made with computer assisted systems or dedicated solutions using industrial PLCs or microcontroller-based modules. Electronic digital transducers provide new measurement solutions with self-calibration, auto-diagnosis or bus communication modules. Data acquisition and virtual instrumentation enabled the development of intelligent measurement software, data processing, data storage or plotting various graphical diagrams.
Modeling and simulation of electro-hydraulic drives is a part of modern engineering design, drastically reducing production costs and time-to-market for a product or a system. Taking into consideration the discrepancies between physical systems and virtual models of the same system and using appropriate software environments, design engineers can easily put to the (virtual) test and optimize their ideas. The authors used for modeling and simulation FESTO FluidSIM Hydraulics.

Acknowledgments

This work has been funded by University Politehnica of Bucharest, through the "Excellence Research Grants" Program, UPB – GEX 2017. Identifier: UPB-GEX2017, contract. No. 56/2017 (DIGIPRESS)".

References

[1] Jelali, Mohieddine, & Andreas Kroll. *Hydraulic servo-systems: modelling, identification and control*. Springer Science & Business Media, 2012.
[2] Rădoi, Radu Iulian, Iulian Duțu, and Marian Blejan. "Stand and equipments for determining the dynamic performances of electrohydraulic proportional directional control valves." Paper presented at the International Salon of Hydraulics and Pneumatics HERVEX 2011. Calimanesti-Caciulata, Romania, Nov. 9-11, 2011: 365-372.
[3] http://www.hydraulicspneumatics.com. Accessed September 3, 2018.
[4] Popescu, Teodor Costinel, Daniela Vasiliu and Nicolae Vasiliu. *Chapter 19- Numerical Simulation - a Design Tool for Electro Hydraulic Servo Systems*: 425-446, DOI: 10.5772/13332. In International volume *Numerical Simulations - Applications, Examples and Theory*. Lutz Angermann (Ed.), ISBN: 978-953-307-440-5, published in January 2011, by InTech-Austria. Accessible online at http://www.intechweb.org/books/show/title/numerical-simulations-applications-examples-and-theory.
[5] Popescu, Teodor-Costinel, Polifron-Alexandru Chiriță, and Alina Iolanda Popescu. "Increasing energy efficiency and flow rate regularity in facilities, machinery and equipment provided with high operating pressure and low flow rate hydraulic systems." Paper presented at the 18th International Multidisciplinary Scientific GeoConference SGEM 2018. Albena, Bulgaria, 30 June-9 July 2018: 401-408.
[6] https://eu.hsm.eu. Accessed October 18, 2018.
[7] https://www.festo-didactic.com/ov3/media/customers/1100/698530_fl_sim_h42_en_offset.pdf. Accessed October 8, 2018.

The 3D Geometry Reconstruction of a Scaled Axial Blade by Photogrammetry

Prof. PhD. Eng. **Dorian NEDELCU**[1], PhD. Student Eng. **Sorin-Laurenţiu BOGDAN**[2],
Assoc. Prof. PhD. Eng. **Ioan PĂDUREAN**[3]

[1] “Eftimie Murgu” University of Reşiţa, d.nedelcu@uem.ro

[2] “Eftimie Murgu” University of Reşiţa, bsl_1984@yahoo.co.uk

[3] "POLITEHNICA" University of Timișoara, padurean58@yahoo.com

Abstract: *The paper illustrates the Reverse Engineering of an axial blade geometry, who was scanned through Photogrammetry technique and processed with the following software packages: Agisoft Photoscan and Geomagic Design X; the solid geometry and the drawing of the blade were generating using the SolidWorks software. The 3D blade geometry was compared with the blade mesh generated in Geomagic Design X based on point cloud obtained in Agisoft Photoscan software. Ultimately, three plane intersections of the blade were compared with measured points on the real blade on CNC machine.*

Keywords: *Reverse Engineering, Photogrammetry, Turbine, Axial Blade*

1. Introduction

As it can be noticed from regional preoccupation in the field, but also by extrapolation as a national and worldwide approach, the exploitation at maximum efficiency of the water courses hydropower potential by developing viable small hydroelectric plants [1], as also the efficiency mounting for existing peak hydroelectric arrangements by acquiring pumped-storage hydroelectric power plants [2], are directly related to the optimization of the engaged hydropower machines, a goal that can be achieved by a high precision design of the axial turbine’s blades. Using the Reverse Engineering technology, the geometry of a scaled blade of axial type with the mass equal to 0.528 kg, Fig. 1, will be reconstructed by following the next steps:

- 3D scanning of the blade using Photogrammetry and the Agisoft Photoscan software;
- the blade reconstruction using the Geomagic Design X and SolidWorks software packages.

Fig. 1. The axial blade

2. Acquisition of the images

The acquisition of photographic images was done with the NIKON D610 camera positioned on a tripod, generating 78 snapshots from different successive angles, covering 720 degrees on two levels of the blade periphery, Fig. 2. The following shooting parameters were used: Focal length 50, F-stop F / 11, ISO 1600, Shutter 1/125. Contactless scanners and photo devices use light in capturing data. This creates problems when light hits glossy surfaces, so the blade surfaces must be prepared before scanning, temporarily applying a fine layer of powder, Fig. 2.

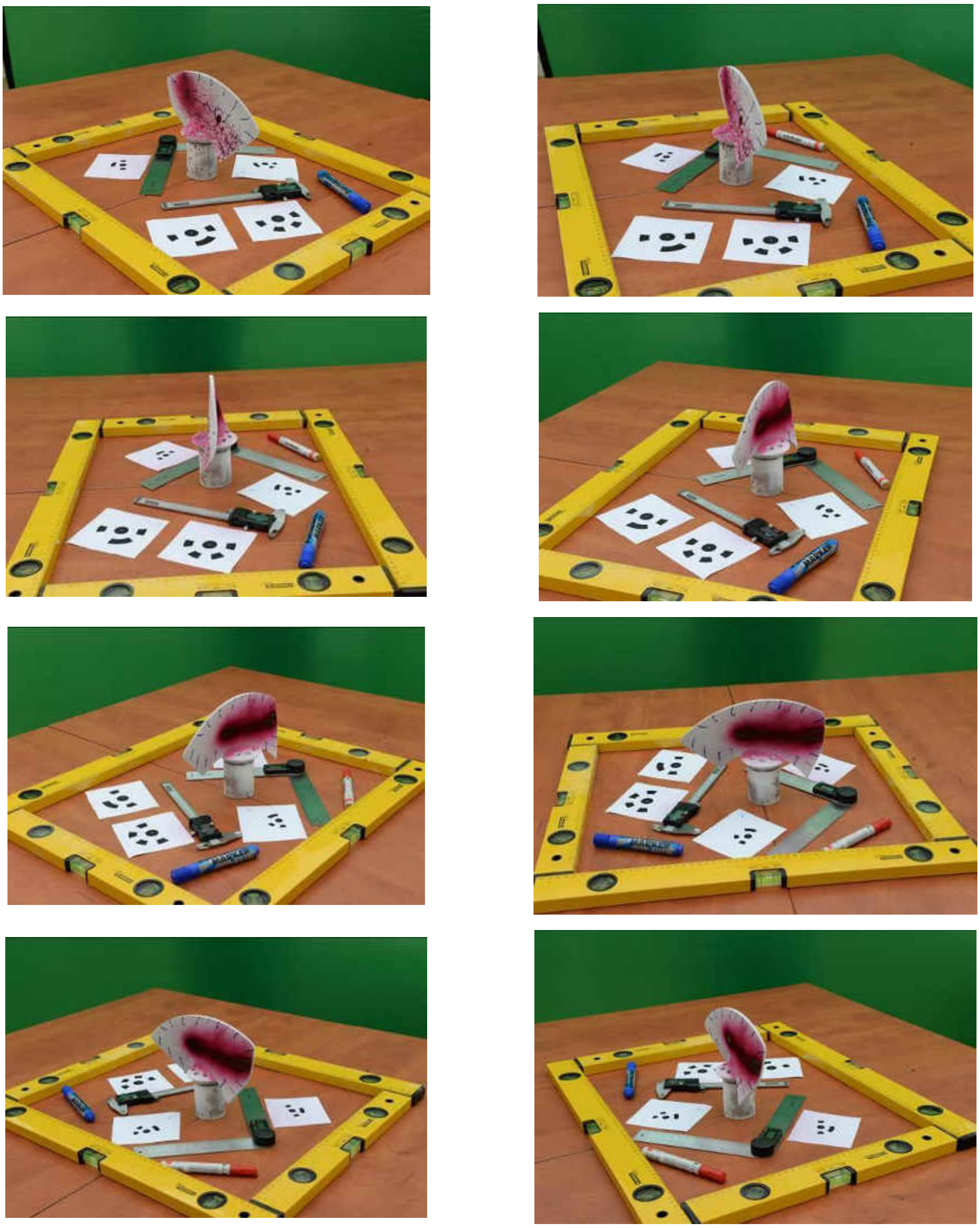

Fig. 2. The images sequence of the scaled axial blade

3. Cloud Point Generation in Agisoft Photoscan software

The import of photos into the Agisoft Photoscan software is shown in Fig. 3. The sparse cloud of 169,445 points is shown in Fig. 4; the dense cloud of 1,780,197 points is shown in Fig. 5. The point cloud calibration (scaling the geometry to real values) based on known distances is shown in Fig. 6. The dense point cloud generated in the Agisoft Photoscan software was exported in OBJ format to be imported into the Geomagic Design X software.

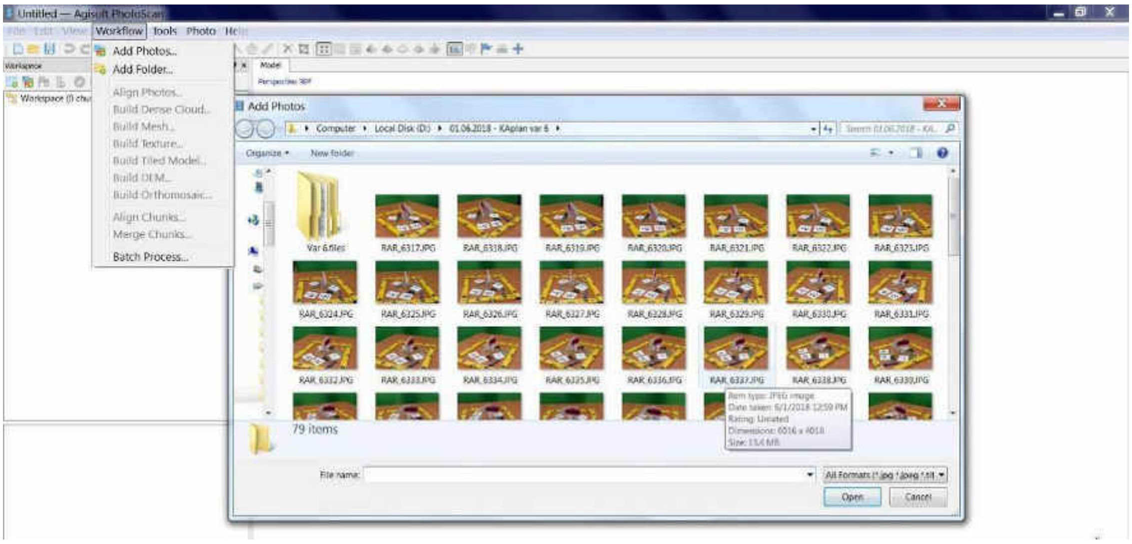

Fig. 3. Images inserted into the Agisoft Photoscan software

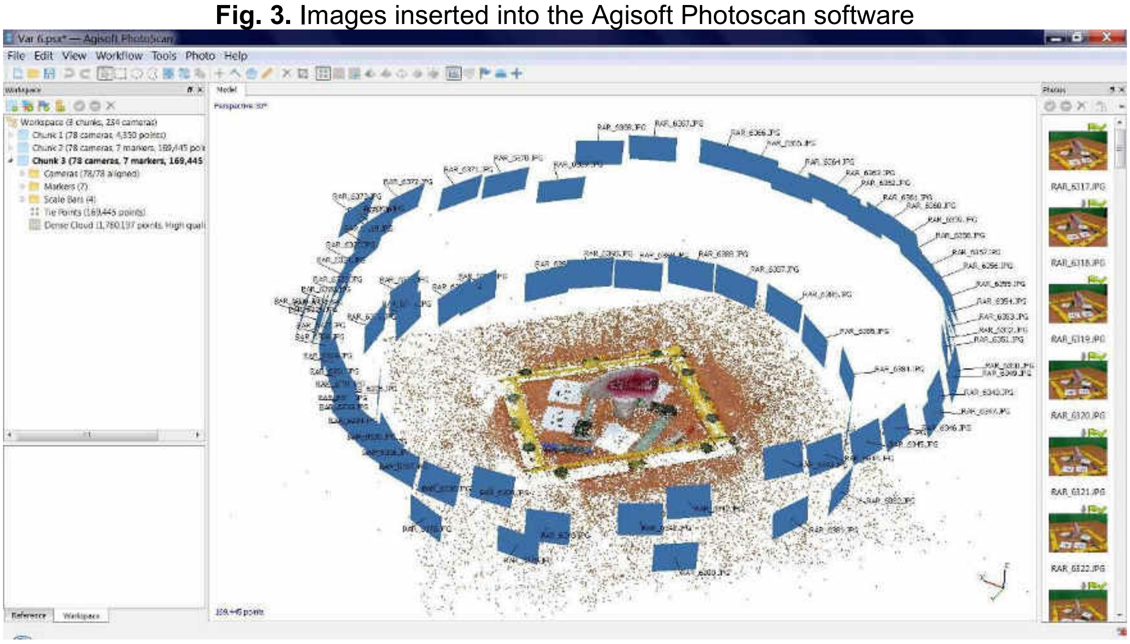

Fig. 4. Images aligned in Agisoft Photoscan and sparse cloud generation of 169,445 points

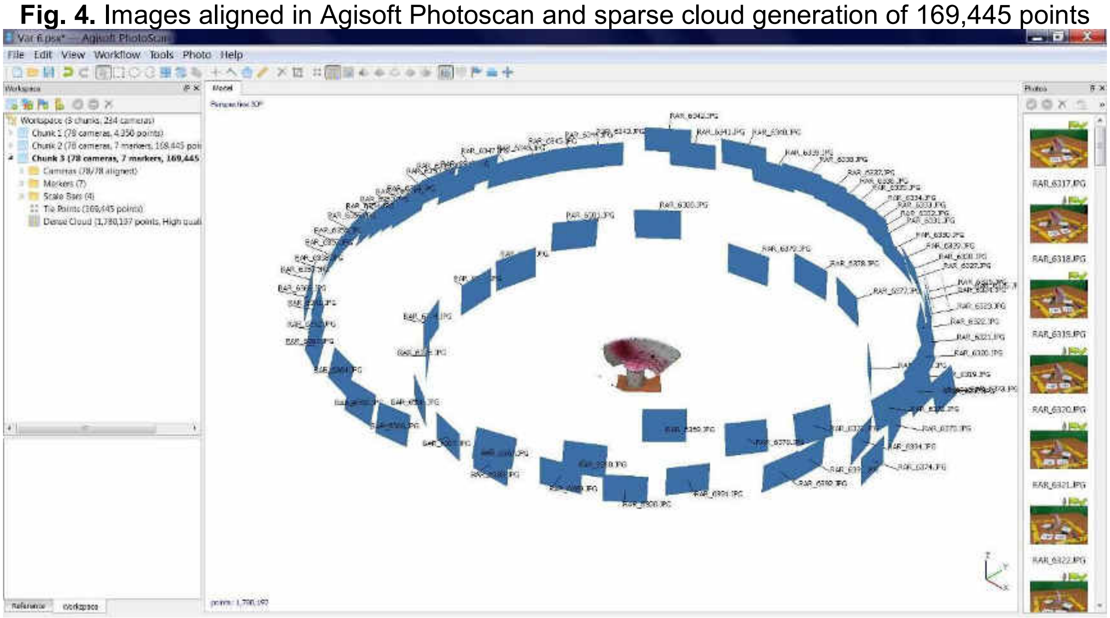

Fig. 5. Dense cloud generation of 1,780,197 points in Agisoft Photoscan software

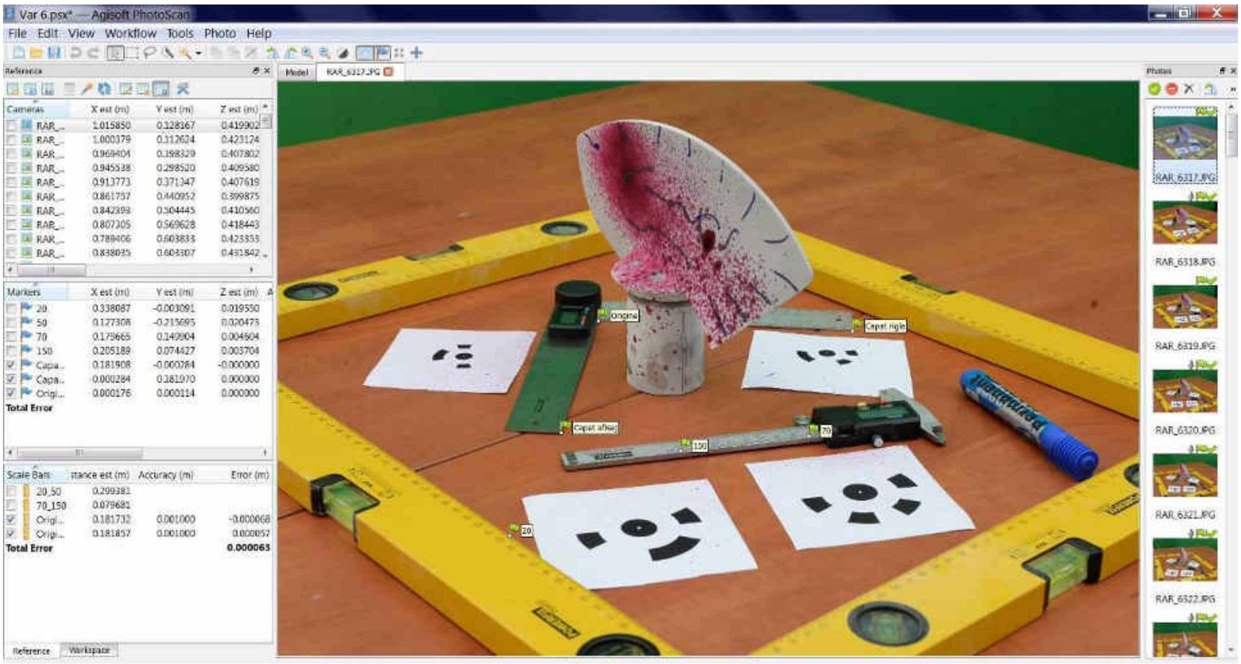

Fig. 6. Points cloud calibrating in Agisoft Photoscan software

4. Generate the blade profiles in Geomagic Design X software

The following stages are required to generate the blade profiles:

- the dense cloud import (1,780,197 points) into Geomagic Design X, Fig. 7;
- generate the mesh of the points cloud; at this stage the software generates a network of triangles similar to meshing in the finite element analysis; for this blade 863,228 triangles were generated, Fig. 8;
- the generation of 6 profiles in Geomagic Design X, resulted from the intersection of the mesh with 6 cylinders with the following imposed radii: 92, 107, 122, 137, 152, 167 mm; also, the characteristic circles of the blade trunnion have been generated, Fig. 9;
- export the 6 intersection profiles and trunnion circles to SolidWorks.

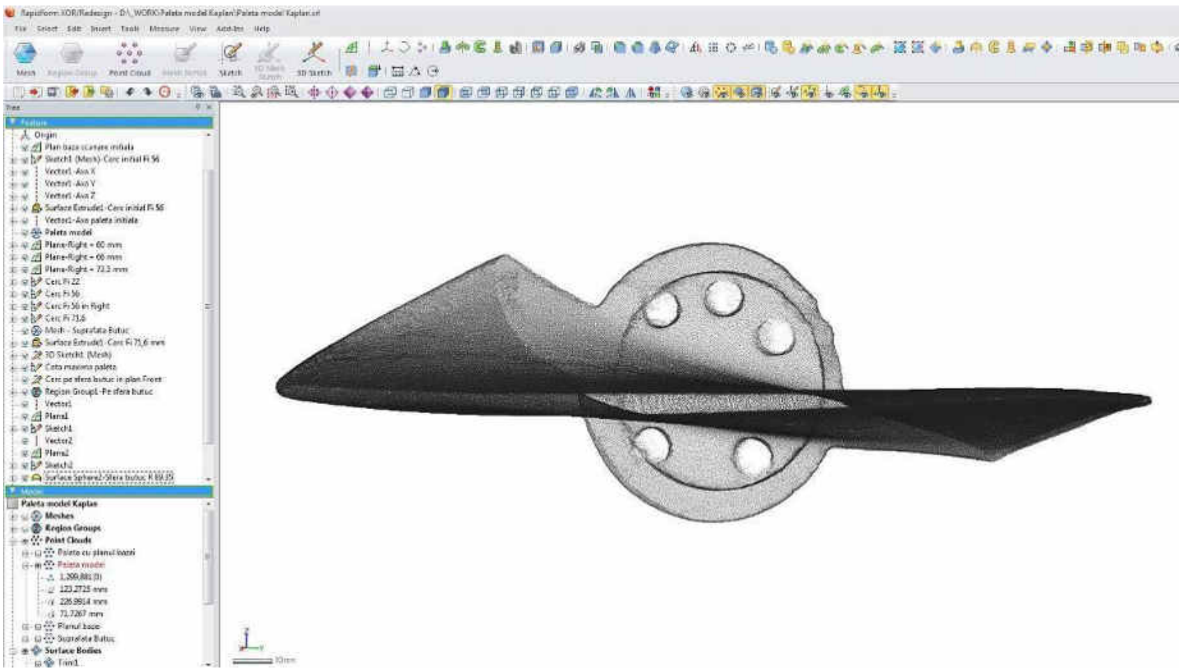

Fig. 7. Points cloud imported in Geomagic Design X software

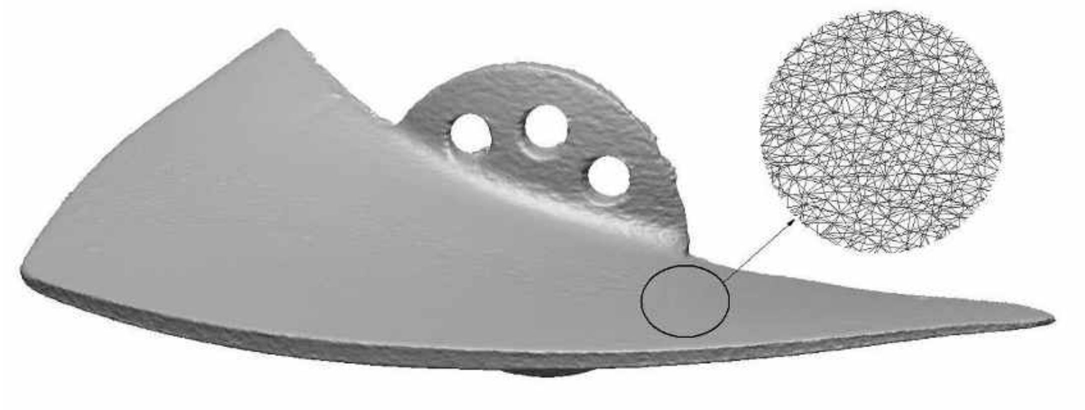

Fig. 8. The mesh of the points cloud imported in Geomagic Design X software

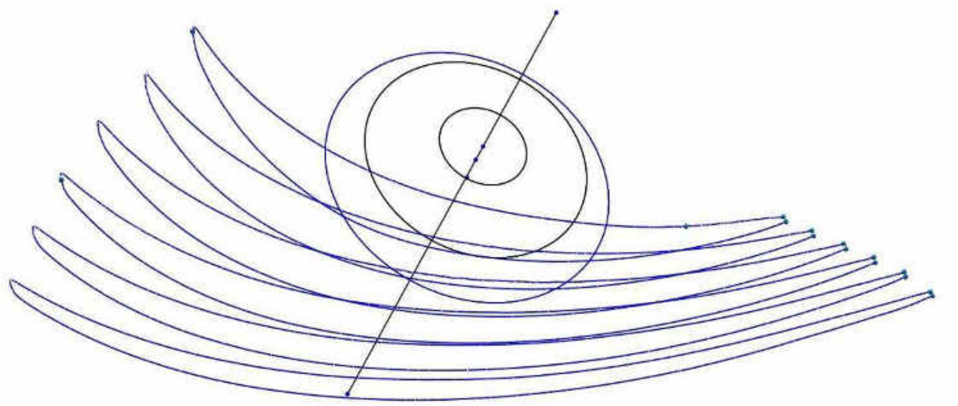

Fig. 9. The six profiles of the blade generated in Geomagic Design X software

5. Generate the blade geometry in SolidWorks software

The intersection profiles and the trunnion circles were imported into SolidWorks software. The intersection of scaled blade geometry with the cylinders can generate profiles with a slightly irregular shape, especially in the leading-edge area. This is a common problem for scanners, which can generate errors in areas with lower brightness, such as chamfers, fillets, holes, threads or the leading edge, as is the case here, as shown in Fig. 10.

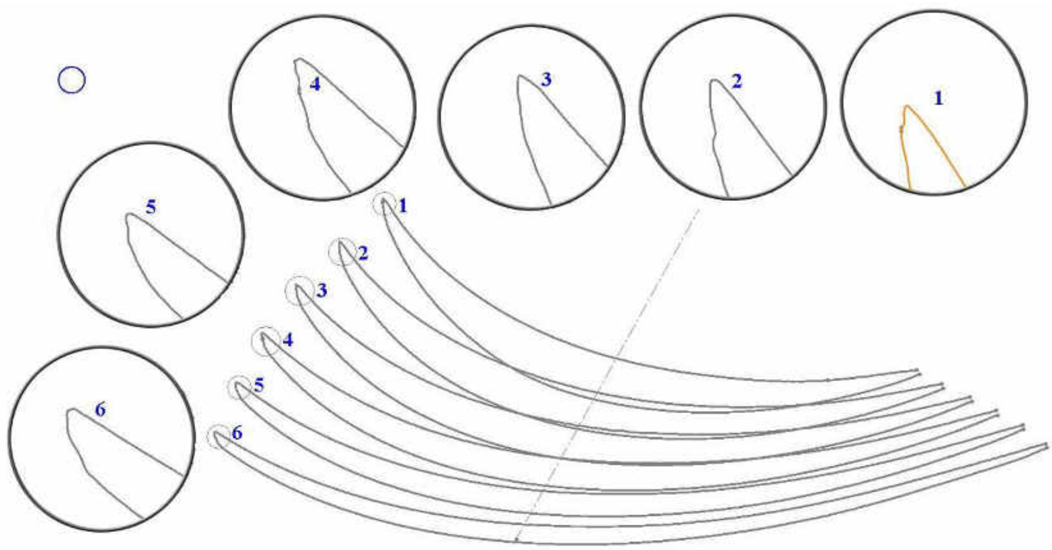

Fig. 10. The profiles imported in SolidWorks software with leading edge irregularities

For each profile, the leading-edge area was corrected with a 3D spline curve to eliminate the irregularities from Fig. 10. Next, 100 three-dimensional coordinates (X, Y, Z), Fig. 11, were extracted from profiles through a macro in Visual Basic, from the suction and pressure side of the profile and exported to an Excel file, where a smooth algorithm was applied to profiles points according to the methodology presented in [4]. Finally, the corrected points were imported back to SolidWorks software, where the 3D blade geometry was generated as solid format, Fig. 12. The mass of the solid blade reported by SolidWorks is 0.544 kg.

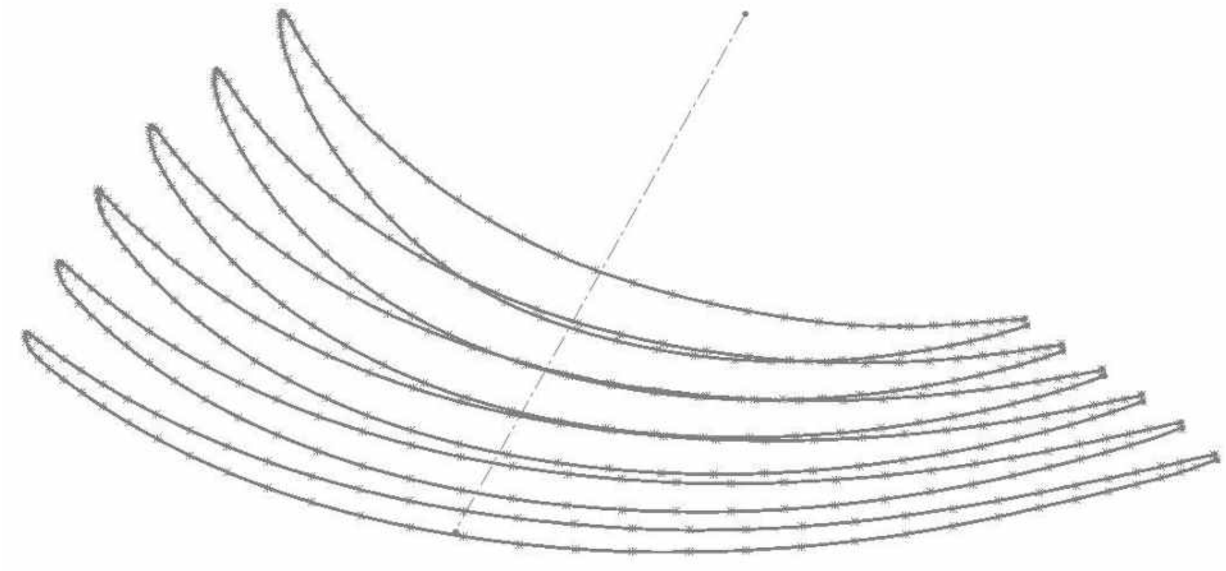

Fig. 11. Points generated with macro on the profiles shape

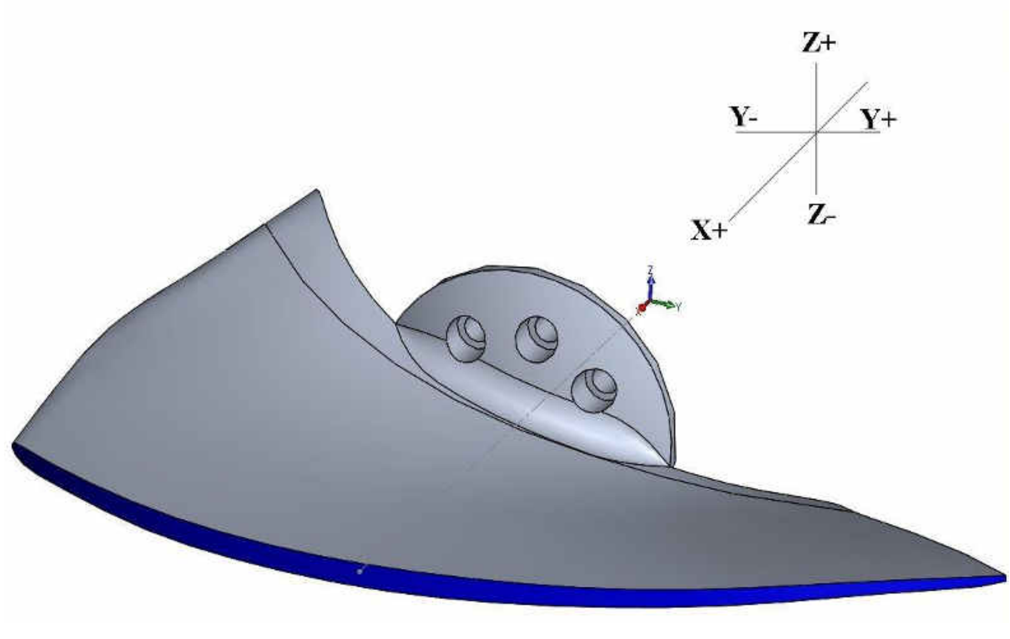

Fig. 12. The 3D blade geometry in solid format

6. Comparison of the blade mesh with those reconstructed as solid format

Fig. 13 present the comparison of the blade mesh from Fig. 8, with the blade reconstructed as solid format. The two geometries were imported into the GOM Inspect application; the blades were aligned with automatic best-fit alignment algorithm, so the geometry of the reconstructed blade overlaps with minimum deviations over the mesh blade. The most significant errors are in the area of the blade trunnion -1.57 ÷ +1.73 mm, but the rest of the values are within ± 0.1 mm.

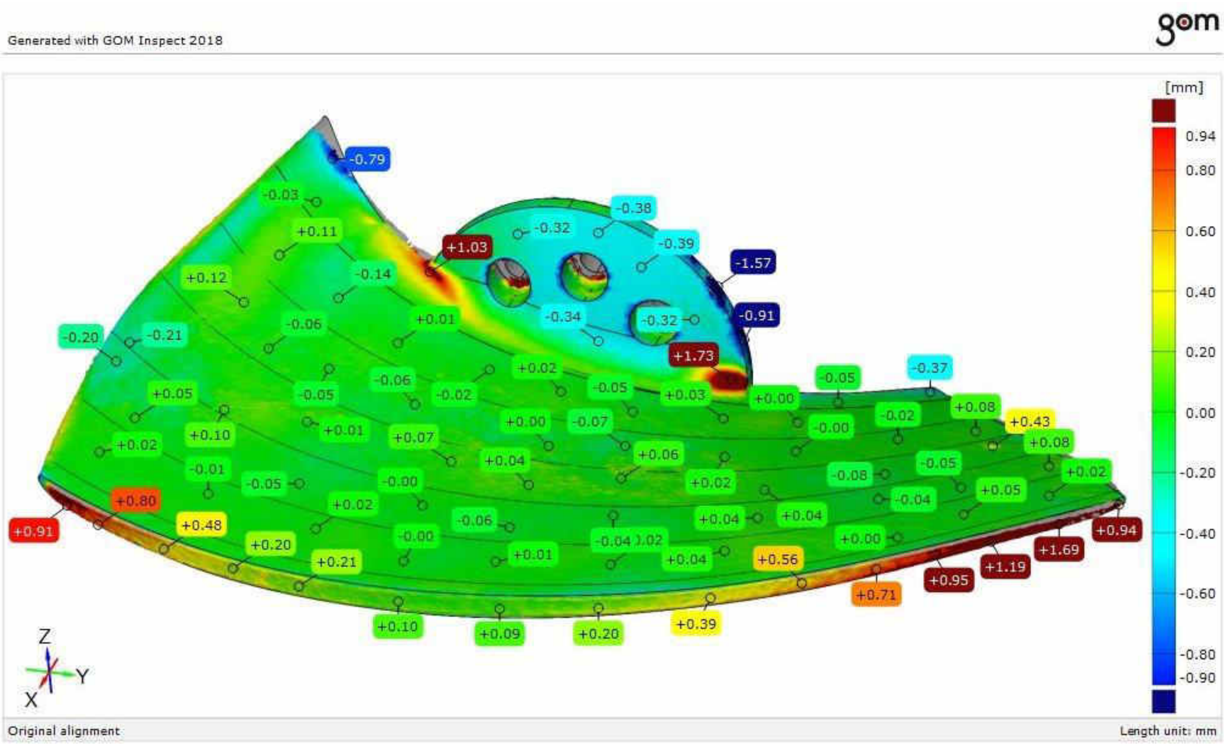

Fig. 13. The mesh comparison of the blade with those in solid format

7. Comparison of the measured blade with those reconstructed as solid in SolidWorks

To verify the accuracy of the blade reconstruction, it was measured on the DMF 180 DECKEL MAHO CNC machine, Fig. 14. The measurements were performed on the suction side, Fig. 15, and pressure side, Fig. 16, at three planes placed at X = 40, 60 and 80 mm from the trunnion end plane. The comparison is presented in Fig. 17, 18 and 19. These figures show a correct overlap of the comparison curves, small deviations due to cumulative scan errors, solid geometry generation and measurement. These errors also include the small changes applied to the theoretical profiles due to their smoothing operation. The minimum and maximum deviations range for the plane placed at X = 40, 60 and 80 mm were -0.33018 / +0.094484, -0.37405 / +0.29926 and -0.04589 / +0.476279 respectively.

Fig. 14. CNC machine DMF 180 DECKEL MAHO

Fig. 15. Measuring the suction side of the blade

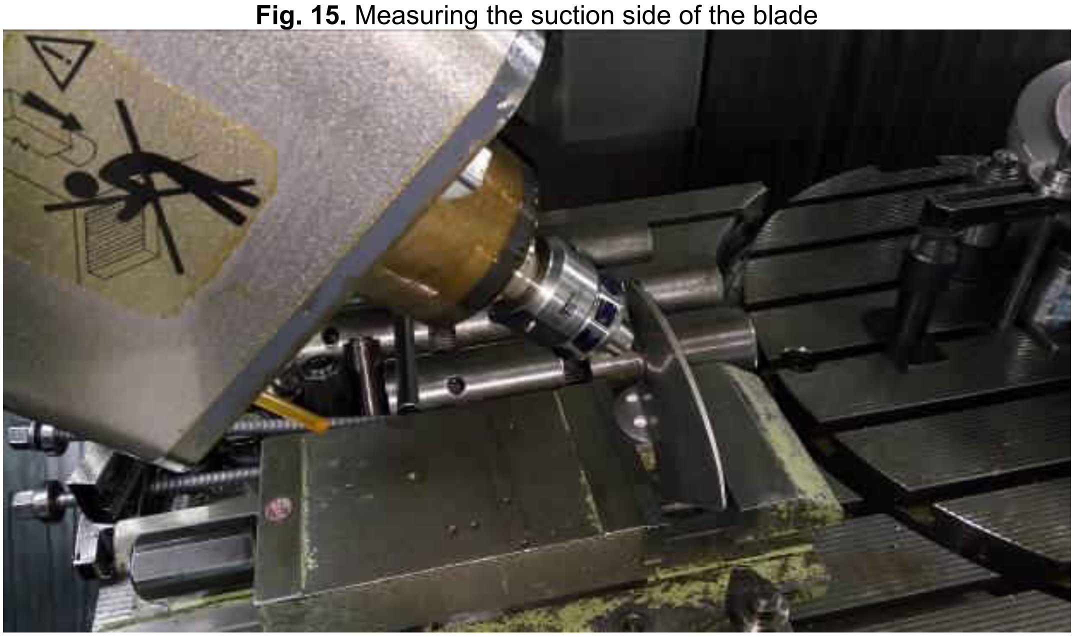

Fig. 16. Measuring the pressure side of the blade

8. Conclusions

Scanning geometry is a laborious task, necessary but not enough. The result of the scan is a point cloud of three-dimensional coordinates. To use geometry in computer aided design applications is required to move to a higher level, like cloud points transformation into surface or solid geometry. That's it can only be done through specialized applications, like Geomagic Design X and/or SolidWorks. The objective of the paper is to describe the reverse engineering stages to transform a real blade object into a virtual geometry, using the Photogrammetry techniques. For the axial blade, it was necessary to smooth the profiles to attenuate the scanning errors, especially those in the leading-edge area. From the comparison of point cloud mesh with the blade reconstructed in SolidWorks, it was concluded that the largest errors occurred in the 1.55 ÷ +1.73 mm range at the blade trunnion, but most of the values were included within ± 0,1 mm. From the measurements made on the real blade, the suction and pressure side deviations of the reconstructed blade fall within the deviations range between a minimum of -0.37405 and a maximum of +0.476279 mm.

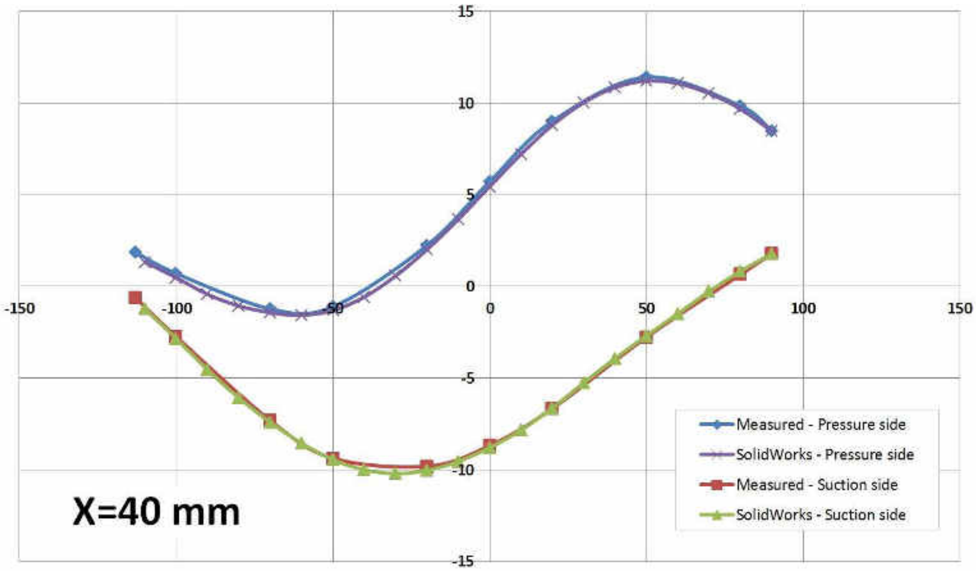

Fig. 17. The points comparison of the blade at X=40 mm plane

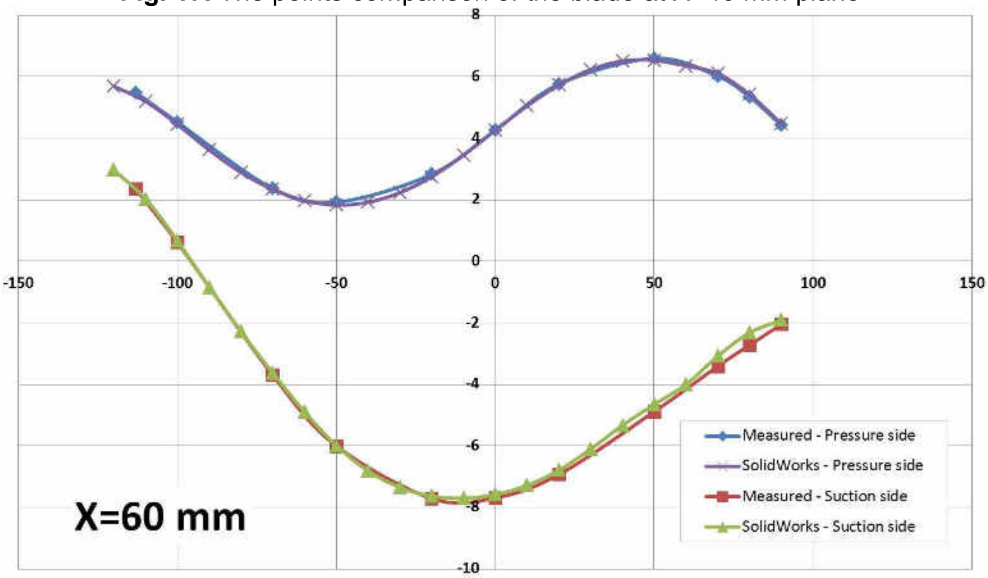

Fig. 18. The points comparison of the blade at X=60 mm plane

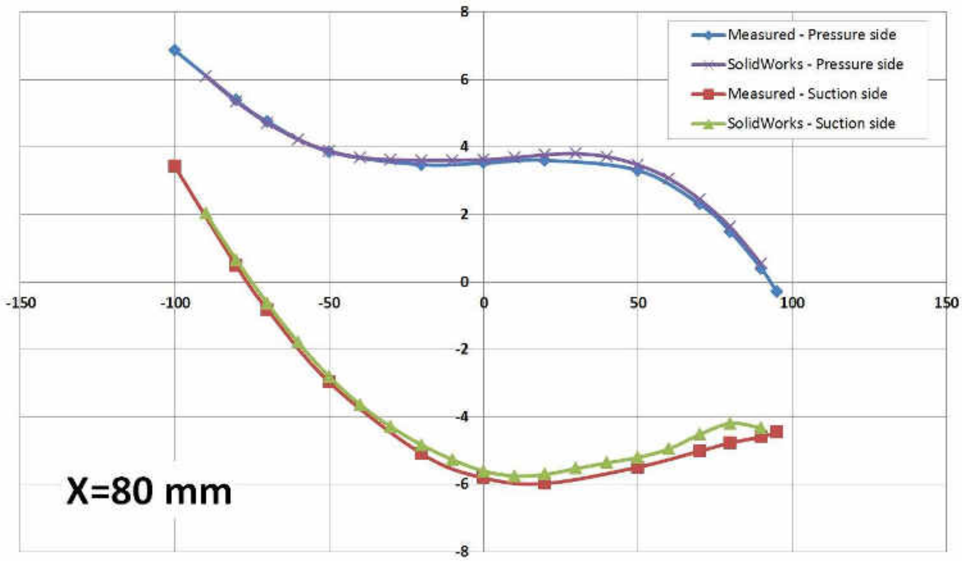

Fig. 19. The points comparison of the blade at X=80 mm plane

Acknowledgments

This paper was supported by "Eftimie Murgu" University of Reşiţa, "Traian Vuia" Square, No. 1-4, 320085, Caraş-Severin county, Reşiţa, Romania.

References

[1] Popescu-Buşan, A.I., Gh. Lazăr, A.T. Constantin, and Ş.V. Nicoară. „Water Flow Transition on a Hydropower Virtually Developed Sector of Bârzava River in the Town of Reșița", *HIDRAULICA* No. 3/2018 - Magazine of Hydraulics, Pneumatics, Tribology, Ecology, Sensorics, Mechatronics, pg.46-55, ISSN 1453 – 7303, Bucharest.
[2] Constantin, A.T., I. David, A. Chebuţiu, Ş.V. Nicoară, and M. Vişescu. „The possibility of fitting a pumped storage plant within the complex water development on upper Bârzava, Romania", Paper presented at the 25th IAHR Symposium on Hydraulic Machinery and Systems, 20–24 September 2010 'Politehnica' University of Timişoara, Romania, IOP Conference Series: Earth and Environmental Science, Volume 12, No.1, 10.1088/1755-1315/12/1/012109, 8 pag, 2010.
[3] Agisoft LLC. "Fully automated professional photogrammetric kit", Accessed October 21, 2018, http://www.agisoft.com/pdf/photoscan_presentation.pdf
[4] Bogdan, Sorin-Laurenţiu, Dorian Nedelcu, and Ioan Pădurean. "Determining the geometric parameters of a blade runner that has a geometry obtained through the Photogrammetry technique." Paper presented at the 10th International Conference on Machine and Industrial Design in Mechanical Engineering Novi Sad, Serbia, June 6-8, 2018, http://iopscience.iop.org/article/10.1088/1757-899X/393/1/012127.

ISSN 1453 – 7303 **"HIDRAULICA" (No. 4/2018)**
Magazine *of Hydraulics, Pneumatics, Tribology, Ecology, Sensorics, Mechatronics*

Approaching Mean Air Temperature-Rainfall Models by Means of Genetic Programming under Climatic Change Scenarios

M. Eng. **Gonzalo Daniel MEJIA SANTANA[1]**, Dr. **Maritza Liliana ARGANIS JUAREZ[2]**, M. Eng. **Margarita PRECIADO JIMÉNEZ[3]**, M. Eng. **Nikte OCAMPO GUERRERO[2]**, Dr. **Jeanette ZAMBRANO NÁJERA[4]**, M. Eng. **Eliseo CARRIZOSA ELIZONDO[1]**

[1] National Autonomous University of Mexico, Institute of Engineering, Mexico, GMejiaS@iingen.unam.mx

[2] National Autonomous University of Mexico, Faculty of Engineering, Mexico, MArganisJ@iingen.unam.mx, nikteocg@yahoo.com.,mx

[3] Instituto Mexicano de Tecnología del Agua, Jiutepec, Morelos, Mexico,preciado@tlaloc.imta.mx

[4] Nacional University of Colombia, Manizales, Colombia, jdzambranona@unal.edu.co

Abstract: *The study of how climatological variables had been or will change over time under emissions of greenhouse gases, has been the subject of several researches since the late nineteenth century and they have increased since the eighties of the XXI Century. The population growth in the medium and short term means a greater urbanization with the consequent change in land use in a country; civil protection measures to be implemented will be essential to alert and protect future populations to the occurrence of extraordinary weather events, providing necessary measures in cases such as heatwaves, frosts and floods. In this study ten weather stations with daily records of precipitation and air temperature located in different points of Mexico were selected; monthly behavior patterns of historical rainfall depending on the temperature in a representative year were identified, and genetic programming (GP) was applied to obtain mean temperature-rainfall models. Additionally, climate change models were applied using the system SEDEPECC of the Mexican Institute of Water Technology (IMTA), with horizons from 50 up 10000 years, obtaining forecasts of precipitation and temperature. The GP models were applied with the forecasted data of temperature to approach the rainfall and the annual patterns in some cases were similar to historical values.*

Keywords: *Mean Rainfall, Mean air temperature, Genetic programming (GP) models, climate change*

1. Introduction

The study of the way in which weather variables have gone or will change in the face of greenhouse gas emissions, has been the subject of numerous investigations since the late nineteenth century that have increased since the eighties of the 20st century (De Lima, 2012, Buddaa & Dewalleb, 2001, Boccolari & Malmusi, 2013, Abderrahmane, 2008, Magaña, 2006).
Studies of the analysis of the behavior of precipitation according to climatic variables have been carried out, either correcting their values (Allerup, 2000), or modifying the statistical bias of precipitation and temperature used in hydrological models or in predictions of regional climate change (Piani, 2010, Chistensen, 2008). Homogeneity adjustments have also been made to temperature and precipitation series (Toumenvirta, 2001, Berget, 2005, Brunetti, 2005, Cahalan, 1996). Other studies have analysed the effect of annual total precipitation and average air temperature in annual runoff (Cho, 2011). The effects of the variation in soil cover on annual precipitation and near-surface air temperature have also been studied. (Strack, 2008, De Lima, 2012). Other studies include adjustment to daily or monthly precipitation data or precipitation data given in grids (Yang, 1998, Benning & Yang, 2005, Adam & Lettenmaier, 2003.
Unlike previous studies, where we seek to simulate relatively constant variables, in this paper we try to identify variables that change moderately throughout a fairly wide geospatial territory.
Evolutionary computation, genetic algorithms, genetic programming and other bioinspired algorithms have gained popularity in their use in engineering problems since the last two decades of the 20th century; we can mention the works of Fuentes, 2015. In particular, genetic programming has been used in hydrology and hydraulics to obtain mathematical models in which a dependent variable is related to one or more independent variables. Within the evolutionary computation, genetic algorithms and genetic programming (PG) are tools that help to obtain

parameters of proposed models or to obtain completely new models in their form with which the behavior pattern of a dependent variable can be reproduced in function of n independent variables (Cramer, 1985, Koza, 1989, Goldberg, 1989).
The objective of this study was to obtain, with a genetic programming algorithm, models of the pattern of the behavior of the monthly precipitation based on the temperature of the air that they have observed historically and to use these models to estimate the monthly precipitation with air temperature data, generated under climate change scenarios, in order to identify the agreement between the measured and calculated data. To make the analysis, 10 climatological stations of the Mexican Republic, representative of the different regions of the country, were selected.
The article is organized as follows: first the methodology used is presented from the data analysis, the description of the genetic programming, then the separation of the data is done (horizontal and vertical dissection, based on the differences obtained in those directions with the models that considered all the data) to obtain new models with genetic programming, considering groups of non-consecutive months, the application is subsequently made, the results obtained are highlighted and finally the conclusions derived from the study are reported.

1. Methods

1.1. Data collection and analysis

In Mexico a system of compilation of the normal of the climatological stations is used which is of public domain and is in charge of the National Water Commission (CONAGUA), in this site the following data were extracted from the stations mentioned above:

- Precipitation
- Evaporation
- Maximum air temperature
- Minimum air temperature
- Mean air temperature

But as in any system there is loss of information due to technical failures either as a result of an extreme event, system crash or maintenance of the same station, for which reason it was necessary to resort to adjacent information, that is, to information from attached or nearby stations, which fulfilled the criterion that the distance between one and another did not exceed 20 km apart.
Monthly mean air temperature and precipitation data were selected from 10 weather stations of the CONAGUA, distributed throughout the country (Table 1 and Figure 1).

Table 1: Climatological stations distributed throughout the National Territory

Station	State	Name	Municipality	ID CONAGUA
A	Sinaloa	San Joaquin	Sinaloa	25172
B	Queretaro	Coyotillos	El Marques	22043
C	Chiapas	Cuauhtemoc	Ixtapa	7343
D	Sonora	Colonia Morelos	Agua Prieta	26022
E	Yucatan	Santa Elena	Santa Elena	31027
F	Veracruz	Chicontepec	Chicontepec	30041
G	Michoacan	Acahuato	Apatzingan	16228
H	Guerrero	Acapulco	Acapulco	12142
I	Baja California Sur	Ojo de Agua	Comondu	3039
J	Coahuila	Ejido Primero de Mayo	Escobedo	5147

Fig. 1. Map location of climatological stations

1.2. Genetic programming (GP)

Genetic programming (GP) (Koza, 1992) takes place in a few years later the genetic algorithms (Goldberg, 1989), in order to build computer programs and mathematical models using evolutionary random algorithms used as optimization methods.
The genetic programming algorithm includes the establishment of the independent variables and the dependent variable in the problem, operators and constant vector to be considered for the construction of the models to be tested must also be defined. It should provide a probability of exchange or cross (crossing) of the best individuals (set of selected operations) and a probability of mutation must be given. A number of generations (iterations) is proposed to finish the optimization process. In this study objective function consisted in minimizing the mean square error between the measured and the calculated rainfall data with the models tested by the GP algorithm.
The GP algorithm starts with the random generation of an initial population of n individuals (each individual corresponds to a mathematical model consisting of different operators, variables and constants), individuals are then evaluated in the objective function and the best ones are selected (selection can be performed by obtaining a relative frequency of the result obtained by each individual in the objective function divided by the average value given by all tested individuals), individuals with higher relative frequency can be used more than once to be exchanged or crossover, and mutation may also create new individuals and the individuals with lower performance are eliminated and no longer enter the exchange process and / or mutation; so that the new population is again size n. The new individuals are again tested on their performance, selected and the best ones creates new individuals who pass to the next generation, this process is repeated until the number of generations or iterations is reached and the best individual in the last generation will be the one with higher performance and represents the optimal mathematical model found; in Figure 2 there is a flow chart of GP Algorithm.

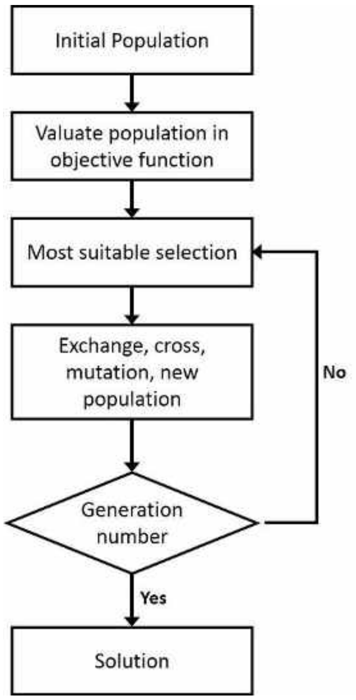

Fig. 2. GP Algorithm

In this study the set of arithmetic operators TS = [+,-,*] was considered, a vector of constants obtained randomly, there were considered the independent variable air temperature T and the rainfall hp as dependent variable. Populations of 200 individuals (models) of 25 nodes (consisting of operators, variables and constants), a crosses a probability of 0.9 and mutation probability of 0.05 were considered; finally, 5,000 generations to complete the process were considered.
The objective function consisted of minimizing the mean square error between the measured and calculated data with the test model.

$$Z = \min \frac{1}{n} \sum_{i=0}^{n} \left(Hp(T) - \widehat{Hp(\bar{T})} \right)^2 \qquad (1)$$

Where *Hp(T)* is the historical monthly rainfall intensity in mm/day, *Hp(T̅)* is the calculated rainfall intensity in mm/day, as a function of the monthly average temperature *T in C°*

1.3. Domain Splitting

For each station, a monthly precipitation model was obtained with genetic programming based on the temperature, considering all the months of the representative year (12 data); a graphic comparison was made between the measured and calculated precipitation data and it was decided to divide the domain of the problem considering the months of registration separately; genetic programming was re-applied to obtain new functions; that is, on this occasion 12 different equations were obtained, taking as reference the time of year.

1.4. SEDEPECC Platform

The SEDEPECC Platform of IMTA uses different scenarios of climate change and its records were taken as a basis in this work; but such platform does not provide a suitable accuracy for each climatological station of the CONAGUA database, the platform only estimates site data with an approximation of 0.5 °, since the coordinates are limited to a type of scenario A1B (High Emissions), for a period from January 2010 to January 2060, with data corresponding to the normal or means for each year, the temperature and rainfall intensity data were collected. (Figure 1 shows the location of the points near the stations of the CONAGUA that were considered for the data download of the SEDEPECC platform). Figures 3 to 8 illustrate the steps taken for the compilation of climate change data.

Fig. 3. The type of Climate Change Scenario is selected, in this case the A1B

Figure 4: The variable (Temperature or Precipitation) is defined.

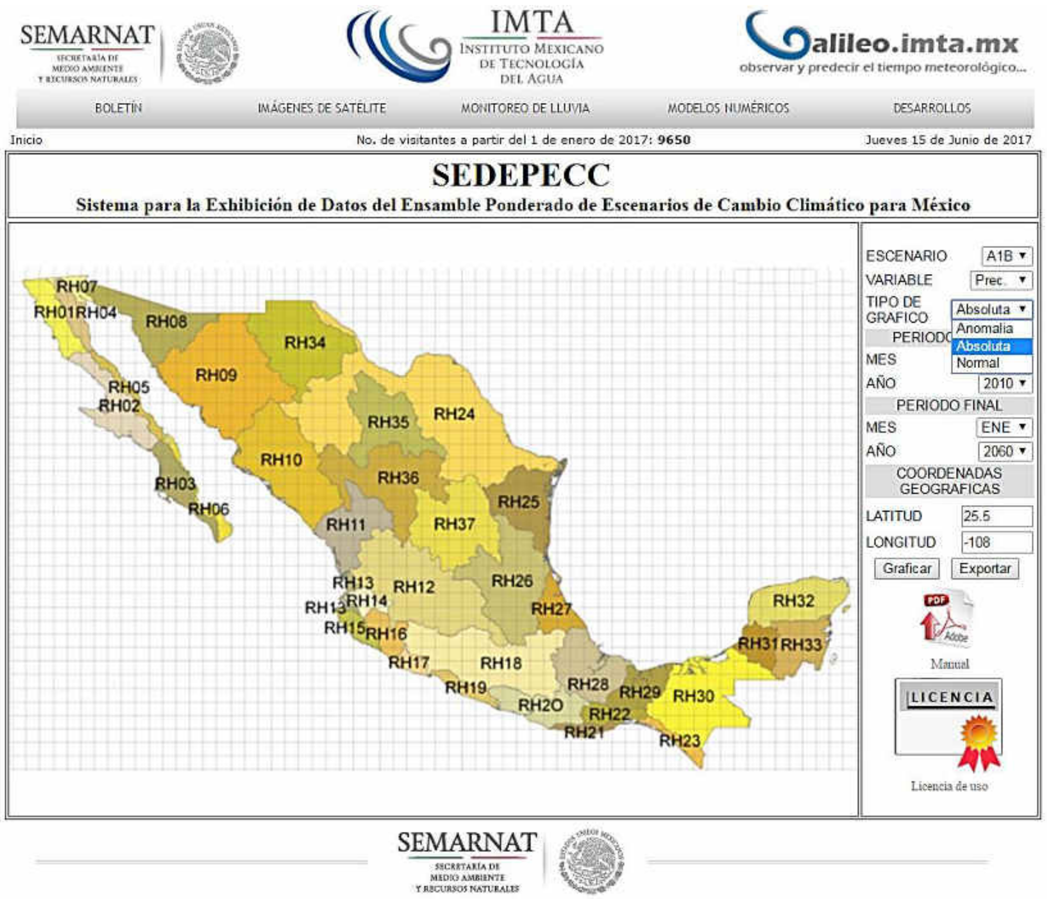

Fig. 5. To obtain data for each month, an ABSOLUTE graph is specified

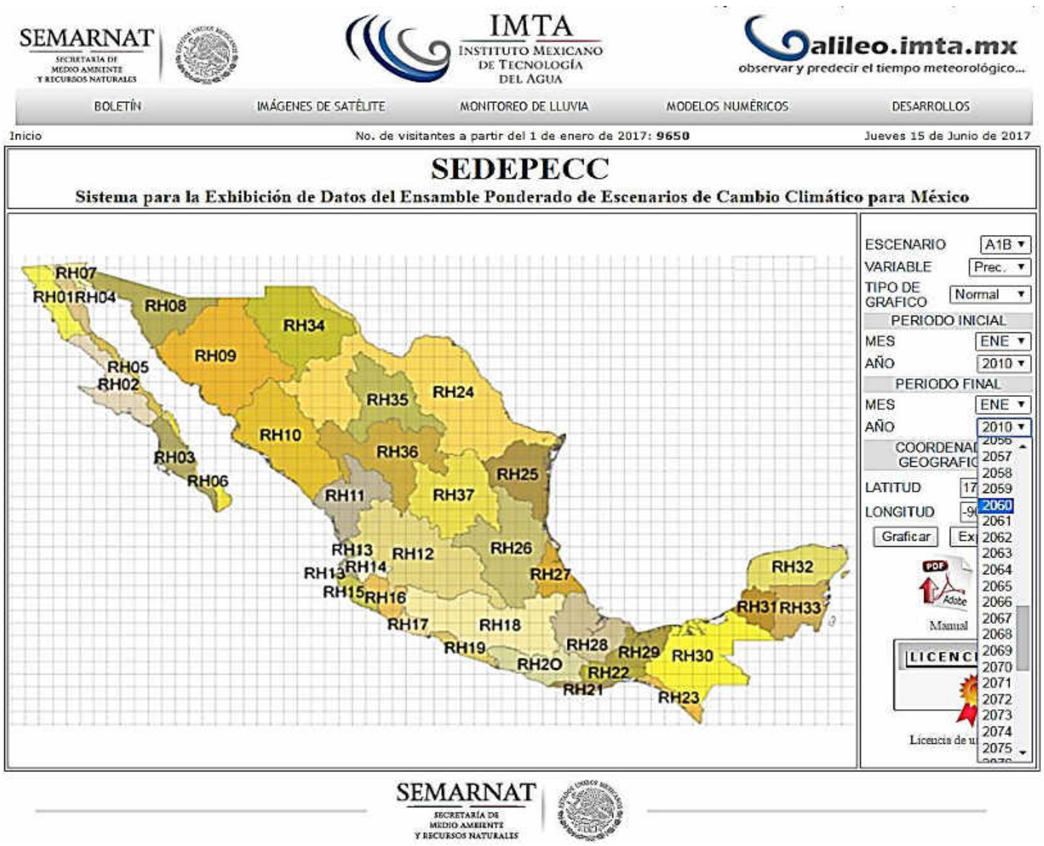

Fig. 6. The period to be analyzed is limited

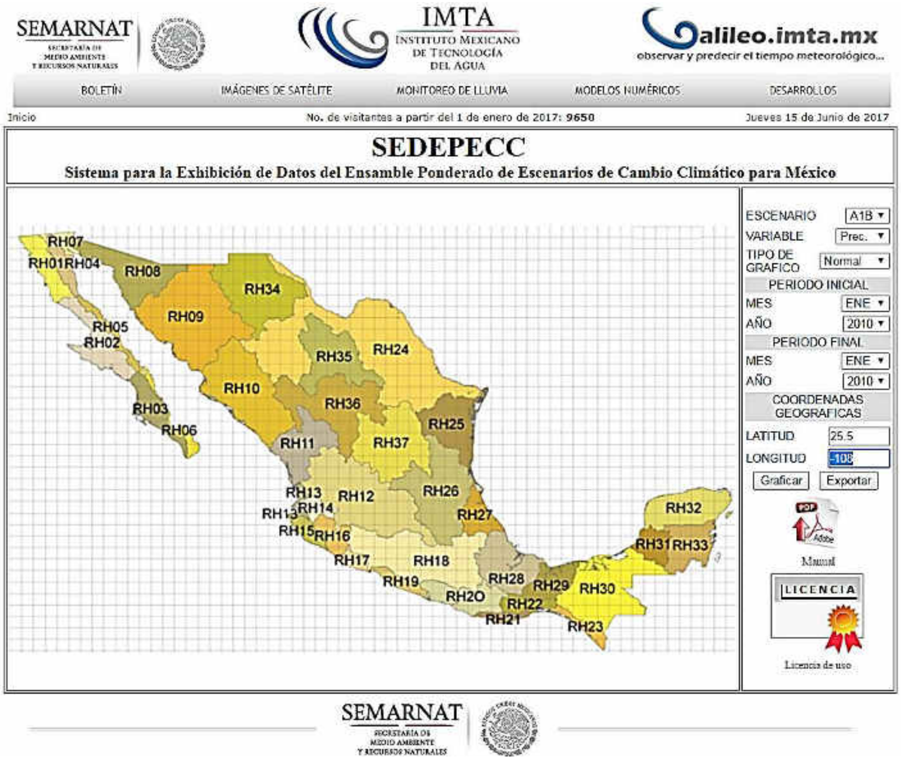

Fig. 7. The coordinates of the site under study are loaded, bearing in mind that the platform has an accuracy of 0.5°

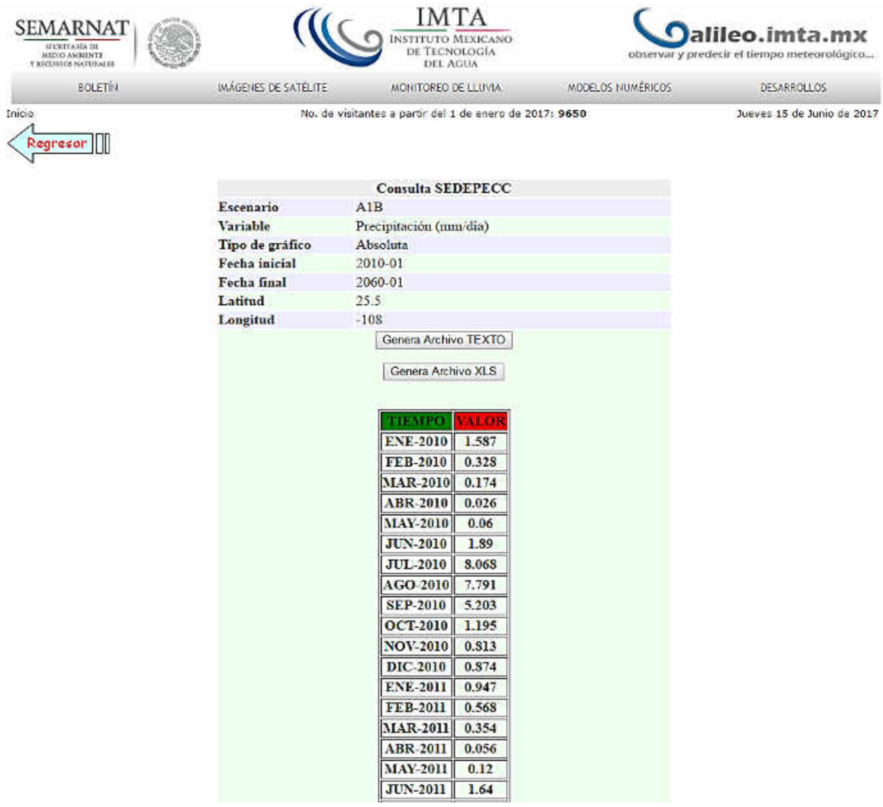

Consulta SEDEPECC	
Escenario	A1B
Variable	Precipitación (mm/dia)
Tipo de gráfico	Absoluta
Fecha inicial	2010-01
Fecha final	2060-01
Latitud	25.5
Longitud	-108

TIEMPO	VALOR
ENE-2010	1.587
FEB-2010	0.328
MAR-2010	0.174
ABR-2010	0.026
MAY-2010	0.06
JUN-2010	1.89
JUL-2010	8.068
AGO-2010	7.791
SEP-2010	5.203
OCT-2010	1.195
NOV-2010	0.813
DIC-2010	0.874
ENE-2011	0.947
FEB-2011	0.568
MAR-2011	0.354
ABR-2011	0.056
MAY-2011	0.12
JUN-2011	1.64

Fig. 8. The option EXPORT is chosen and later it can be used in the desired format

1.5. Application of PG models to series of climate change scenarios

In order to simulate the behavior obtained with the representative year and with the horizontal and vertical dissections, the models were fed with air temperature records extracted from climate change scenarios from the SEDEPECC platform to obtain the indispensable equation to calculate the precipitation of the site study. Initially records with a length of 50 years were used, later periods between January 2010 and January 2045 were adopted (that is 35 years to obtain the model), with the intention of testing the equations in the subsequent 15 years, seeking to represent the behavior of the simulations represented in the SEDEPECC.

2. Results

Notably the values calculated with the PG follow the same behavioral trend as the data disseminated by the SEDEPECC, this is of note, since, when trying to reproduce the patterns in the following 15 years of study with the formulas obtained with the initial 35 years, the behavior of the figures coincides and, in addition, the divergence is lower between those calculated and those taken as a basis. The scope of these results is visible in table 2 and from figure 9 to 11.

Table 2: Precipitation Intensity Equations (mm/day), obtained with PG according to the month of adjustment

San Joaquin Station, Sinaloa, ID: 25172	
January Equation	$Hp= 0.94$
February Equation	$Hp= -0.004T^2-0.01T+2.03$
March Equation	$Hp= 0.801-0.0000029T^4$
April Equation	$Hp= 0.0802$
Mayo equation	$Hp= 0.0005T^2+0.00003T-0.223$
June equation	$Hp= 4.789-0.097T$
July equation	$Hp= 8.321$
August equation	$Hp= -0.0006T^3+0.0084T^2+0.499T-0.089$
September equation	$Hp= 0.0076T^2-0.0329T$
October equation	$Hp= 4.667-0.11T$
November equation	$Hp= 0.635$
December equation	$Hp= -0.0000017T^4+0.00019T^3+0.00011T^2+0.000016T$

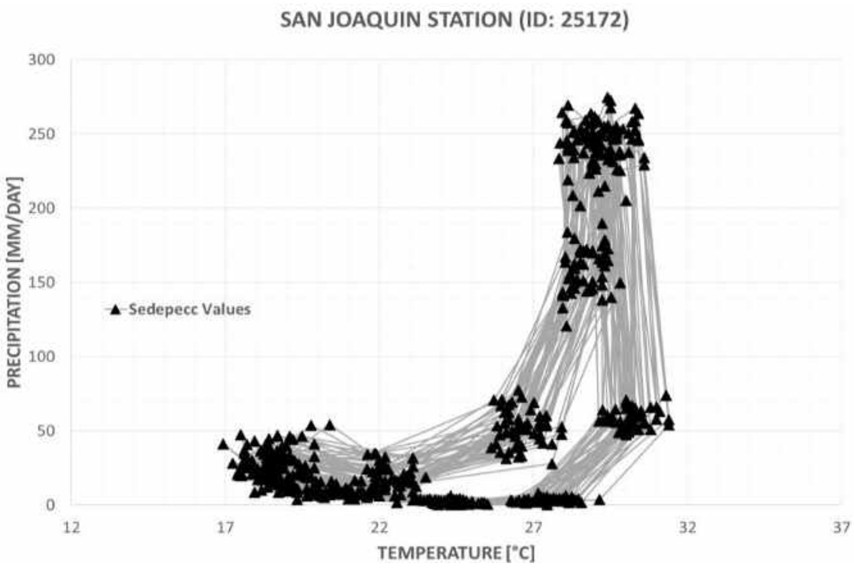

Fig. 9. Values of the SEDEPECC platform, corresponding to an A1B scenario, with a period between January 2010 and January 2045. Site near San Joaquin Station

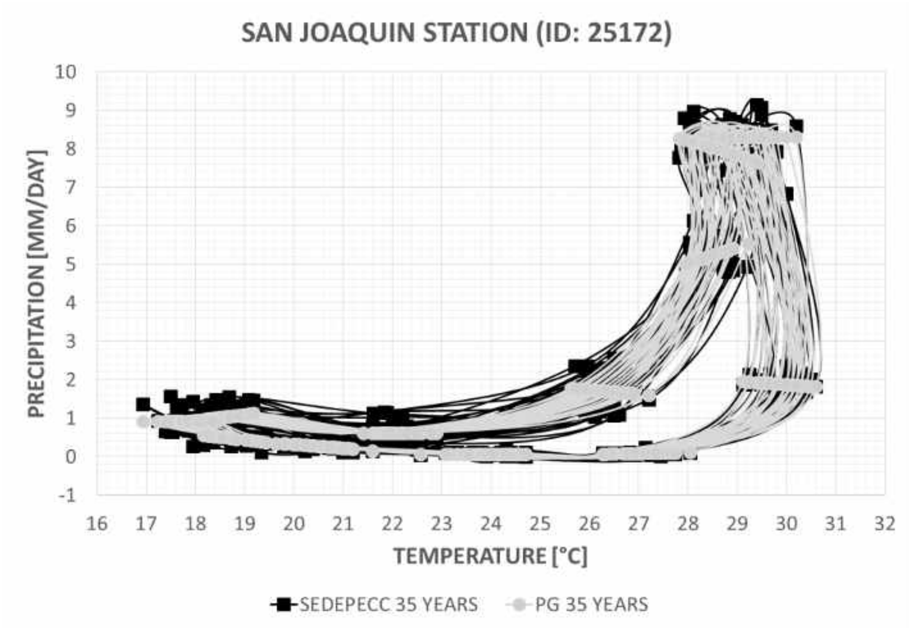

Fig. 10. Precipitation against Temperature, PG and SEDEPECC first 35 years

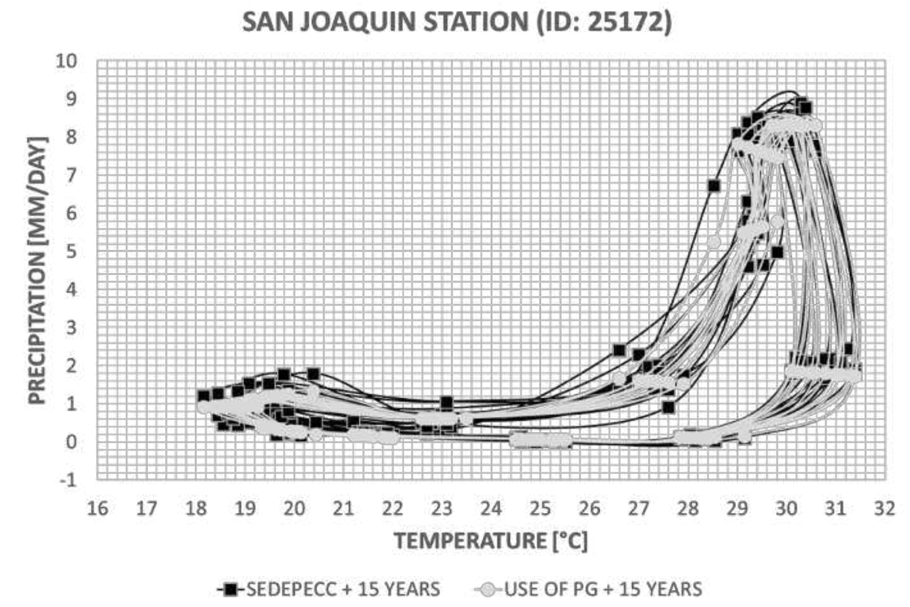

Fig. 11. PG model obtained with firs 35 years used to the subsequent 15 years

Figure 12 shows the efficiency of the method since it is possible to reproduce the annual behavior pattern of precipitation from the average air temperature data. Below are the graphs that are obtained by applying the same equations to a much longer time span, for this case from February 2045 to December 2098.

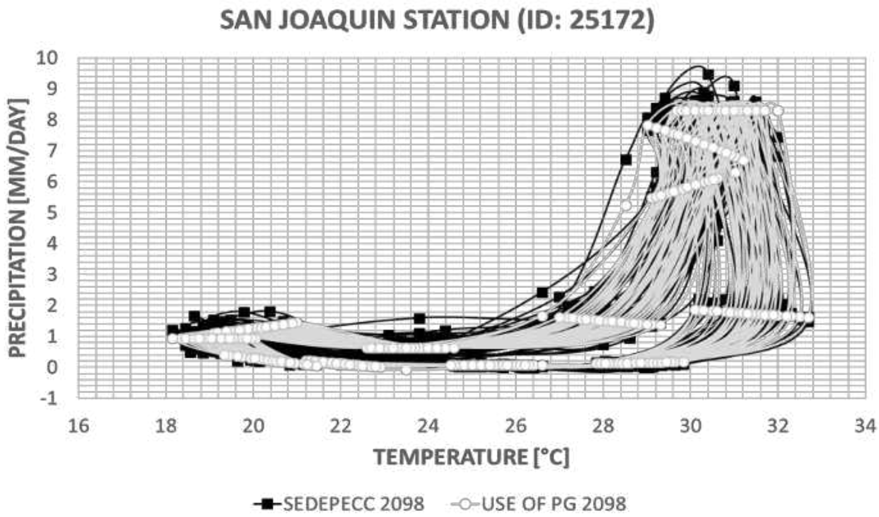

Fig. 12. PG with 35 initial years used for a period of time longer than 53 years on the chart of the SEDEPECC records for the same subsequent period

The parameters obtained from this process are listed below (Table 3), show that Genetic Programming can be used to calculate long and short term behavior based on an initial period of 35 years.

Table 3: Parameters calculated for different subsequent periods

San Joaquin Station, Sinaloa, ID: 25172	
Mean Square Error 35 initial years	*0.08*
Mean Square Error Feb 2045 to Jan 2060 PG	*0.09*
Mean Square Error Feb 2045 to Dec 2098 PG	*0.15*
Variation 35 initial years	*8.51*
Variation 35 years PG	*0.08*
R^2 35 years PG	*0.99*
Variation Feb 2045 to Jan 2060	*8.68*
Variation Feb 2045 to Jan 2060 PG	*0.11*
R^2 Feb 2045 to Jan 2060 PG	*0.99*
Variation Feb 2045 to Dec 2098	*7.92*
Variation Feb 2045 to Dec 2098 PG	*0.21*
R^2 Feb 2045 to Dec 2098 PG	*0.97*

3. Discussion

There is still a long way to go when it comes to predicting climatological variables, but what is detailed in this work will be used to generate opinions and highlight the importance of being prepared as a society in the face of extreme events. the results shown in graphs and make an analysis in the peaks in both low and high temperatures and how these can give indications of the behavior of the climate in specific regions.

4. Conclusion

In this work, models were obtained to reproduce the patterns of precipitation behavior based on their average temperature in different sites of Mexico, with unique physiographic and hydrographic characteristics, providing a tool for the prediction of meteorological phenomena of certain regions, before of short and long-term climate change.

In the modeling of data based on the same figures of SEDEPECC, and used in later periods in the short and long term, excellent adjustments were also found, such as the San Joaquín Station, Sinaloa, Code 25172, since the parameter of R2, was the highest in its three periods of analysis.

As mentioned previously, this research has covered 10 stations in the Mexican national territory, so it is important to capture the most outstanding results in a general manner, in figure 13 and 14 a global summary of this study is shown.

Month	Station				
	San Joaquin	Coyotillos	Cuauhtemoc	Colonia Morelos	Santa Elena
January	0.94	0.706-0.02998T	3.840-0.104T	-0.025T+0.62	0.8228
February	-0.004T^2-0.01T+2.03	0.002T^2-0.085T+1.16	3.24-0.075T	-0.0044T^2-0.0022T+0.81	0.7659
March	0.801-0.0000029T^4	1.197	2.71-0.0578T	-0.00016T^2+0.986	0.9052
April	0.0802	-0.003T^2-0.0006T+1.8	4.858-0.129T	0.0396	1.0894
May	0.0005T^2+0.00003T-0.223	7.3-0.26T	5.207-0.067T	-0.0009T^2+0.0023T	2.82-0.006T
June	4.789-0.097T	-0.03T^2+0.82T-0.053	12.378-0.217T	0.995-0.0239T	-0.02T^2+0.77T-0.52
July	8.321	-0.039(T-24.04)(T-1.99)	-0.029T^2+0.917T+1.09	0.436T-0.0125T^2	12.32-0.27T
August	0.0084T^2+0.499T-0.089	6.155-0.155T	-0.03T^2+1.05T-0.021	0.0599T+0.785	4.32
September	0.0076T^2-0.0329T	7.05-0.19T	9.025	5.892-0.193T	23.49-0.61T
October	4.667-0.11T	0.074T+0.159	0.115T+3.53	0.712	5.34-0.053T
November	0.635	0.00002T^3-0.002T^2+0.798	-0.0099T^2+0.358T+0.087	0.41	1.446
December	0.00011T^2+0.000016T	0.8229-0.0449T	-0.01T^2+0.32T-0.214	0.612	2.499-0.044T

Month	Station				
	Chicontepec de Tejeda	Acahuato	Acapulco de Juarez	Ojo de Agua	Ejido Primero de Mayo
January	-0.003T^2+0.065T+1.173	-0.00035T^2+1.28	1.008-0.038T	0.0096T+0.159	2.124-0.13T
February	1.495	1.09-0.002T^2	1.05-0.046T	0.856-0.0459T	-0.00003T^2+1.31
March	1.125	2.72-0.12T	1.43-0.06T	0.0516	0.223
April	5.108-0.118T	-0.001T^2	0.994-0.001T^2	0.267-0.013T	0.762
May	-0.007T^2+0.255T+0.79	0.92	1.32	0.0175	3.765-0.075T
June	-0.0169T^2+0.665T+2.168	-0.036T^2+1.08T+1.314	-0.029T^2+1.012T-0.69	0.00001T^3	5.78-0.14T
July	11.21-0.18T	-0.039T^2+1.235T+0.73	7.197	0.002T^2-0.03T-0.0123	8.11-0.22T
August	5.25	9.71-0.05T	-0.017T^2+0.64T+1.46	1.57	1.35
September	-0.02T^2+0.9997T+0.799	0.26T+3.56	-0.029T^2+1.12T-0.0297	1.33	-0.011T^2+0.45T-1.12
October	0.224T+0.04	0.37T-4.31	-0.0049T^2	-0.008T^2+0.129T+0.667	1.0447
November	8.41-0.25T	0.78	0.043T	0.746-0.0329T	-0.005T^2+0.065T+1.219
December	0.12T-0.73	2.22-0.102T	0.0014T+0.031	0.3919	0.2576

Fig. 13. Equations obtained monthly

Parameter	Statiion									
	San Joaquin	Coyotillos	Cuauhtemoc	Colonia Morelos	Santa Elena	Chicontepec de Tejeda	Acahuato	Acapulco de Juarez	Ojo de Agua	Ejido Primero de Mayo
Mean Square Error 35 initial years	0.08	0.09	0.17	0.04	0.07	0.15	0.12	0.13	0.02	0.07
Mean Square Error Feb 2045 to Jan 2060 PG	0.09	0.1	0.17	0.04	0.08	0.16	0.13	0.13	0.02	0.07
Mean Square Error Feb 2045 to Dec 2098 PG	0.15	0.17	0.2	0.06	0.1	0.19	0.17	0.18	0.03	0.09
Variation 35 initial years	8.51	1.98	6.71	0.73	3.3	11.05	14.26	12.64	0.29	0.51
Variation 35 years PG	0.08	0.09	0.17	0.04	0.07	0.15	0.12	0.13	0.02	0.07
R^2 35 years PG	0.99	0.96	0.97	0.95	0.98	0.99	0.99	0.99	0.93	0.87
Variation Feb 2045 to Jan 2060	8.68	1.99	6.52	0.73	3.13	11.06	14.08	11.99	0.3	0.5
Variation Feb 2045 to Jan 2060 PG	0.11	0.13	0.16	0.05	0.11	0.18	0.14	0.12	0.03	0.08
R^2 Feb 2045 to Jan 2060 PG	0.99	0.94	0.98	0.94	0.96	0.98	0.99	0.99	0.9	0.84
Variation Feb 2045 to Dec 2098	7.92	1.91	5.67	0.8	2.94	10.98	14.14	11.88	0.24	0.5
Variation Feb 2045 to Dec 2098 PG	0.21	0.23	0.24	0.08	0.12	0.23	0.21	0.25	0.04	0.11
R^2 Feb 2045 to Dec 2098 PG	0.97	0.88	0.96	0.9	0.96	0.98	0.99	0.98	0.84	0.78

Fig. 14. Parameters obtained monthly.

Acknowledgments

We want to thank the Institute of Engineering, UNAM for the support for the realization of this project.

References

[1] De Lima, M. Isabel P., Fátima Espírito Santo, Alexandre M. Ramos and Ricardo M. Trigo. "Recent changes in daily precipitation and surface air temperature extreme in mainland Portugal, in the period 1941–2007". *Atmospheric Research*, 2012.

[2] Budaa, Anthony. *Potential effects of changes in precipitation and temperature on wet deposition in central Pennsylvania,* Atmospheric Environment, 2002.

[3] Boccolari, M. "Changes in temperature and precipitation extremes observed in Modena, Italy." Department of Materials and Environmental Engineering, University of Modena and Reggio Emilia, Italy. 2013. *Atmospheric Research* 122 (March 2013): 16-31.

[4] Yagouti, Abderrahmane. *Observed changes in daily temperature and precipitation indices for southern Québec, 1960–2005*, Atmosphere-Ocean, 2008.

[5] Magaña Rueda, Victor. *Cambio Climático: Una Visión desde México*, Instituto Nacional de Ecología, 2006

[6] Allerup, Peter, Henning Madsen and Flemminf Vejen. "Correction of precipitation based on off-site weather information." *Atmospheric Research* 53 (May 2000): 231-250.

[7] Piani, C. "Statistical bias correction of global simulated daily precipitation and temperature for the application of hydrological models." *Journal of Hydrology* 395 (December 2010):187–192.

[8] Christensen, Jens H., Fredrik Boberg, Ole B. Christensen and Philippe Lucas-Picher. "On the need for bias correction of regional climate change projections of temperature and precipitation." *Geophysical Research Letters* 35 (October 2008): 1-6.

[9] Tuomenvirta, H. "Homogeneity adjustments of temperature and precipitation series—Finnish and Nordic dat." *International Journal of Climatology* 21. (April 2001): 495-506.

[10] Begert, Michael, Thomas Schlegel and Walter Kirchhofer. "Homogeneous temperature and precipitation series of Switzerland from 1864 to 2000." *International Journal of Climatology* 25 (January 2005): 65-80.

[11] Brunetti, Michele, Maurizio Maugeri, Fabio Monti and Teresa Nanni. "Temperature and precipitation variability in Italy in the last two centuries from homogenised instrumental time series." *International Journal of Climatology* 26 (March 2005): 345 -381.

[12] Cahalan, Robert F., Lawrence E. Wharton and Man-Li Wu. "Empirical orthogonal functions of monthly precipitation and temperature over the United States and homogeneous stochastics models." *Journal of Geophysical Research*, 101 (November 1996):26309-26318.

[13] Cho, Jaeil, Hikaru Komatsu, Yadu Pokhrel, Pat J.-F. Yeh, Taikan Oki and Shinjiro Kanae. "The effects of annual precipitation and mean air temperature on annual runoff in global forest regions." *Climatic Change* 108 (September 2011): 1-8.

[14] Strack, John E., Roger A. Pielke Sr., Louis T. Steyaert, and Robert G. Knox. "Sensitivity of June near-surface temperatures and precipitation in the eastern United States to historical land cover changes since European settlement." *Water Resources Research* 44 (November 2008): 1-13.

[15] Yang, Daqing, Barry E. Goodison, Shig Ishida and Carl S. Benson. "Adjustment of daily precipitation data at 10 climate stations in Alaska: Application of World Meteorological Organization intercomparison results." *Water Resources Research* 34 (February 1998): 241 -256

[16] Benning, Jennifer and Daqing Yang. "Adjustment of Daily Precipitation Data at Barrow and Nome Alaska for 1995-2001." *Arctic, Antarctic, and Alpine Research* 37 (August 2005): 276-283.

[17] Adam, Jennifer C. and Dennis P. Lettenmaier. "Adjustment of global gridded precipitation for systematic bias." *Journal of Geophysical Research Atmospheres* 108 (May 2003): 1-9.

[18] Cramer, Nichael Lynn. "A representation for the adaptive generation of simple sequential programs. In Proceedings of the International Conference on Genetic Algorithms and Their Applications." Paper presented at an International Conference on Genetic Algorithms and the Applications, 1985.

[19] Koza, John R. "Hierarchical Genetic Algorithms Operating on Populations of Computer Programs. In Proceedings of the 11th International Joint Conference on Artificial Intelligence." Paper presented at IJCAI'89 the 11th international joint conference on Artificial intelligence, Detroit, Michigan, August 20-25, 1989

[20] Goldberg, David E. *Genetic algorithms in search, optimization and machine learning.* Boston: Addison-Wesley, 1989.

Phenomenon of Transiency in Water Supply Systems

Assistant professor PhD Student **Nikolett FECSER**[1]

[1] Széchenyi István University, 1 Egyetem tér, Győr, H-9026, e-mail: fecser.nikolett@sze.hu

Abstract: *Transient is a flow condition in which velocity and pressure change rapidly with time. A transient normally occurs when a flow control component changes status and this change flows through the system as a pressure wave. Due to the devastating effects a hydraulic transient can cause, its analysis is very important in determining the values of transient pressures. I present the measurements carried out at Pannon-Víz Zrt and their results in my study.*

Keywords: *Transient, pressure wave, flow, analysis, measurements, pump*

1. Introduction

Transient operating states occur in water supply systems under pressure. Transient operating states place such extreme loads on the pipes that they might cause burst water pipes. The main reasons of the occurrences of transient phenomena are, for example, a sudden change in flow or power failures at pump stations. In extreme situations, transient phenomena can endanger the soundness of the pipe itself [1,2,3].

2. The venue of the measuring process

Pannon-Víz ZRt, the largest water and sewage service in Győr-Moson-Sopron county, operates several regional drinking water supply systems. My measuring instruments were installed at the booster station in Pápai út, Győr. I applied 1 Sebalog D-3 measuring instrument to monitor the transient state in the pipeline system.

Fig. 1. Measurement venue (Pápai út)

3. Describing the measuring instrument

Sebalog D-3 is a compact, robust and extremely versatile data logger. The device can record the readings of various sensor types in user-defined intervals. When using the internal pressure sensor, in addition to the standard pressure measurement the recording of sudden pressure fluctuations is possible. Recorded measuring data are stored in the memory of the logger and can be retrieved via short range radio. Loggers equipped with a GSM module can also send the data regularly to an FTP server, from where they can be downloaded to any Internet-capable computer [4].

Table 1 shows the technical data of the measuring instrument.

Table 1: Parameters of measuring instrument [4]

Parameters	Value
Communication	Short-range radio/
Inputs / outputs	2 or 4 freely programmable channels
Internal pressure sensor	optional: 16 bar / 25 bar / 35 bar; accuracy: +/- 1 %; resolution: 0.006 bar
Log interval standard measurement pressure surge means	Pressure surge measurement 0.1 sec or 1 sec selectable
Memory	4 MB internal memory
Alarm	Switching input and threshold monitoring for each channel possible
Battery	Internal lithium batteries
External power supply	12 V DC
Operating temperature	-20°C…..+70°C
Storage temperature	-20°C…..+70°C
Dimensions	185 x 115 mm
Weight	0.9 kg
Degree of protection	IP 68

Fig. 2 shows the structure of the measuring instrument.

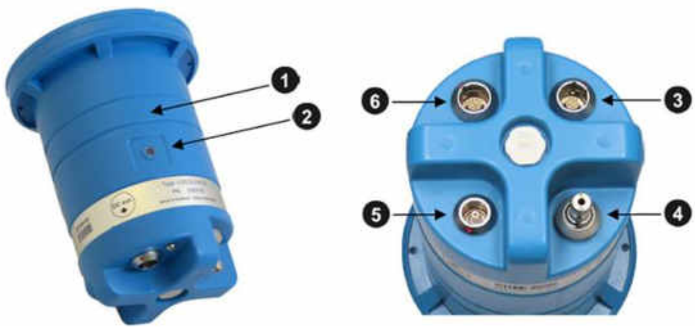

Fig. 2. Measuring instrument

Table 2 shows the structure of the measuring instrument.

Table 2: Structure of measuring instrument

Item	Description
1	contact area (On/Off)
2	control lamp (I/O)
3	DC ext. socket
4	Pressure sensor
5	GSM socket
6	IN socket

The SebaDataView-3 software is used on a PC to program the logger before the measurement and to retrieve the collected data after the measurement. A short-range radio is used for communication between the devices.

Fig. 3 shows the operation of the measuring instrument.

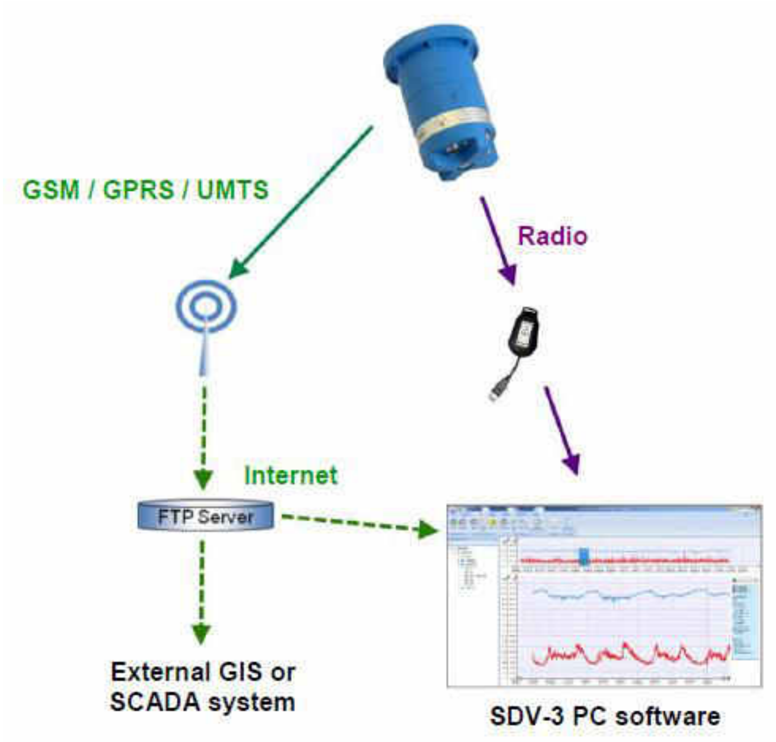

Fig. 3. Operation of measuring instrument [2]

4. Presenting measurement results

Fig. 4. illustrates the measurements of Sebalog D-3 measuring instrument.

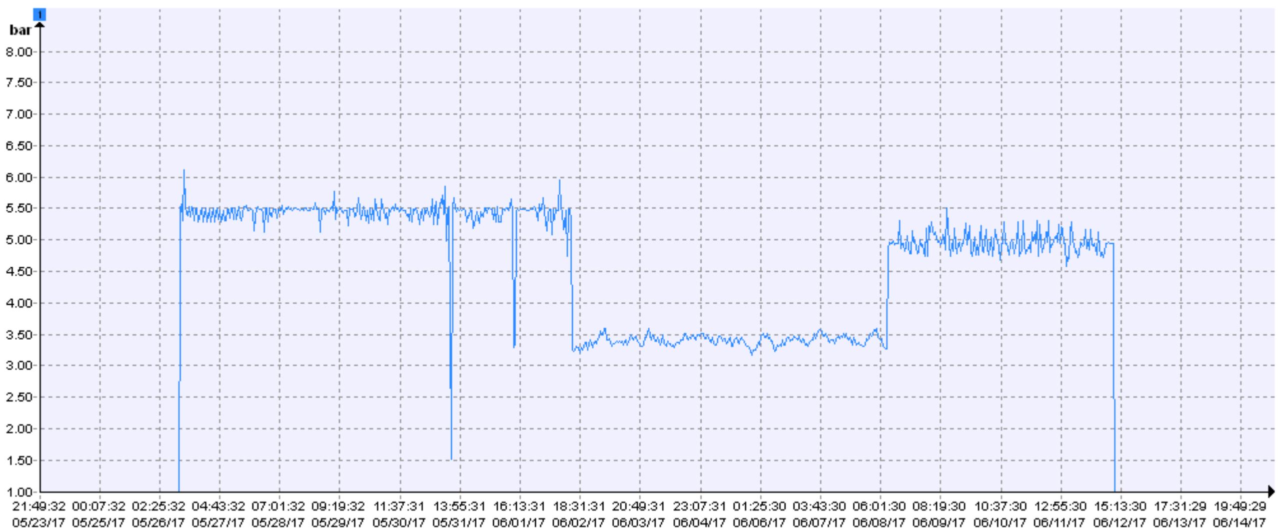

Fig. 4. Operation of measuring instrument [3]

The series of measurements covered 12 day. Table 3 shows the value of transient.

Table 3: The value of transient

Time		Pressure value [bar]
05.26.	12:15	6.119
05.27.	14:00	6.212
	18:15	6.217
	22:45	5.991
05.28.	01:45	5.760
	05:40	5.827
05.29.	05:55	6.166
	06:00	5.770
	07:20	6.166
05.30.	15:25	5.785
	18:55	5.791
05.31.	06:00	5.734
	06:30	5.847
	06:00	5.734
	13:20	6.063
	16:35	5.714
06.01.	09:55	5.755
	23:50	5.940
06.02.	01:30	5.965
	03:20	5.873
	03:25	6.171
	05:55	5.739
	08:10	6.063
	08:20	6.032
	08:25	6.012
	08:40	5.945
	08:45	6.058
	08:50	6.042
	08:55	6.048
	09:00	6.032

Conclusion

In my study I intended to draw attention to the existence of the phenomenon of pressure transiency. The phenomenon of pressure transiency is a potential danger to any water system. My goal is to reveal what might cause the appearance of transient in the water supply systems.

Acknowledgment

Thanks for that „EFOP-3.6.1-16-2016-00017 Internationalization, initiatives to establish a new source of researchers and graduates, and development of knowledge and technological transfer as instruments of intelligent specializations at Szechenyi University" project which supported me.

References

[1] Szlivka, Ferenc. *Csővezetékekben fellépő tranziens jelenségek / Transient phenomena in pipelines.* Budapest, Hungary, 2012. http://www.ontozesmuzeum.hu/download/7ViZGAZDHirtelenzaras.pdf
[2] György, István. *Vízügyi létesítmények kézikönyve. Szivattyúüzemi kézikönyv / Handbook of water facilities. Pump Manual*. Technical Publishing House, Budapest, Hungary, 1974, pp. 11-45.
[3] Csongrádi, Zoltán, Nikolett Fecser, and Bálint Lajtai. "Studying Transients in Water Supply Systems." *Hidraulica - Magazine of Hydraulics, Pneumatics, Tribology, Ecology, Sensorics, Mechatronics*, Romania, 2018.
[4] SebaKMT. *User Manual, Data Logger, Sebalog D-3*. Accessed April 13, 2017. https://www.sebakmt.com/en/portfolio-reader/sebalog-d-3-en.html.

ISSN 1453 – 7303 **"HIDRAULICA" (No. 4/2018)**
Magazine *of Hydraulics, Pneumatics, Tribology, Ecology, Sensorics, Mechatronics*

Estimation of Water Infiltration at a Given Embankment Dam with Sealing Deficiencies by a 3D Numerical Model

Lecturer dr.eng. **Albert Titus CONSTANTIN**[1], Assoc.prof.dr.eng. **Gheorghe LAZĂR**[2], Lecturer dr.eng. **Şerban-Vlad NICOARĂ**[3]

[1] POLITEHNICA University Timişoara, albert.constantin@upt.ro

[2,3] POLITEHNICA University Timişoara

Abstract: *The paper presents a way of studying the water infiltration at the Motru embankment Dam (river ballast fill, clay core sealing) by a 3D numerical model covering the deficient right supporting bank. Since due to sealing imperfections the reservoir runs under level restrictions, the calculations were performed in two stages. First, the model was set up and checked for the existing running situation and then it was endowed with a proposed supplementary ground sealing element that would allow the reservoir running at its designed full capacity. The final goal of the study would be to estimate the maximum appropriate value of the water exfiltration discharge for a dam safety operation under the load given by the originally designed water level. This parameter may than be considered as representative for the expected deep sealing quality, under the required condition of accepting an exfiltrated water turbidity below the value pointed out by stored water.*

Keywords: *Embankment dam, core sealing, ground sealing, water infiltration, numerical modelling.*

1. Motru dam – general description

The Motru Dam on Motru River in Gorj County, Romania, is a ballast-fill embankment sealed with a clay core (figure 1), with a maximum height of 48 m with respect to the foundation level [1,2]. The dam crest is situated at 484.00 mSL and the reservoir usual operation water level is designed at 480.00 mSL. The high-waters are to be discharged by a funnel spillway and eventually by the bottom outlet, both driven by the left supporting bank. As part of the complex Cerna-Motru-Tismana-Bistriţa Water Development, the main purposes of Motru water reservoir are energy production at Tismana Hydro-Power Station and water supply of downstream towns.

The foundation ground in the streambed and towards the left bank shows the fundamental supporting layer – crystalline rock of low permeability and moderate cracking – close to surface, while for the right bank it leaves space for alluvia thick deposits of various granulometries and of larger permeability coefficient (figure 2).

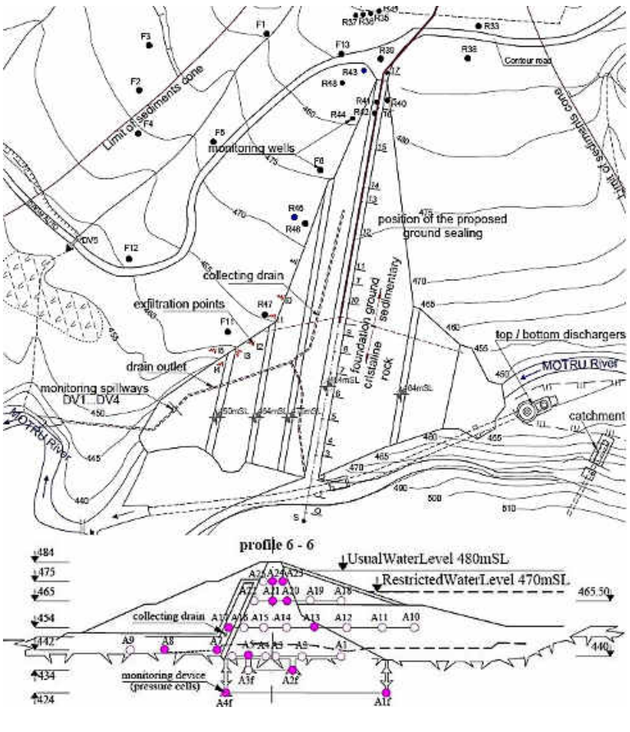

Fig. 1. Motru Dam – overview and cross section

After a short period from the moment of entering into operation in the year of 1983, important water exfiltration was noticed at the dam (producing also transport of fine material) and consequently water level constraint had to be imposed at 470.00 mSL. It was further on perceived that the water infiltration from reservoir happened predominantly by the right bank terrace, at a relatively high permeability ratio ranging from 0.5 to 50 m/day. Several field studies were performed throughout time, proving that exfiltration come mainly from the reservoir by the superficial layers of the right bank under- and side-passing the sealing core, layers not properly sealed during the accomplishment of the retaining structure.

The Institute Studies and Projects in Hydropower developed in 2006 a rehabilitation documentation that proposes the accomplishment of a continuous slurry wall imbedded into the fundamental supporting layer. Driven from the dam crest, the wall was estimated at a total surface of about 10900 m^2 [2]. The project was revised, so the final solution assumes now the foundation ground sealing on the streambed and the right supporting bank.

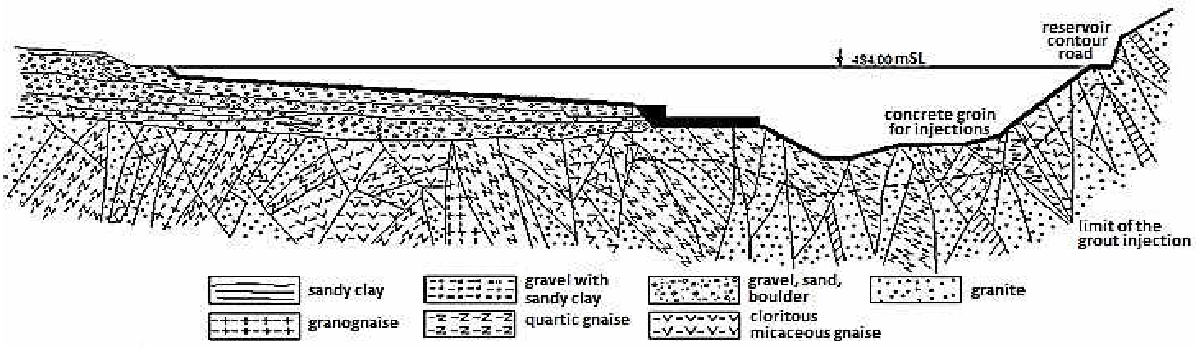

Fig. 2. Valley profile along the Motru Dam axis showing the general geological layer disclosure

In order to develop the infiltration numerical model focusing the right side of the dam and its foundation ground, as according to the revised rehabilitation solution, a three-dimensional volume (figure 3) following a given geometrical configuration was sliced from the entire space of the dam emplacement [3]. The execution quality of the proposed ground sealing could be checked by the help of a numerically estimated acceptable value for the water exfiltrated discharge under a load provided by the originally designed usual retaining water level in the reservoir. This acceptable limit to be assessed by the developed numerical model will have to fulfil the specific condition of an exfiltrated water turbidity below or at most equal to its level in the reservoir.

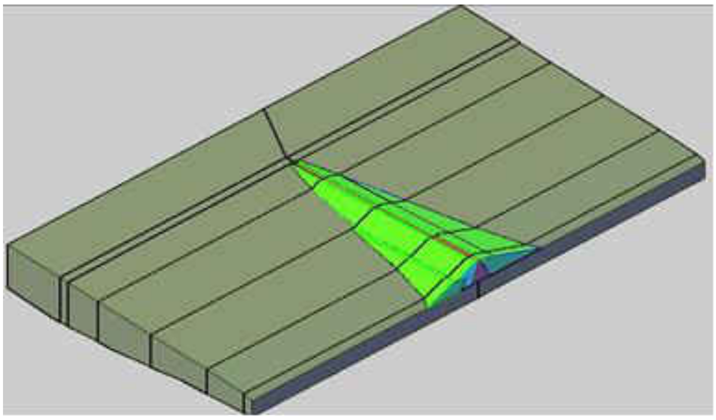

Fig. 3. General geometrical configuration of the modelled dam - emplacement ground domain considered from the streambed towards the right bank

2. Development of the dam - emplacement ground numerical model

The three-dimensional model was obtained by meshing the considered domain by employing SOLID70 thermal type 3D finite elements (figure 4) offered by ANSYS software package [4].

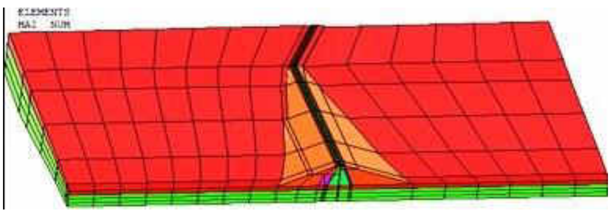

Fig. 4. 3D meshed domain, dam - emplacement ground according to the revised rehabilitation solution

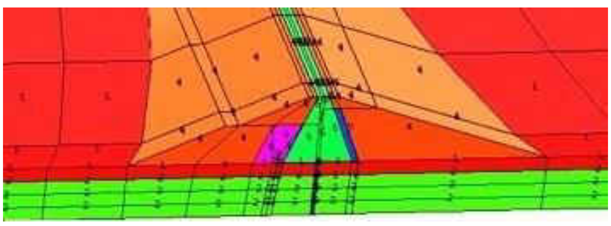

Fig. 5. Detailed view of the Motru Dam central zone indicating the materials' codes

The given values of the permeability coefficient corresponding to the involved materials (supporting ground and embankment fill, [2]) are presented by table 1. Figure 5 brings a zoomed-in view that points out the materials' codes and the modelled downstream draining element. The collecting drain at the bottom of the downstream filter is accomplished by a prefab pipe of 0.80m in diameter encased in a perimetrical concrete massive of square cross section of 1.50m in side. The concrete element is perforated so to collect the infiltrated water and gravitationally discharges by a monitored outlet placed along the streambed.

Table 1: Engaged permeability coefficients for the involved materials

Crt. no.	Type of material	Permeability coefficient, k	
		m/sec	m/day
1	gravel-sand-boulder	0.0001	8.64
2	alluvia deposits	0.0025	216.00
3	sealing screen 1	1.0e-5	0.864
4	embankment fill	0.000347	29.98
5	clay core	1.0e-8	0.000864
6	downstream filter	0.0005291	45.72
7	upstream filter	0.000012	1.0368
8	drainage equivalent -step1 drainage equivalent -step2	0.00615 0.9419	531.50 81380
9	sealing screen 2	2.0e-7	0.0216
10	sealing screen 3	0.0004	34.56
11	sealing screen 4	0.0002	17.28

The automatic mesh of the designed domain led to a model of 1373 finite elements (SOLID70 with 8 joints) and 2094 joints. The numerical simulation of the unsteady regime model engaged a time step of 1 day to consider the storage water level fluctuation and a time step of ½ day to perform the iterative calculations [5]. The boundary conditions are given by water level fluctuation at a number of specific joints – on the dam upstream face, at the wells on dam downstream part and at the equivalent drain, respectively.

2.1 Adjustment of the numerical model for the transitory regime

Given the entire available data base represented by the water level time development in the reservoir and several monitoring wells driven on the right mountainside downstream and aside of the retention structure (F1, F5, F6, F11, F12, R35) together with the water discharge values at the monitoring spillways DV3 and DV4 on the outlet of the infiltrated waters collector (equivalent drain), a total time interval of 4748 days – from January 1st, 1990, to January 1st, 2003 – was considered for running the numerical model (see figure 1). It was noticed from the supplied data that usually there is no recorded information for nonworking days (weekends and other official holidays). By eliminating these blank moments, a total number of 2274 days remained to perform the analysis.
The infiltration (permeability) coefficient for the modelled collecting drain k_{equiv} is initially unknown, following to be revealed by the numerical model adjustment operation. The properly corresponding final value shall be established by successive tests until the infiltrated discharge values reached by the numerical analysis come to match with the measured ones (Q_{total} = DV3+DV4). The setting operations were initially performed for the 2274 days time interval and it was noticed that for the beginning period, when the reservoir water level is usually above 475mSL and the measured infiltration discharge varies between 50 and 15 l/s, the computed discharge values come close to the measured ones. By the other hand, for the ending period, when the reservoir level is below 474mSL and the infiltrated measured discharge goes from about 10 to 0.5 l/s, the numerical model leads to values spreading away from the target ones.

As considering the downstream drain outgoing part, its hydraulic head is known as equal to the geometrical level 463.85mSL of the joints attached to it (1053, 1054, 1063 and 1064). Still, this condition would match to the numerical model only if the equivalent drain runs as a pipe at full cross section flow. In the situation that the drain operates under a free level flow regime with partial filled cross section (as it happens towards the ending part of the considered time interval), the outgoing water level would result from the model as variable below the specified geometrical level. Artificially, for the situation of low outgoing discharge values (as when Q_{total} = DV3+DV4 tends to range from about 10 to 0.5 l/s – happening mainly along the 2001…2002 period), a new specific equivalent permeability coefficient (k_{equiv1}) was established – drainage equivalent 1 in table 1 – so that the modelled pipe to run at full flow. As a consequence, the 3D numerical model adjustment for a transitory operating regime had to follow two steps:

Step 1 – the equivalent drain running as a pipe under a free level flow regime with its cross section partially filled. There was engaged the k_{equiv1} value while the permeability coefficients describing materials 9, 10 and 11 that model the sealing element were successively altered till the outgoing total infiltrated discharge came out in the range of the corresponding measured values. The three finally estimated values by this first step are to be further on considered as fixed for the second step.

Step 2 – the equivalent drain running as a pipe under a free level flow regime at full cross section. A k_{equiv2} value was then successively adjusted looking to have a fit on the total outgoing infiltrated discharge values. When this condition was fulfilled, the reached k_{equiv2} value was assumed as fixed for the model.

In explicit terms, by considering for step 1 the time interval from January 9, 1997, to December 22, 2002, (meaning from day 1352 to day 2274) with its specific boundary conditions – the water level development at joints attached to dam upstream face (reservoir) and to the wells F1, F5, F6, F11, F12 and R35, and respectively the fixed level of 463.85mSL at the joints attached to drain outgoing (1053, 1054, 1063, 1064) – and proceeding as described to several adjustment numerical computations, the three proper values of permeability coefficients describing the sealing element were revealed and so fixed for the model (as presented by table 1). The representative phenomenon time dependent parameters are then graphically presented for the significant final stage of adjustment step 1 (figures 6a, 7a and 8a).

The values representing the time developments showed in figures 7 and 8 were saved in an outgoing file in order to acquire a correlated development as expressively presented by figure 9, from day 1852 to day 2202.

Afterwards, the time interval from April 27, 1993, to December 23, 1996, (meaning from day 750 to day 1352) was considered for step 2 adjustment operation. By engaging the corresponding boundary conditions (as previously mentioned) and by performing the adjustment operation described for this second step, the proper drain equivalent value k_{equiv2} was established for the modelled drainage (see table 1). After concluding the second adjustment step operation, the representative time dependent parameters were graphically processed (figures 6b, 7b and 8b). The values characterizing time developments in figures 7b and 8b were additionally processed in order to obtain the correlated development presented by figure 10, from day 750 to day 1350 (as ignoring the first 750 days with no registered data at well R35).

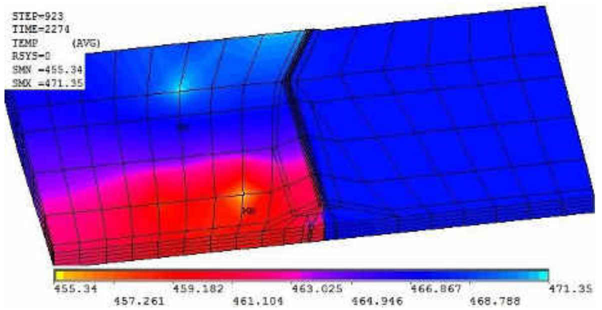

Fig. 6.1 Hydraulic head development at the end of the adjustment step 1 period – day 923 (December 22, 2002), corresponding to a water level of 467.79mSL in the reservoir

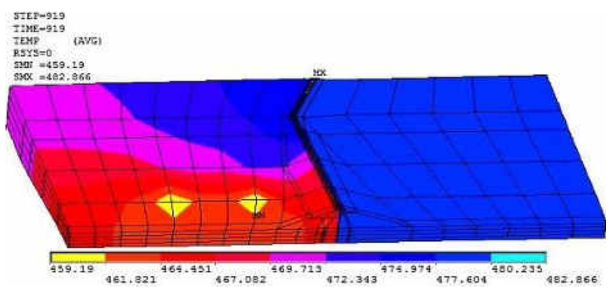

Fig. 6.2 Hydraulic head development on day 919 (April 10, 1994) after the adjustment step 2, corresponding to a water level of 480.00mSL in the reservoir

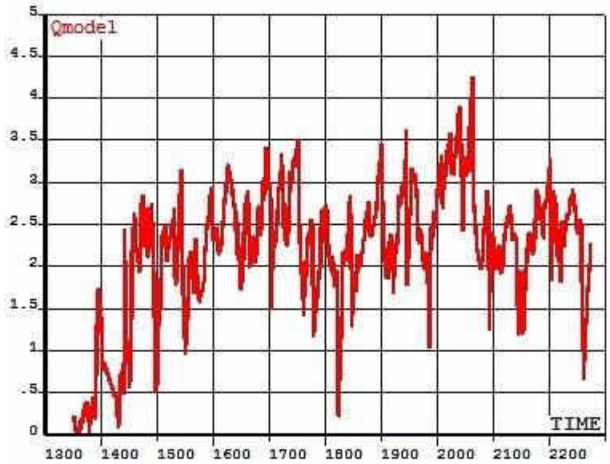

Fig. 7.1 Computed infiltration discharge (DV3+DV4) time development along the adjustment step 1 period of 922 days

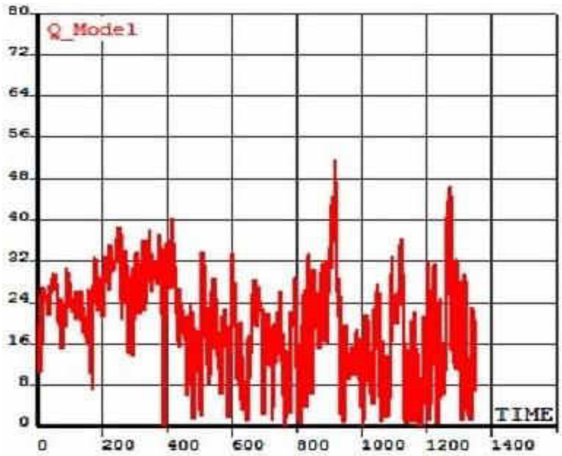

Fig. 7.2 Computed infiltration discharge (DV3+DV4) time development along the adjustment step 2 period of 1352 days

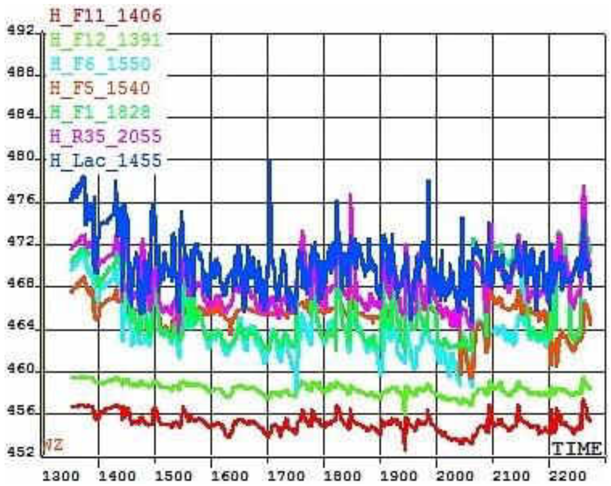

Fig. 8.1 Water level time development in the reservoir and at the six wells along the adjustment step 1 period of 922 days

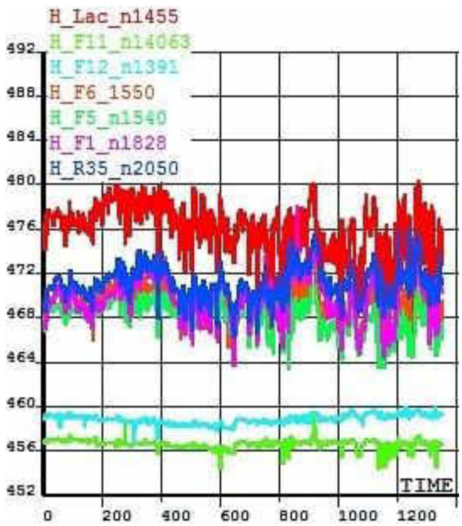

Fig. 8.2 Water level time development in the reservoir and at the six wells along the adjustment step 2 period of 1352 days

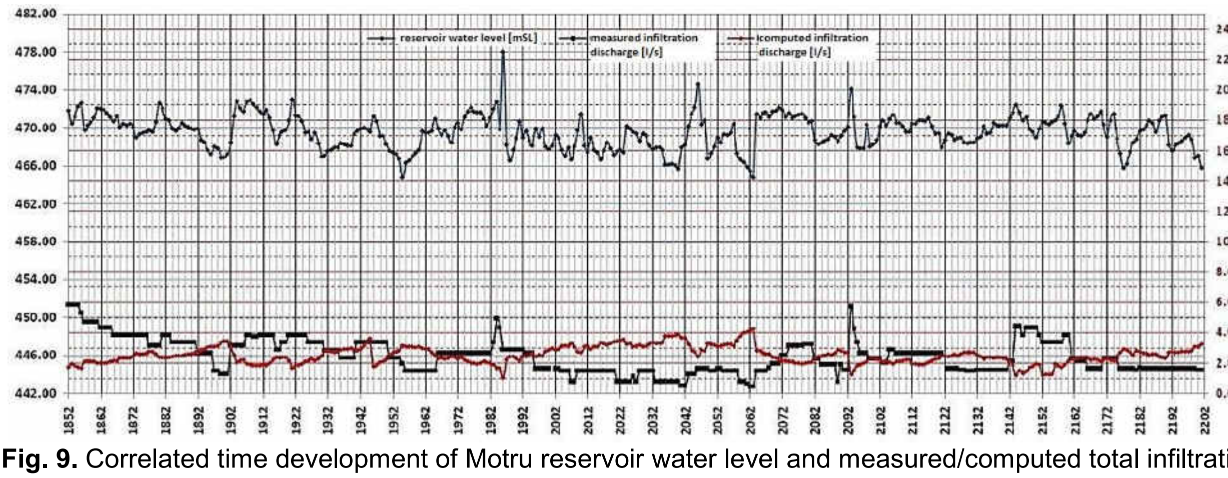

Fig. 9. Correlated time development of Motru reservoir water level and measured/computed total infiltration discharge (DV3+DV4) after the adjustment step 1 (from September 6, 1999, to October 5, 2001)

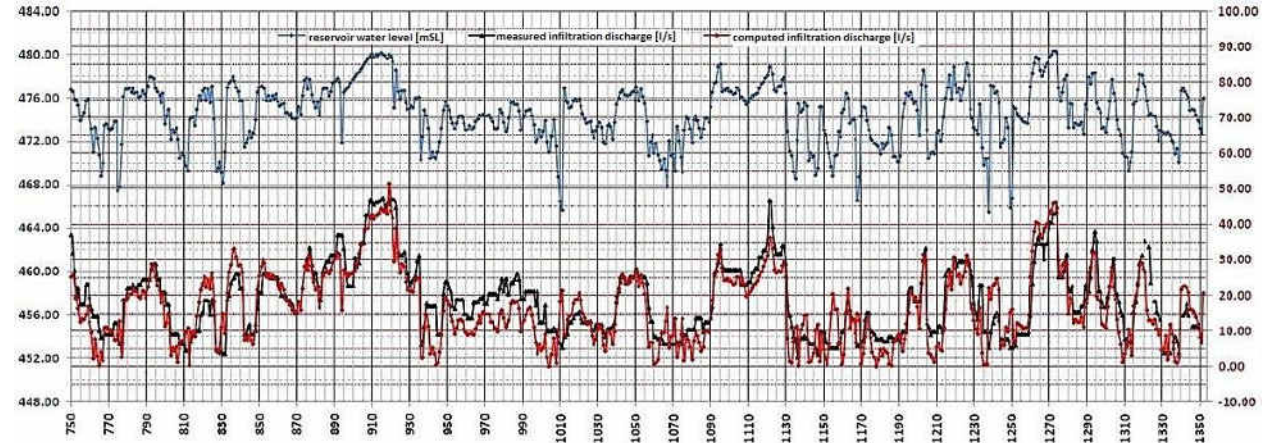

Fig. 10. Correlated time development of Motru reservoir water level and measured/computed total infiltration discharge (DV3+DV4) after the adjustment step 2 (from April 27, 1993, to December 23, 1996)

Studying the numerically reached time development with respect to the measured one (as presented by figure 10), there was accepted that the numerical model of Motru Dam is appropriately adjusted for performing further analysis.

2.2. Infiltrated discharge under transitory running regime during the time period January 3, 2012, to December 24, 2013

The adjusted model behaviour was afterwards examined by running an analysis over a later time period. There was going to consider the time interval of 286 days from January 3, 2012, to December 24, 2013, which is lacking data regarding the measured infiltration discharge at monitoring spillways DV3 and DV4. The equivalent drain would work mainly as a pipe under a free level flow regime with its cross section partially filled. The boundary conditions would refer to the registered water level development in the reservoir and F5, F6, F11 and F12 wells, and the 463.85mSL value fixed for the four joints (1053, 1054, 1063, 1064) attached to the drain outgoing, respectively. The main time dependent parameters – hydraulic head at a given moment (figure 11) or water levels and infiltration discharge – obtained by running the numerical analysis may be correspondingly draw out. A correlated reservoir water level and infiltrated discharge developments with respect to time is given by figure 12 obtained by postprocessing the numerical values.

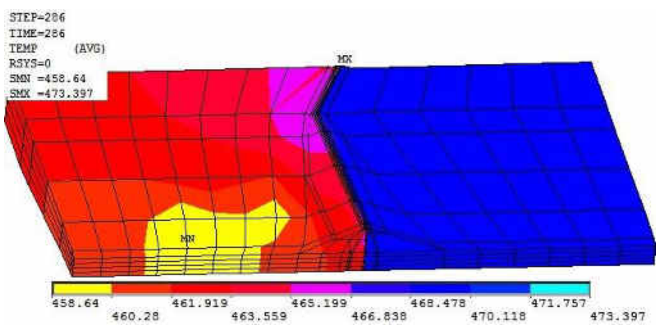

Fig. 11. Hydraulic head development on day 286 (December 24, 2013), corresponding to a reservoir water level of 470.09mSL

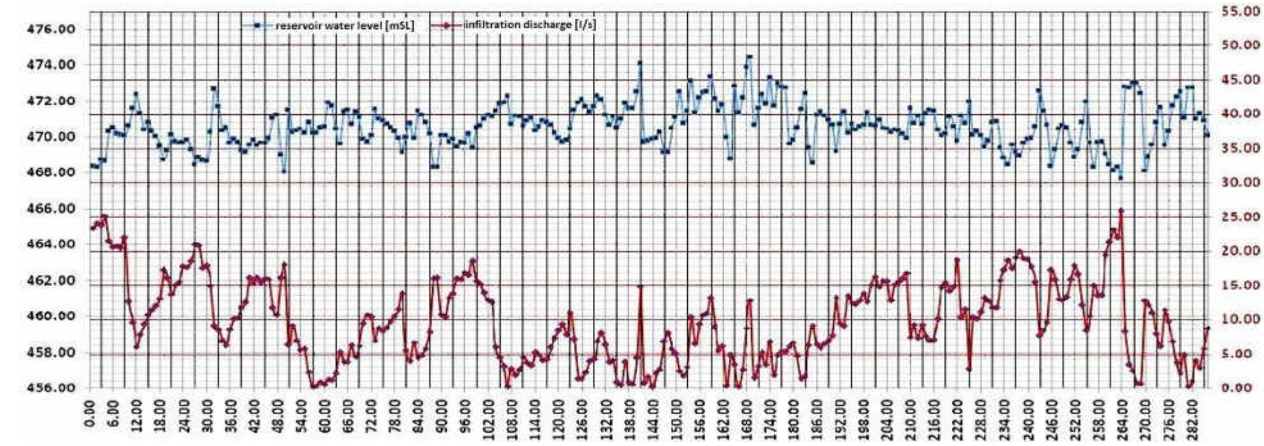

Fig. 12. Correlated time development of Motru reservoir water level and computed total infiltration discharge (DV3+DV4) along the 286 days period of missed registered data (from January 3, 2012, to December 24, 2013)

3. In depth additional sealing at Motru Dam – exfiltrated discharge under transitory regime

As already mentioned, the Institute for Studies and Projects in Hydropower developed in 2006 a documentation that proposes for Motru Dam the accomplishment of a continuous slurry wall driven from the dam crest, going through the deficient underground sedimentation strata and imbedded into the fundamental supporting layer [2]. It was concluded soon after that this additional sealing element should continue the dam core in the ground only from the streambed along the right supporting bank. In order to estimate the infiltration phenomenon that develops mainly by the right side of the barraged section, the previously adjusted numerical model (k_{equiv2} = 0.9419 m/s = 81380 m/day) was endowed with a sealing screen following the proposed geometry and quality. For the new numerical analysis, the defining permeability coefficient of the finite elements in the affected area was accordingly modified [3]. Specifically, the already built elements representing now the designed slurry sealing screen – assigned materials 9, 10 and 11 as indicated in table 1 – are assumed to show a permeability coefficient of k_{screen} = 3.0e-8 m/s = 0.002592 m/day. The detailed views in figure 13 show, beside the already discussed model of the equivalent drain, the modelled configuration of the foreseen sealing screen.

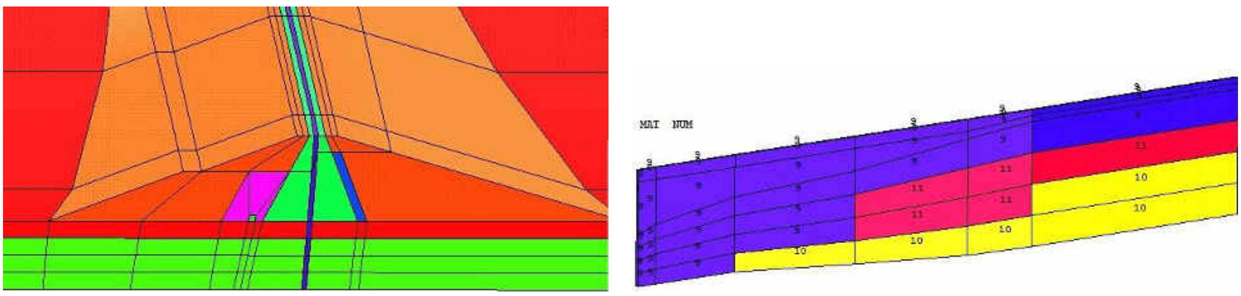

Fig. 13. Detailed view of the Motru Dam central zone endowed with the designed sealing screen (left); profile of the underground sealing screen driven through the right bank indicating the materials' codes (right)

There are further on presented the numerical analysis results for two of the three significant time periods previously considered in the model adjusting stage, meaning from April 27, 1993, to December 24, 1996, and from January 3, 2012, to December 24, 2013, respectively.
The equivalent drain works as a free flow pipe (of an enforced hydraulic head 462.45mSL) and the boundary conditions are represented by the water level time development in the upstream reservoir and several monitoring wells driven downstream on the right bank (the available data at F1, F5, F6, F11, F12 and R35 for the first time period and at F5, F6, F11 and F12 for the second period), and also an enforced water level of 462.45mSL for the joins attached to the drain outgoing. This outgoing level value was reached by several successive alterations in order to fulfil a proper

correlation also during intervals of significant hasty variations of the reservoir water levels (a variation in the total outgoing infiltration discharge would correspond to a previous variation in the reservoir level). The eloquent analysis results would refer to the water head development at a given moment (figures 14) and the total outgoing infiltration discharge at the monitoring spillways DV3+DV4 in correlation to the reservoir and monitoring wells water levels behaviour with time (figures 15). The correlated developments are shown as suggestive over a reduced number of days (602 for the first mentioned time period and 286 for the second one) for which continuous reliable data were available.

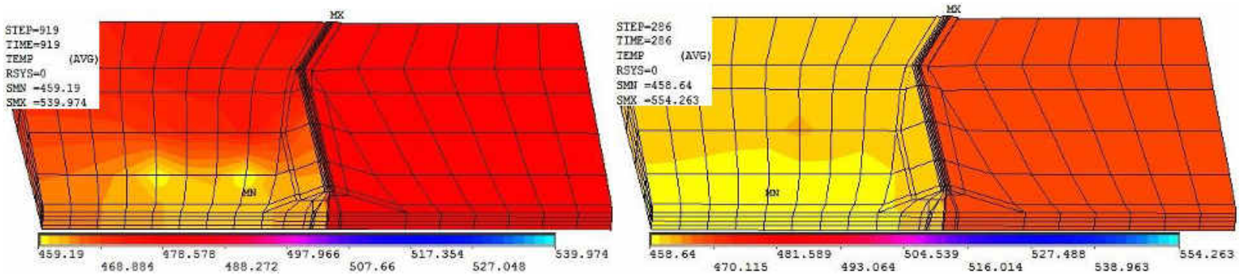

Fig. 14. Estimated hydraulic head development in case of a slurry sealing wall accomplishment – on April 10, 1994, corresponding to 480.00mSL in the reservoir (left) and on December 24, 2013, corresponding to 470.09mSL in the reservoir (right)

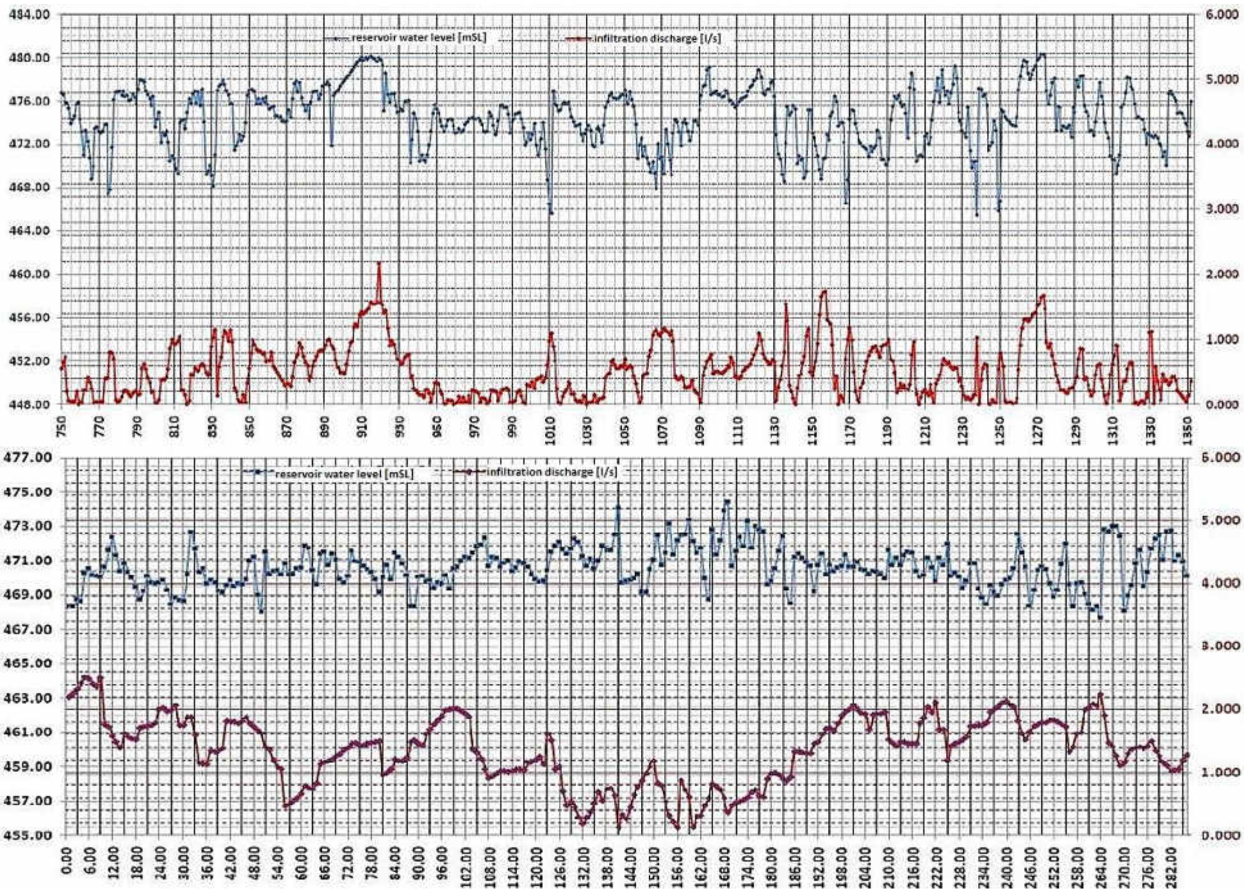

Fig. 15. Correlated time development of Motru reservoir water level and computed total infiltration discharge (DV3+DV4) along the 602 days in-between April 27, 1993, and December 24, 1996, and along the 286 days in-between January 3, 2012, and December 24, 2013 (below), for the retaining structure with designed additional sealing screen

By searching along the numerical data behind the time developments in figures 15, one would notice that the total maximum infiltrated discharge at drain outgoing in the situation of additional sealing screen accomplishment might range from about 2.17 to 2.51 l/s.

4. Conclusions

There can be assumed that throughout the long dam operating period of almost ten years (March 29, 1993 – December 24, 2013) a significant material transport was produced, specifically the fine material from the underground area in the supporting right bank considered to be sealed by the slurry screen. It is also estimated that water level operation constraint at 472.00mSL and shortly after at 470.00mSL determined a reduction in the scouring phenomenon.
As about the rehabilitation solution, by accomplishing an additional sealing element through the dam core and its under side poor sedimentary strata on the right supporting bank, there is estimated that in case the restriction level around 470.00mSL is maintained the total infiltration discharge would go at most to about 2.51 l/s, meaning about ten times less than the existing un-interfered situation.
Assuming the accomplishment of the proposed sealing screen, different procedures can be further on employed to reach an estimation of the infiltration discharge development in time corresponding to an operation reservoir water level around the initially designed value of 480.00mSL, either by altering the available reservoir level data and model rerunning or by numerical extrapolation of the already reached results for the restricted level. A satisfying indicative estimation of the mean infiltration discharge value can be obtained by analysing the built numerical model under a stationary regime given by the usual water level at 480.00mSL.
Proceeding to a numerical extrapolation of the values corresponding to the analysed situation of around 470.00mSL restricted level, there was estimated an amplification ratio of about 3.06 for the infiltration phenomenon in case of increasing the operation reservoir water level at around 480.00mSL. The total infiltration discharge would go under this circumstance at a maximum value of about 7.67 l/s, meaning in the range of the forecasted value (Popovici & Ilinca, 2016) of 7.04 l/s.

References

[1] Cojocar, M. *Hidroconstrucţia 2005 – Tradition and state of the art*. SC Hidroconstrucţia SA Bucureşti, Inkorporateprint, Bucharest, 2005.
[2] ∗∗∗. *Barajul Motru. Etanșare suplimentară a frontului de retenție. Documentație de licitație. Proiect tehnic și caiet de sarcini / Motru Dam. Additional sealing of the retention section. Bidding documentation. Technical project and technology tender specifications*. SC ISPH SA, Subsidiary "Iron Gates", Drobeta Turnu Severin, 2006.
[3] Popovici, A., and C. Ilinca. *Calculul valorii maxime acceptabile a debitului exfiltrat, ca urmare a etanșării suplimentare la barajul Motru. Complex energetic Cerna Motru Tismana / Estimation of the maximum acceptable exfiltrated discharge considering an additional sealing at Motru Dam, Power Arrangement Cerna-Motru-Tismana*, Contract no.17/2016, 2016.
[4] ∗∗∗. *ANSYS/ED – Student Edition, Release 5.3*, Copyright 1971-1996 by SAS IP – ISO 9001-1994.
[5] Lazar, Gh., and S.V. Nicoara. "Numerical modelling by the finite element method of an unsteady water flow through a rockfill dam and its foundation site." Paper presented at the Seventh Benchmark Workshop on Numerical Analysis of Dams, Bucharest, Romania, September 24 - 26, 2003.

Influence of the Rotating Piston Shape on the Flow Rate of a New Type of Rotating Working Machine

Lecturer PhD Student **Ammar Fadhil Shnawa ALMASLAMANI**[1],
Dr. Eng. **Adrian COSTACHE**[1], Prof. Dr. Eng. **Nicolae BĂRAN**[1]

[1] Politehnica University of Bucharest, ammar.fadhil88@yahoo.com

Abstract: *The paper presents a new constructive solution for a rotating pump that contains two profiled rotors; each rotor has two pistons that may be triangular or curvilinear (oval). The area difference of the two pistons in a cross section is calculated; there is a difference in area which at each piston rotation, will reduce the flow rate circulated by the curved pistons.*

Keywords: *Rotating volumetric pump, profiled rotor, pistons.*

1. Introduction

At piston machines, the reciprocating motion of the piston is converted to rotation motion through a crank-rod mechanism; this mechanism generates energy losses due to frictions occurring during its operation. Researcher's attention is directed toward eliminating this mechanism by constructing rotating machines which operates both as motor machines (rotating thermal motors) and as working machines (pumps, fans, compressors).
Researches in the field of rotating machines extend in the sense that these machines transform a form of energy into another form of energy with minimal losses; in these machines there are no alternative rectilinear motion, there are no valves.
A more difficult problem is to produce a rotating machine that can be used as a working machine or a force machine, i.e. theoretically a "reversible" machine [1].
Such a type of machine must ensure:
- transforming the useful moment with minimal loss when operates as a working machine.
- the full use of the energy of the working agent to drive the shaft when it is working as a power machine.

The term "working machine" in the article title refers to the fact that this type of machine can function as a pump, fan, or low-pressure compressor, i.e. the machine can deliver liquids or gases with or without suspensions. In this paper, the operation of the working machine is analysed only as a volumetric pump with profiled rotors.

2. The construction solution and the operating principle of the rotating volumetric pump

The machine (fig.1) has two identical profiled rotors (2, 5) of special shape which rotate with the same speed within a case (1, 4). The synchronous rotation of the two rotors is provided by a cylindrical gear consisting of two inclined gearwheels located inside or outside the machine.
The gearwheels have the same division diameter and are mounted on shafts 7 and 9; it provide a rotational movement so that the rotating pistons (6) of the upper rotor penetrate into the cavities (10) of the lower rotor.

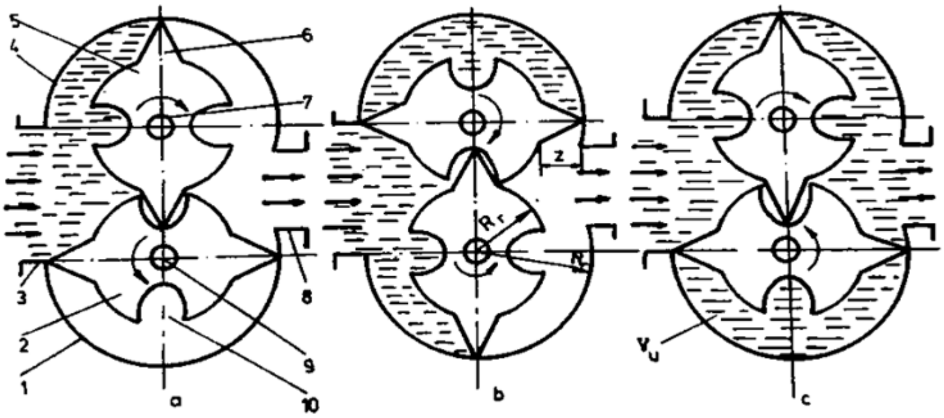

Fig. 1. The operating principle of the rotating volumetric machine
a,b, c, the rotors position after a 90° rotation
1- lower case; 2- lower rotor; 3-sucction chamber; 4- upper case; 5-upper rotor; 6- rotating piston; 7-driven shaft; 8- discharge chamber; 9-driving shaft; 10-cavity in which the upper rotor piston enters

From Figure 1 one can observe that at a 360° rotation of one of the shafts two such volumes will be transported from the suction to the discharge [2]:

$$V_u = \left(\pi \cdot R_c^2 - \pi \cdot R_r^2\right) \cdot l \; [m^3 / rot] \tag{1}$$

where: R_c- case radius [m]; R_r- rotor radius [m]; l- rotor length [m].
Replacing $R_c = R_r + z$, where z is the height of the rotating piston results:

$$V_u = \pi l z \cdot \left(2R_r + z\right) [m^3 / rot] \tag{2}$$

The volumetric flow rate of fluid delivered by a rotor will be:

$$\dot{V} = \pi \cdot l \cdot z\left(2R_r + z\right) \cdot \frac{n}{60} \left[m^3 / s\right] \tag{3}$$

where: n - machine speed [rot / min];
For the entire machine, which has two identical rotors, the flow rate will be:

$$\dot{V} = 2 \cdot \dot{V} = \pi \cdot l \cdot z\left(2R_r + z\right) \cdot \frac{n}{30} \left[m^3 / s\right] \tag{4}$$

The theoretical power required to drive the machine will be [2]:

$$P_m = \dot{V}_m \cdot \Delta p\left[W\right] \tag{5}$$

where: $\Delta p = p_r - p_a$ [N/m^2]
p_r-pressure to discharge; p_a - suction pressure.
From equation (4) one can observe that:
- the volumetric flow rate increases linearly with the rotor length, the rotor radius (l, R_r) and the speed (n);
- the volumetric flow rate increases with the square of the piston height (z).

From Figure 1 one can observe that the shape of the rotating piston also influences the volumetric flow rate through the value of V_u; the rotating piston may have the form of a triangle as in Figure 1 or may be curvilinear (Figure 2).

3. Analysis of the shape of the rotating piston

The rotating piston may be in the form of a blade (Figure 2.a), a triangle (Figure 2.b), or it may be curvilinear (Figure 2.c).

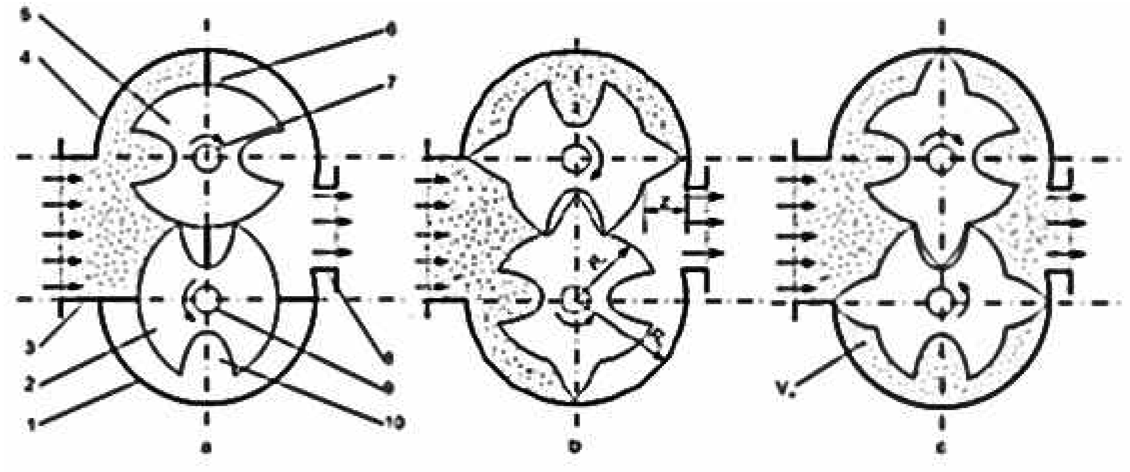

Fig. 2. Section through the rotating machine.
1- lower case; 2- lower rotor; 3-sucction chamber; 4- upper case; 5-upper rotor; 6- rotating piston; 7-driven shaft; 8- discharge chamber; 9-driving shaft; 10-cavity in which the upper rotor piston enters

Blade -type pistons do not withstand high working pressures, therefore, in the analysis of the shape of the rotating piston, the triangular and curvilinear pistons are more robust [3].
Figure 3 shows a section through a portion of the upper rotor in which a triangular piston is attached; with dashed line the curvilinear piston is drawn.
The figure shows that the area of the curvilinear piston section is greater than the area of the triangular piston; as a result, there will be a difference in the flow rate from the rotating machine.
The main dimensions of the profiled rotors are (Figure 3):
- Rotor radius: R_r = 50mm;
- Height of the rotating piston: z = 30mm;
- Case radius: R_c = 80mm;
- Rotor length: l = 50mm;
- Diameter of the driven shaft on the rotor mounting area: d = 30mm.

In rotational motion, the pistons of a rotor penetrate into the adjacent rotor cavities.
Both rotating pistons and cavities have a special shape determined on the basis of mathematical equations; these equations have been established by the research team as a result of numerous efforts.
Based on these equations, the profile contour coordinates were established in the xOy axis system; this allows the construction of rotors on C.N.C.

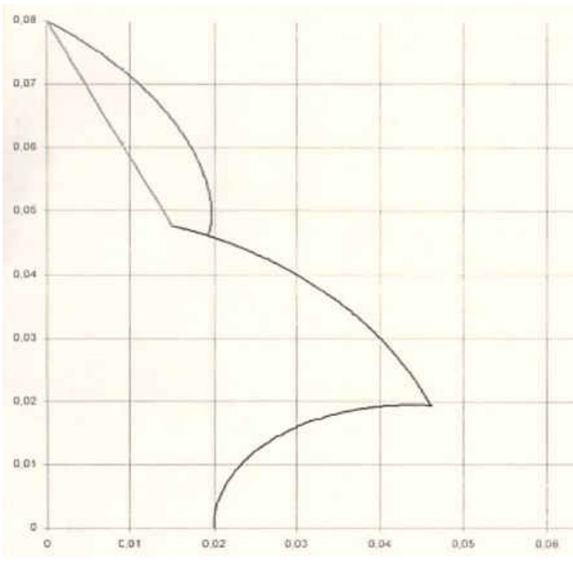

Fig. 3. The contour of a piston quarter

Figure 3 shows the contour of a piston quarter in both studied versions:
A. Triangular profile;
B. Curvilinear profile;

4. Computation of the section area of the triangular and curvilinear piston

In order to establish the rotor contour, a series of different mathematical relations were developed on the three rotor portions (Figure 4):
- contour of the curvilinear piston (A, B)
- the contour of the circular portion (B, C)
- the outline of the cavity in the rotor (C, D)

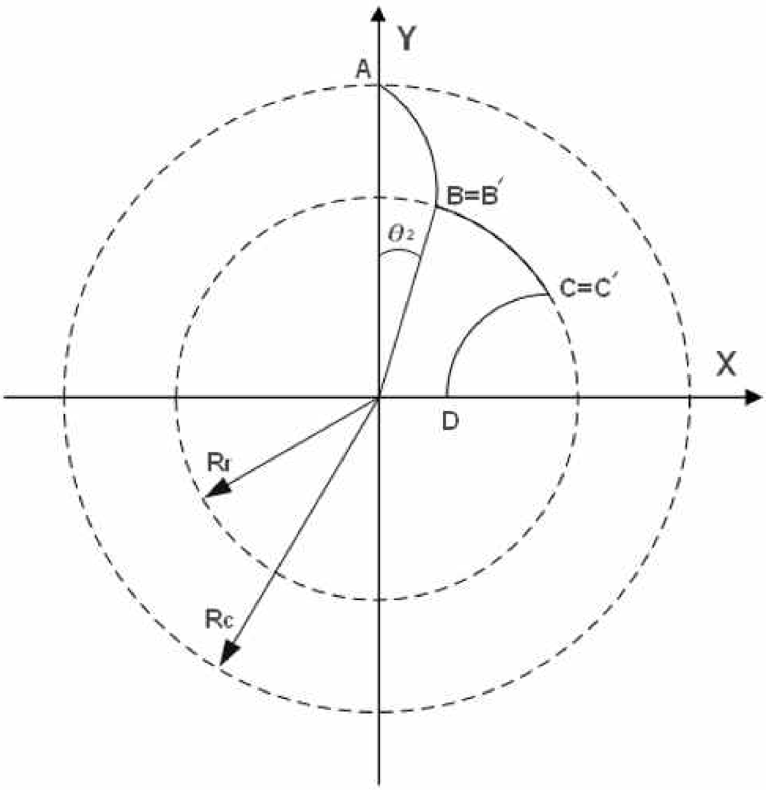

Fig. 4. Computing notations

A computational program [4] [5] was developed, resulting the coordinates (x_i y_i) of the curvilinear piston contour.
Data calculated in meters with an accuracy of five decimal are specified in Table 1.

Table 1: Calculated data

No.	x	y	No.	x	y	No.	x	y
1(A)	0,00	0,08	42	0,01684	0,06112	83	0,01967	0,04793
2	0.00049	0,07964	43	0,01704	0,06069	84	0,01956	0,04776
3	0,00111	0,07921	44	0,01723	0,06026	85	0,01963	0,04761
4	0,00172	0,07876	45	0,01742	0,05984	86	0,01961	0,04746
5	0,00232	0,07832	46	0,01759	0,05942	87	0,01959	0,04732
6	0,00291	0,07787	47	0,01776	0,059	88	0,01956	0,04719
7	0,00349	0,07742	48	0,01792	0,05859	89	0,01954	0,04707

8	0,00406	0,07696	49	0,01807	0,05818	90	0,01952	0,04695
9	0,00461	0,0765	50	0,01821	0,05778	91	0,0195	0,04684
10	0,00516	0,07604	51	0,01835	0,05739	92	0,01947	0,04674
11	0,00569	0,07558	52	0,01848	0,057	93	0,01945	0,04665
12	0,00621	0,07511	53	0,0186	0,05661	94	0,01943	0,04657
13	0,00672	0,07464	54	0,01871	0,05623	95	0,01941	0,04649
14	0,00722	0,07417	55	0,01882	0,05586	96	0,01939	0,04642
15	0,00771	0,0737	56	0,01892	0,05549	97	0,01937	0,04636
16	0,00818	0,07323	57	0,01901	0,05513	98	0,01936	0,0463
17	0,00865	0,07275	58	0,0191	0,05477	99	0,01934	0,04626
18	0,0091	0,07228	59	0,01918	0,05442	100	0,01933	0,04622
19	0,00954	0,0718	60	0,01925	0,05408	101	0,01932	0,04618
20	0,00998	0,07132	61	0,01932	0,05374	102	0,01931	0,04616
21	0,0104	0,07085	62	0,01938	0,05341	103	0,01930	0,04614
22	0,01081	0,07037	63	0,01944	0,05308	104(B)	0,01929	0,04613
23	0,01121	0,06989	64	0,01949	0,05277			
24	0,01159	0,06942	65	0,01954	0,05246			
25	0,01197	0,06894	66	0,01958	0,05215			
26	0,01234	0,06846	67	0,01965	0,05156			
27	0,01269	0,06799	68	0,01967	0,05128			
28	0,01304	0,06752	69	0,0197	0,051			
29	0,01338	0,06704	70	0,01971	0,05074			
30	0,0137	0,06657	71	0,01973	0,05047			
31	0,01402	0,06611	72	0,01974	0,05022			
32	0,01432	0,06564	73	0,01975	0,04997			
33	0,01462	0,06518	74	0,01975	0,04974			
34	0,0149	0,06471	75	0,01975	0,0495			
35	0,01518	0,06425	76	0,01975	0,04928			
36	0,01544	0,0638	77	0,01974	0,04906			
37	0,0157	0,06334	78	0,01974	0,04885			
38	0,01595	0,06289	79	0,01973	0,04865			
39	0,01618	0,06244	80	0,01972	0,04846			
40	0,01641	0,062	81	0,0197	0,04827			
41	0,01663	0,06156	82	0,01969	0,0481			

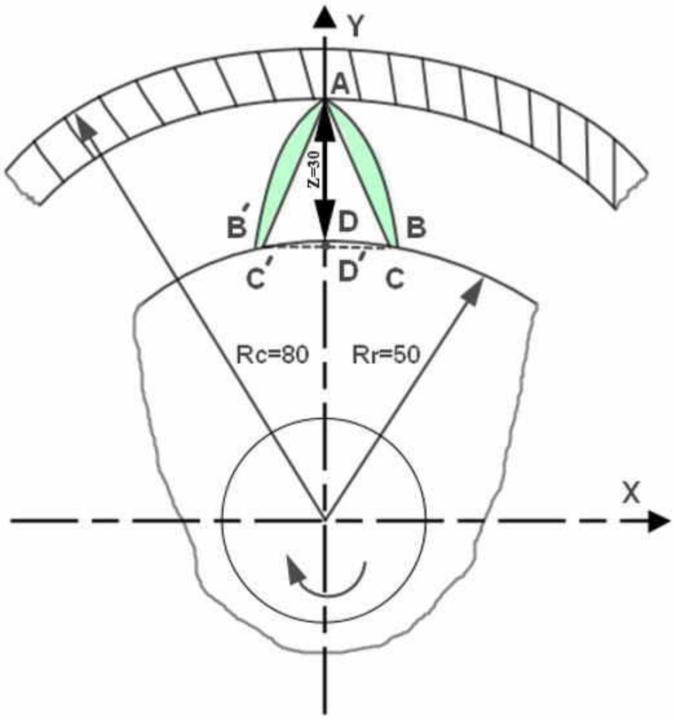

Fig. 5. Computing notations

For triangular piston:
A (x = 0; y = 80)
C (x = 15.8; y = 47.64); C '(x = -15.8; y = 47.64)
For the curvilinear piston:
A (x = 0; y = 80)
B (x = 19.29; y = 46.13); B '(x = -19.29; y = 46.13)
R_c - case radius: R_c = 80 mm
R_r - rotor radius: R_r = 50 mm
z - piston height: z = 30 mm
• For the triangular piston, approximating the BB 'circular arc with a straight line, the section area will be [6][7]:

$$A_{tr} = \frac{BB' \cdot AD}{2} = \frac{31.6 \cdot 30}{2} = 474 \left[mm^2\right] \tag{6}$$

• For the curvilinear plunger, in a first approximation, it is considered as an C'AC triangle of area:

$$A_{curb} = \frac{CC' \cdot AD}{2} = \frac{38.58 \cdot 33.87}{2} = 653.35 \left[mm^2\right] \tag{7}$$

CC' = 38 .58 mm; AD= 80-46.13=33.87 mm^2
The difference between the two areas is:

$$A_{curb} - A_{tr} = 653.35 – 474 = 179.35 \text{ mm}^2$$

If the piston has a length of 50 mm, the volume difference between the pistons will be:

$$\Delta V_1 = 1 (A_{curb} - A_{tr}) = 50 (179.35) = 8967.61 \text{ mm}^3$$

This difference occurs for a rotor rotation of 180^0; for a complete rotation:

$$\Delta V_1 = 28967.61 = 17935.23 \text{ mm}^3\text{/ rot}$$

$$\Delta V_1 = 0.017935 \text{ m}^3\text{/ rot}$$

For a more accurate calculation of the section area of the curvilinear piston, the "trapezoidal method" mathematical analysis is used.
The calculation points in Table 2 are chosen for 0,10,20,30 ...... 100,104 and shall be calculated as follows:

$$A_{20-30} = \frac{9.98 + 13.70}{2}\left(7.18 - 6.65 \right) = 62.75 \left[mm^2 \right] \quad (8)$$

Table 2: Calculation points

$A_{0,10}$	$A_{10,20}$	A_{20-30}	A_{30-40}	A_{40-50}	A_{50-60}	A_{60-70}	A_{70-80}	A_{80-90}	A_{90-100}	$A_{100-104}$
10.32	31.79	62.75	67.72	73.04	70.05	65. 06	39.02	29.62	14.17	1.73

TOTAL: A = 465.27 mm^2, for 1/2 for the area of the curvilinear piston.

$$A_{curb} = 2 \cdot 465.27 = 930.54 \text{ mm}^2$$

A difference in area of:

$$\Delta A = 930.54 - 474 = 456.54 \text{ mm}^2$$

$$\Delta V_2 = \Delta A \cdot l = 456{,}54 \cdot 50 = 22827 \text{ mm}^2/\text{rot}$$

$$\Delta V_2 = 0.0228 \text{ m}^3/\text{rot}$$

5. Conclusions

From the above calculations, the versions of the rotating piston used to increase the flow rate of the fluid are:

- $\Delta V_2 > \Delta V_1$
- Curved piston rotor
- Triangular piston rotor
- A blade type piston rotor

The advantages of this new type of machine are:

a. The construction solution can be made as follows:

- As working machine: pump, fan, blower;
- As a power machine: steam or combustion engine, pneumatic engine, hydrostatic engine.

b. When operating as a pump, this solution eliminates the disadvantages of other types of rotating pumps (gearwheels, pallet) in which the conveyed fluid must be free of solid particles; this type of rotating volumetric pump has no valves and can be used for the following fluids: with impurities, viscous fluids, rheological fluids, wastewater.

c. The rotating machine construction solution allows its use as a fan or blower for the transport of dry or wet gases.

d. Used as a blower this machine is more advantageous than the Roots compressor.

References

[1] Băran, Nicolae, Petre Răducanu et al. *Bazele termodinamicii tehnice, vol.3, Termodinamică tehnică*. Bucharest, Politehnica Press Publishing House, 2010.

[2] Motorga, Alin. *Influența parametrilor constructivi și funcționali asupra performanțelor mașinilor rotative cu rotoare profilate*. PhD thesis, Faculty of Mechanical Engineering and Mechatronics, Politehnica University of Bucharest, 2011.

[3] Băran, Nicolae, Antonios Detzortzis, and Maria Bărăscu. "Influence of the rotor shape on the flow rate transported by a machine with profiled rotors." *Termotehnica* 16, no.1 (2012): 89-94.

[4] Pătulea, Alexandru. *Influența parametrilor funcționali și a arhitecturii generatoarelor de bule fine asupra eficienței instalațiilor aerare*. PhD thesis, Politehnica University of Bucharest, 2009.

[5] Detzortzis, Antonios. *Influența arhitecturii rotoarelor asupra performanțelor compresoarelor volumice cu rotoare profilate*. PhD thesis, Politehnica University of Bucharest, 2014.

[6] Exarhu, Mihai. *Mașini și instalații hidraulice și pneumatice*. Bucharest, Andor Tipo S.R.L. Publishing House, 2006.

[7] Țurcanu, C., N. Ganea. *Pompe volumice pentru lichide*. Bucharest, Technical Publishing House, 1987.

Technological and Constructive Considerations on the Realization of Components and Parts Using 3D Printing FDM-Type Technology

Assist.Prof. PhD.Eng.Ec. **Mircea Dorin VASILESCU**[1]

[1] POLITEHNICA University Timisoara, mircea.vasilescu@upt.ro

Abstract: *The work is addressed both the constructive considerations and the analysis of specific deformations generated by gaseous or liquid medium on specific components of the pneumatic or hydraulic installation. The work is structured on several part that addresses at first the general considerations after that considerations for classifying the analysed components and at the end of the generation, realization of components through 3D printing and final the analysed of constructive elements generated to the medium used for functional activity. The analysis of the material behaviour on requests from an effective point of view will be the subject of a subsequent work, starting from the considerations of analysing deformations and modifying the structure and shape of components based on the elements observed where this is required.*

Keywords: *Repair, 3D printing, hydraulic/pneumatic, constructive modelling*

1. Introduction

In this paper there was conducted a study on the possibilities of replacement of components or assemblies used in hydraulic/pneumatic installations with components made by generation methods of 3D printing FDM system. Both parts of a hydraulic/pneumatic installation and sub-assemblies, which may be replaced by a single component, shall be concerned with the improvement of both the technological precision of the component, but also the provision of a component with a much better structure than that of the assembly achieved by conventional technological processes. At the same time by using the 3D printing technology, the old parts or assemblies, obtained with polluting technologies, are replaced with some at which the generating part is clean, the energy consumption is reduced and the costs of regenerating the parts, or smaller sub-assemblies than those obtained by more polluting traditional technologies [1]. For example, we will take a component of a hydraulic/pneumatic made of aluminium or cast iron, two types of polluting materials both in the raw material, but also in the phase of realization itself, through the technological methods of casting. If the same milestone is achieved through 3D printing through the FDM method with PLA material, we can see the following. The PLA is a material with mechanical properties is like those of aluminium to compression [2, 3]. It can also be observed that FDM as a material generation technology that is a method that does not pollute the environment, being the lowest degree of volatile particles emitted in the workspace relative to other 3D printing technologies.

It can also be observed that for replacing the aluminium or cast iron, with another aluminium or cast iron or with the same marker, we can have the following solutions:

- technological variant welding for repair, relatively polluting method;
- recycle of melting and casting, method also polluting.

For the FDM case, the marker is broken into pieces with a tooth mill, a method with a low level of pollution, is introduced in a proportion of 50% new material and reused and the creation of a new files, with which the new part will be achieved through the process called FFF method the same unpolluting method.

If the comparison is made at the level of the cost of realisation only if we are to consider the costs of achieving the melting of aluminium minimum 700 degrees Celsius, with the plasticizing of the PLA maxim 220 degrees Celsius, we will clearly realize the advantages FDM technology.

The achievement of 3D printed parts is ensured by its variants, which are numbering five type [4] and involving lower or higher output costs [3] primarily dependent on the raw material used in the performance of the 3D printed component, but also by how to achieve printing so the technology used.

It should be noted that by any of the five solutions, the obtaining of components can be made technologically efficient, with reduced manufacturing costs, low energy consumption and not least with the use of renewable materials and/or biodegradable. Some of these technologies because they use size particles of the order of tens or hundreds of microns and can produce particulate matter and thereby pollution of the working space.

2. Classification of types of hydraulic/pneumatic components from a dimensional and functional point of view

A hydraulic/pneumatic installation can be distinguished, the existence of several types of components, which may be demanded from the point of view of static but also dynamic applications. We can thus classify them:

- part with functional or no functional or positional and unsolicited role;
- functional parts which are little requested, and which do not encounter in contact with the pressure environment;
- functional parts that encounter with the pressure environment and are required by it.

A few of these parts are presented in the paper and a brief analysis of their main characteristics is being made.

2.1 Part with functional or no functional or positional and unsolicited role

For their case, precision is the element that has an important role in constructive and functional terms. Precision is provided by the 3D printing technology by making dimensional corrections at the level of the quotas that must ensure the required dimensional precision. At the same time, depending on the orientation of the usual static and wear of the surface, the structure used is for printing with a heterogeneous or homogeneous component, with a lower or higher density of the 3D printed interior structure. From among these elements, the coupling elements of the ducts must be presented to the components of the hydraulic or pneumatic circuit of the type coupling part (Figure 1).

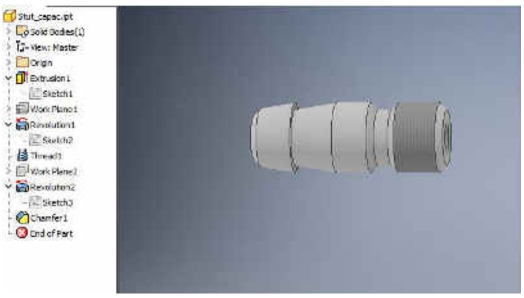

Fig. 1. Coupling pneumatic/hydraulic part 4 mm inner diameter at left and ring for pneumatic/hydraulic sealing at right

For the coupling part case, a FEA modeling was made using the inner-specific load of the central tube with a pressure of 10 MPa and the threaded side and the surfaces that is in contact with the connection tube were loaded with a pressure of 1 MPa (Figure 2). From the analysis for compressed air pressure the requests are small deformities being insignificant by the order of micron. For higher hydraulic pressures of order 10 MPa the deformations become larger and, in some areas, approaching the limit resistance of the material. It should be noted that due to the specificity of the material and the mode of generation FEA modeling must be accompanied by the mechanical test to validate the model.

The 3D modeled part is saved in STL format and is then processed to generate layers and numerical command. Great importance in the process of made the part that is subject to the process of generating the numerical command, is the verification from several viewpoints of the STL part generated.

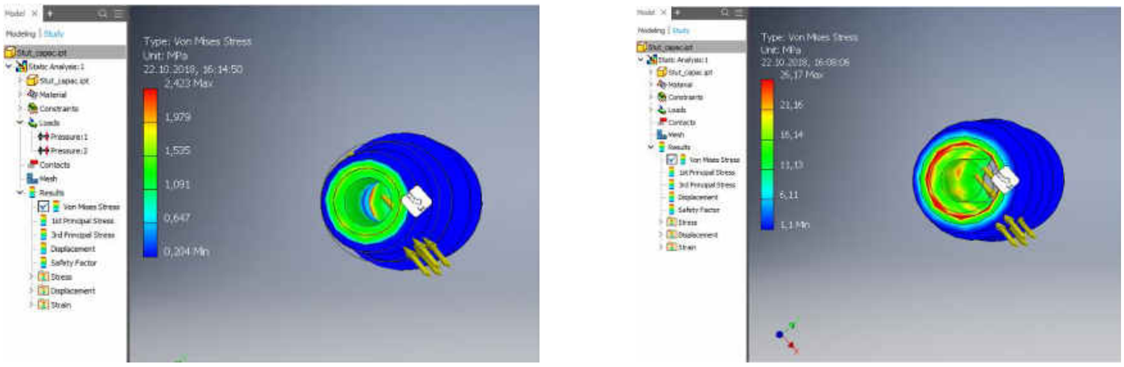

Fig. 2. Coupling pneumatic 1 MPa left / hydraulic 10 MPa right part 4 mm inner diameter

It must be shown at this point that there are two important phases. The first is related to the implementation of the STL file which must respect both the dimensional conditions and the resolution of the implementation of the STL generation of the triangle generated. The second is the verification of how to generate are and correct the errors.
The generation of the part was carried out with the Fabrikator Mini printer, which provides the processing of part with the size of 80 mm^3 and to which the program for generating is Cura for layers generation and under Repetiter Host was used for generation of them. It should be noted that both previously mentioned programs are of FREE type. In (Figure 3) you can see the settings for generation and on the right side of generation with the generation of 1 minute and 1 second, with a thread length of 1 metre and a number of layers of 2 pieces. The track generated can be seen in (Figure 4).

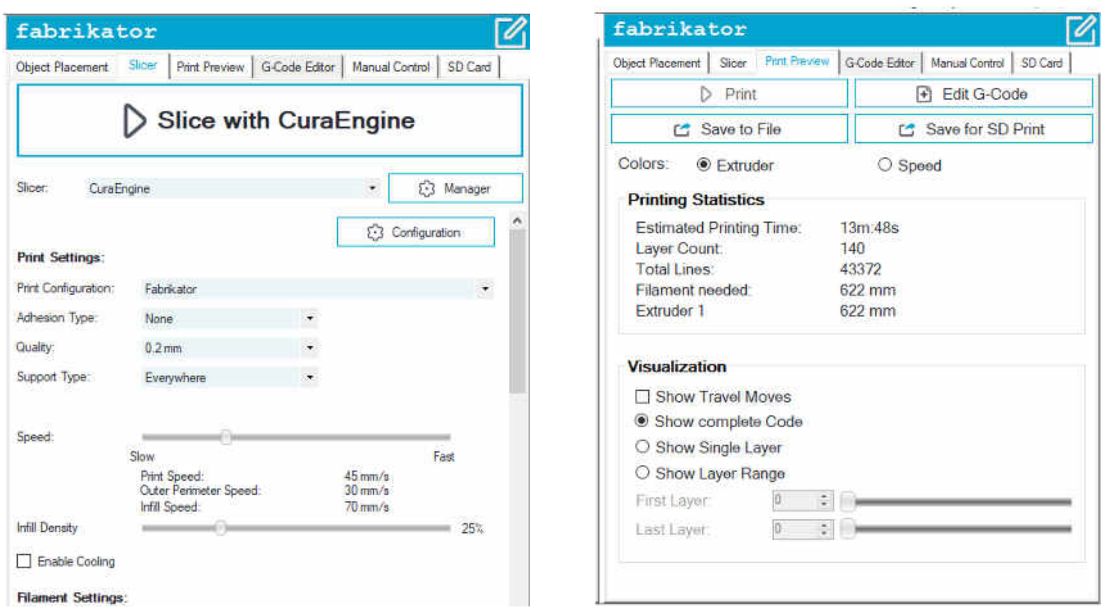

Fig. 3. Coupling pneumatic slice generated parameter at left and printing statistic at right

It can therefore be concluded that for parts without a functional role the realization through this process is very good at low pressures and satisfactory at high pressures, where it begins to be recommended to use the achievement of parts through the processes of 3D printing SLS.

2.2 Functional parts that are low in demand and do not encounter the pressure medium

This type of components is those that are medium requested, but that do not come or come into direct contact with the hydraulic or pneumatic medium. For these components function the interconnection mode with the other components, an important role has both the dimensional component for the achievement of the games and/or centres and the tightening of the conjugated components, but also the direction and the way in which forces appear at surface level and in the structure of 3D printed components. The major advantage of 3D printing from other materials processing technologies through traditional procedures is given by the fact that it allows for the replacement of several components made by traditional technological methods, with a single component, achieved through 3D printing.

Fig. 4. Coupling pneumatic at left and printing statistic at right generated by FDM 3D printing solution

One of the elements which is in this category is the cap of the body of a cylinder for a hydraulic or pneumatic installation (Figure 5) shall be presented from among these items. The generation of both components was carried out in the INVENTOR in the light of their functional role.

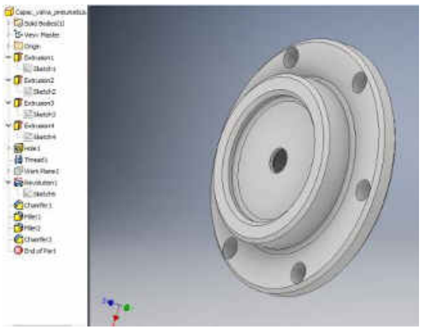

Fig. 5. Cap of a cylinder for a hydraulic or pneumatic installation

It must be shown at this point that there are two important phases. The first is related to the implementation of the STL file which must respect both the dimensional conditions and the resolution of the implementation of the STL generation of the triangle generated. The second is the verification of how to generate are and correct the errors.

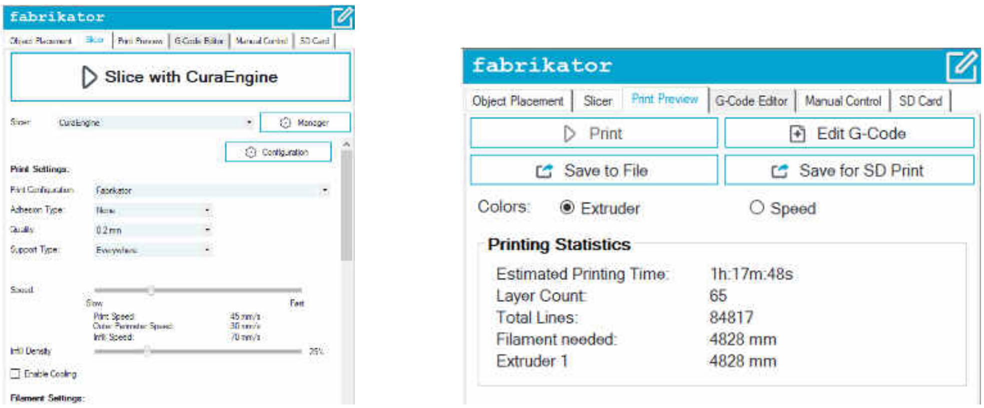

Fig. 6. Cap of a cylinder for a hydraulic or pneumatic installation slice generated parameter

The generation of the part was carried out with the Fabrikator Mini printer, which provides the processing of part with the size of 80 mm^3 and to which the program for generating is Cura for layers generation and under Repetiter Host was used for generation of them. It should be noted that both previously mentioned programs are of FREE type. In (Figure 5) you can see the settings for generation and on the right side of component for one of this elements. The track generated can be seen in (Figure 7).
The 3D modeled part is saved in STL format and is then processed to generate layers and numerical command. Great importance in the process of made the part that is subject to the process of generating the numerical command, is the verification from several viewpoints of the STL part generated.

Fig. 7. Cap of a cylinder for a hydraulic or pneumatic installation slice generated parameter

To solve the modelling problem with the finite element was defined in the program INVENTOR 2019 educational variant. The material from which the part was made is the PLA [5] to which the resistance characteristics have been considered (Figure 8).

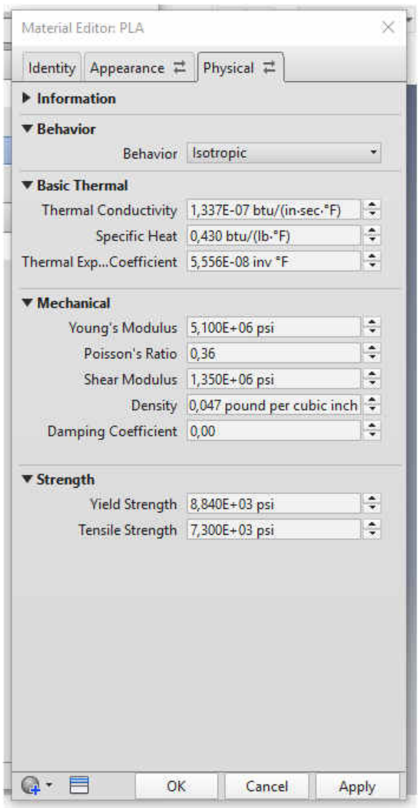

Fig. 8. Cap of a cylinder for a hydraulic or pneumatic installation PLA definition characteristics

For the cap of a cylinder, a FEA modeling was made using the frontal load force with a pressure of 1 MPa or 10 MPa and fixed part of the orifice (Figure 9). From the analysis for compressed air pressure the requests are small deformities being insignificant by the order of micron. For higher hydraulic pressures of order 10 MPa the deformations become larger and, in some areas, approaching the limit resistance of the material. It should be noted that due to the specificity of the material and the mode of generation FEA modeling must be accompanied by the mechanical test to validate the model.

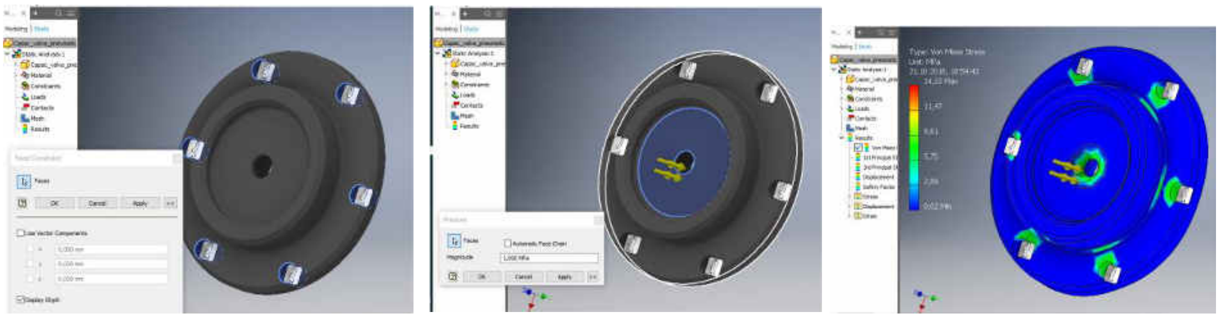

Fig. 9. Cap of a cylinder for a hydraulic or pneumatic installation PLA load force, fixed point and deformation

The numerical value of the FEA modelling it is presented in (Figure 10). At left for 1 MPa and at right for 10 MPa. The displacement is 2 microns for small pressure and 20 microns for medium pressure.

⊟ **Result Summary**

Name	Minimum	Maximum
Volume	20519,6 mm^3	
Mass	0,0266781 kg	
Von Mises Stress	0,0244432 MPa	14,3325 MPa
1st Principal Stress	-6,83642 MPa	16,8795 MPa
3rd Principal Stress	-22,6833 MPa	5,89777 MPa
Displacement	0 mm	0,0048324 mm
Safety Factor	4,25253 ul	15 ul
Stress XX	-19,6933 MPa	14,7601 MPa
Stress XY	-5,68141 MPa	4,79292 MPa
Stress XZ	-5,33529 MPa	5,29277 MPa
Stress YY	-17,1446 MPa	12,604 MPa
Stress YZ	-4,78528 MPa	4,79641 MPa
Stress ZZ	-10,6271 MPa	8,19982 MPa
X Displacement	-0,00105085 mm	0,00104971 mm
Y Displacement	-0,00109794 mm	0,00110114 mm
Z Displacement	-0,0047991 mm	0,000140194 mm
Equivalent Strain	0,000000634278 ul	0,000399103 ul
1st Principal Strain	0,000000315894 ul	0,000335701 ul
3rd Principal Strain	-0,000466294 ul	-0,000000413172 ul
Strain XX	-0,00035065 ul	0,000253731 ul
Strain XY	-0,000219738 ul	0,000185374 ul
Strain XZ	-0,000206351 ul	0,000204707 ul
Strain YY	-0,000351884 ul	0,000257688 ul
Strain YZ	-0,000185079 ul	0,000185509 ul
Strain ZZ	-0,000138585 ul	0,000172857 ul

⊟ **Result Summary**

Name	Minimum	Maximum
Volume	20519,6 mm^3	
Mass	0,0266781 kg	
Von Mises Stress	0,244432 MPa	143,325 MPa
1st Principal Stress	-68,3642 MPa	168,795 MPa
3rd Principal Stress	-226,833 MPa	58,9777 MPa
Displacement	0 mm	0,048324 mm
Safety Factor	0,425253 ul	15 ul
Stress XX	-196,933 MPa	147,601 MPa
Stress XY	-56,8141 MPa	47,9292 MPa
Stress XZ	-53,3529 MPa	52,9277 MPa
Stress YY	-171,446 MPa	126,04 MPa
Stress YZ	-47,8528 MPa	47,9641 MPa
Stress ZZ	-106,271 MPa	81,9982 MPa
X Displacement	-0,0105085 mm	0,0104971 mm
Y Displacement	-0,0109794 mm	0,0110114 mm
Z Displacement	-0,047991 mm	0,00140194 mm
Equivalent Strain	0,00000634278 ul	0,00399103 ul
1st Principal Strain	0,00000315894 ul	0,00335701 ul
3rd Principal Strain	-0,00466294 ul	-0,00000413172 ul
Strain XX	-0,0035065 ul	0,00253731 ul
Strain XY	-0,00219738 ul	0,00185374 ul
Strain XZ	-0,00206351 ul	0,00204707 ul
Strain YY	-0,00351884 ul	0,00257688 ul
Strain YZ	-0,00185079 ul	0,00185509 ul
Strain ZZ	-0,00138585 ul	0,00172857 ul

Fig. 10. Cap of a cylinder for a hydraulic or pneumatic installation displacement and stress value

It can therefore be concluded that for parts with a functional role the realization and contact with the medium through this process is good at low pressures and satisfactory at medium pressures, where it begins to be recommended to use the achievement of parts through the processes of 3D printing.

2.3 Parts with a functional role that encounter the pressure medium and are required by it

This type of components is those that are required by the active working environment at maximum values and come into direct contact with it. For these components function the interconnection

mode with the other components, an important role has both the dimensional component for the achievement of the games and/or centres and the tightening of the conjugated components, but also the direction and the way in which the applications appear at the surface level and in the structure of the 3D printed components.
The part it is the body of this cylinder (Figure 11). The generation of both components was carried out in the INVENTOR in the light of their functional role.

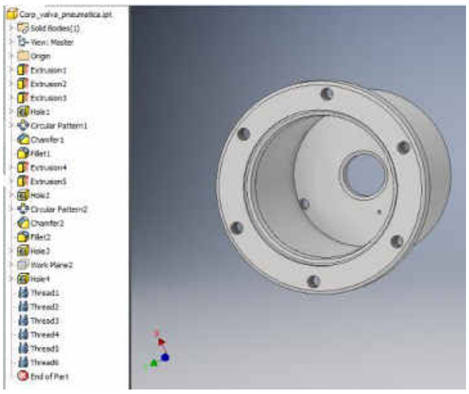

Fig. 11. Body of a cylinder generated in INVENTOR

The generation of the part was carried out with the Fabrikator Mini printer, which provides the processing of part with the size of 80 mm^3 and to which the program for generating is Cura for layers generation and under Repetiter Host was used for generation of them. It should be noted that both previously mentioned programs are of FREE type (Figure 12). In (Figure 13) can see the load for FEA model generation. At left fixed point and force load and on the right side the deformation for this elements.

Fig. 12. Body of a cylinder for a hydraulic or pneumatic installation 3D printed

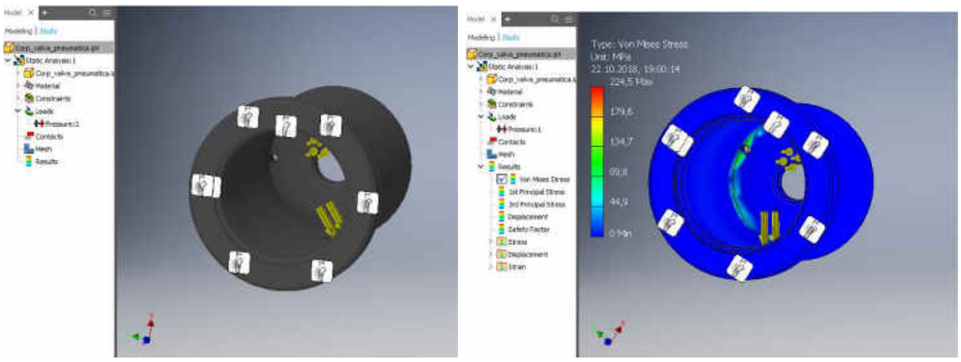

Fig. 13. Body of a cylinder for a hydraulic or pneumatic installation load for FEA modeling

In view of the deformations that occur, the construction of the analysed element has been changed (Figure 14) and it has been concluded that without the use of metallic material solutions in the outer or inner area will not withstand the requests.

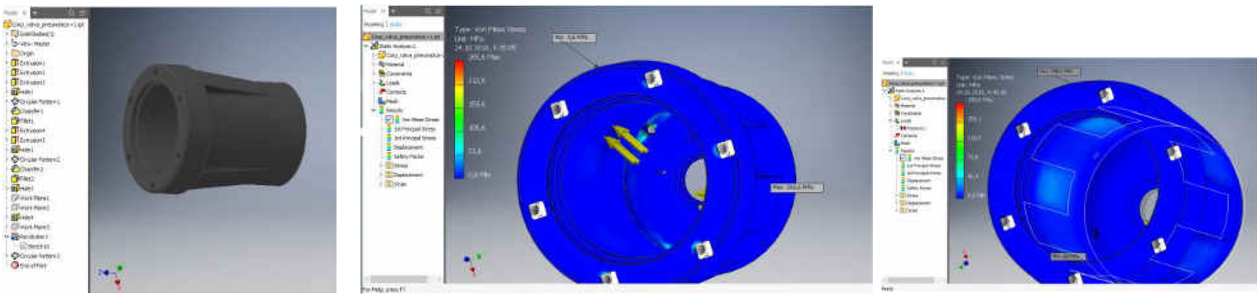

Fig. 14. Body of a cylinder modify for a hydraulic or pneumatic installation load for FEA modeling

It can therefore be concluded that for parts with a functional role for this construction is satisfactory for modified structure at low pressures and mot satisfactory at medium pressures, where it begins to be recommended to use the metallic part for construction of part made by 3D printing.

3. Conclusions

In view of the observations made at the end of each subchapter, it may be concluded that parts generated by 3D printing in hydraulic or pneumatic installations may be used in part. The research will continue with the achievement of the benchmarks according to the results recommendations and the attempt in their work process.

References

[1] ***. How green is 3D printing? --- for details, please see: http://www.ecosmagazine.com/print/EC13276.htm, accessed 09.2018.
[2] ***. 3D Printed Material Strength --- for details, please see: www.lifewire.com/3d-printed-material-strength-2230, accessed 09.2018.
[3] Vasilescu, Mircea Dorin, Tiberiu Aurel Vasilescu, Ioan Vasile Groza. “Economical Considerations over 3D Printing Components for Abrasive Water Jet Machinery.” *Advanced Materials Research*, ISSN: 1662-8985, Vol. 1146, pp 84-91, 2018 Trans Tech Publications, Switzerland.
[4] Vasilescu, Mircea Dorin, Ioan Vasile Groza. “Influence of technological parameters on the roughness and dimension of flat parts generated by FDM 3D printing.” *Nonconvențional Technologies Review*, 2017, 2359-8646, vol.3, 18-23 pag.
[5] ***. Polylactic Acid (PLA, Polylactide) --- for details, please see: https://www.makeitfrom.com/material-properties/Polylactic-Acid-PLA-Polylactide, accessed 09.2018.

Theoretical and Experimental Research on the Technological Process of Spraying and Dynamics of the Motorized Agricultural Platform

Ph.D Student Eng. **Polifron-Alexandru CHIRIȚĂ[1],** PhD. Eng. **Corneliu CRISTESCU[1],**
PhD. Eng. **Radu RĂDOI[1],** Assoc. Prof. PhD. Eng. **Oleg CIOBANU[2]**

[1] Hydraulics and Pneumatics Research Institute INOE 2000-IHP, Bucharest, Romania; chirita.ihp@fluidas.ro

[2] Technical University of Moldova

Abstract: *This article presents the results of a research developed by INOE2000 - IHP, as well as a functional model of a motorized agricultural platform used for spraying in horticulture. This is part of a complex crop monitoring system that, with the help of a quad-copter, generates a map that is used later for remote guiding of the agricultural platform, which is equipped with tracks system and a differential steering system allows it to turn in place or with a very small radius to track as accurately as possible the trajectory generated by the remote guidance system. The spraying equipment of this agricultural platform is designed to be used in a wide variety of horticultural crops with the ability to adjust both the direction and the spraying distance.*

Keywords: *Horticulture, remote spraying, motorized agricultural platform, hydraulic automation.*

1. Introduction

Nationally and internationally, there are a variety of spraying systems of different sizes, some worn/ pushed by humans, tractor, helicopter, airplane or self-propelled. In the world, there are many companies that produce and market, including in Romania [1], such as: ROYAL BRIKMAN, global specialist in horticulture, GREGSON-CLARK, focusing on high-quality sprinkler equipment in green industry, EMPAS, in horticulture spraying equipment, HYDRO SYSTEMS EUROPE with irrigation and horticultural applications, MARTIN LISHMAN Ltd and others [2,3,4]. Some of the machines produced by these companies are shown in Figure 1.

Fig. 1. Examples of spraying equipment available worldwide.

In the market of Romania, except those carried by humans, there are conventional sprayers. Generally large spraying sizes for large crops with high productivity, not fully satisfying market requirements, requiring medium-sized self-propelled machines that need small-scale SMEs in horticulture. Sprayed crops are sprayed using systems worn or towed by humans. In Romania there is no spraying technology and no specialized equipment. Recognizing this market failure, the beneficiary SME is requesting funding for this project, which will launch an innovative product based on new, productive and competitive technology, useful and necessary in horticulture in Romania.

The necessity and usefulness of spraying equipment is given by the modernization of the technologies for the realization of the horticultural works, but especially by the introduction of innovative equipment, ensuring both high productivity and quality food production, knowing that on the market, is an increasing demand for clean organic / ecological products to ensure healthy food for the population. One of the agricultural activities, which is quite frequent in the horticultural sectors, is the spraying of crops, both for outdoor purposes, but especially for crops growing in sheltered areas such as solariums, greenhouses, etc. At world level, there are particular concerns and achievements with regard to crop spraying equipment in the horticultural sectors. These equipment are very diverse in terms of how they are transported / brought to the place where the spraying is to be performed. These can be: manned equipment; equipment worn on tractors; trailed spraying equipment and self-levelling equipment. Worldwide there are airplane-mounted spraying equipment, helicopters even drone, which reacts the automatic sprinkling of crops located on designated stations.

2. Theoretical aspects of the spraying process

The nozzle spraying process is characterized, first of all, by the particle velocity and the spraying distance, under a certain working pressure and a given nozzle diameter.

For the mathematical modelling of the nozzle spraying process, a nozzle of diameter d, fed through a pipe of diameter D, with a flow Q, from a pump P, to the pressure p, controlled by means of a limiting valve SLP pressure. The nozzle of length h is horizontally stacked and spans, over a certain distance, on a trajectory considered to be a semi-parabola.

Figure 2 shows the physical modelling of the spraying process with specific main parameters, as well as the parabolic trajectory the water drops through.

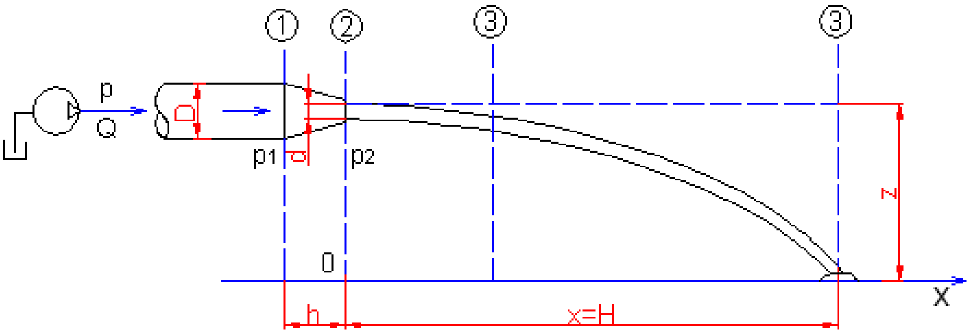

Fig. 2. Particle trajectory at spray nozzle

For the mathematical modelling of the spraying process, the BERNOULLI [5] equation used in points 1 and 2 above leads to equality (1):

$$z_1 \quad \frac{p_1}{\gamma} + \frac{V_1^2}{2g} = z_2 + \frac{p_2}{\gamma} + \frac{V_2^2}{2g} \tag{1}$$

Since the nozzle is horizontal, $z_1=z_2$ and the exit nozzle pressure is $p_2=p_a$, where p_a is the atmospheric pressure which is equal to 0 bar as real pressure. The relationship (2) is obtained:

$$\frac{p_1}{\gamma} + \frac{V_1^2}{2g} = 0 + \frac{V_2^2}{2g}, \tag{2}$$

Which allows the liquid velocity v_2 to be calculated at the outlet of the nozzle, with the relation (3):

$$V_2 = \sqrt{\frac{2}{\rho} \cdot p_1 + V_1^2} \tag{3}$$

To determine the maximum sprinkling distance, consider the equation of the classical parabola (4):

$$y = az^2 + bz + c \tag{4}$$

The shape of the liquid particle trajectory is represented by the positive part of the graph in Fig. 3.

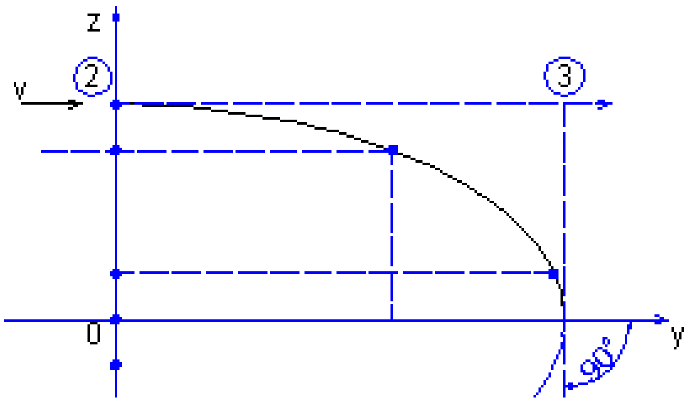

Fig. 3. The trajectory travelled by the liquid particle

It is believed that the nozzle is at a height sufficient for the particle to lose all the energy from the pressure even when it reaches the surface of the ground, and from this point the particle will fall vertically with the gravitational acceleration g. that the parabola is symmetrical with respect to the y-axis and the boundary conditions at points 2, where the velocity of the liquid particle is the velocity v_2 determined above, and in point 3 is null, the equation of the parabola of the form (5):

$$y = -\frac{g}{2} \cdot z^2 + y_{max} \tag{5}$$

Based on this equation, it is possible to determine the particle velocity of the liquid at each point of the trajectory and the maximum spraying distance, taking into account the actual nozzle height of the nozzle from the point 2 to point 0. The above, along with pipeline flows, are used to develop the numerical simulation model of the spraying process.

3. Numerical simulation of the spraying process

On the basis of the elaborated mathematical model, coupled with aspects of pipe pressure losses, a complex model [6] has been developed which has allowed a numerical simulation of the spraying system shown in Figure 4.

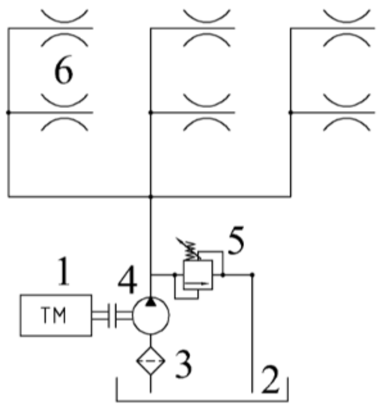

Fig. 4. Hydraulic scheme underlying the numerical simulation model
1 - thermal engine, 2 - tank, 3 - filter, 4 - hydraulic pump, 5 - pressure valve and 6 - spray nozzles.

Parameters of simulation and its results are presented in the graphs in the figures below.

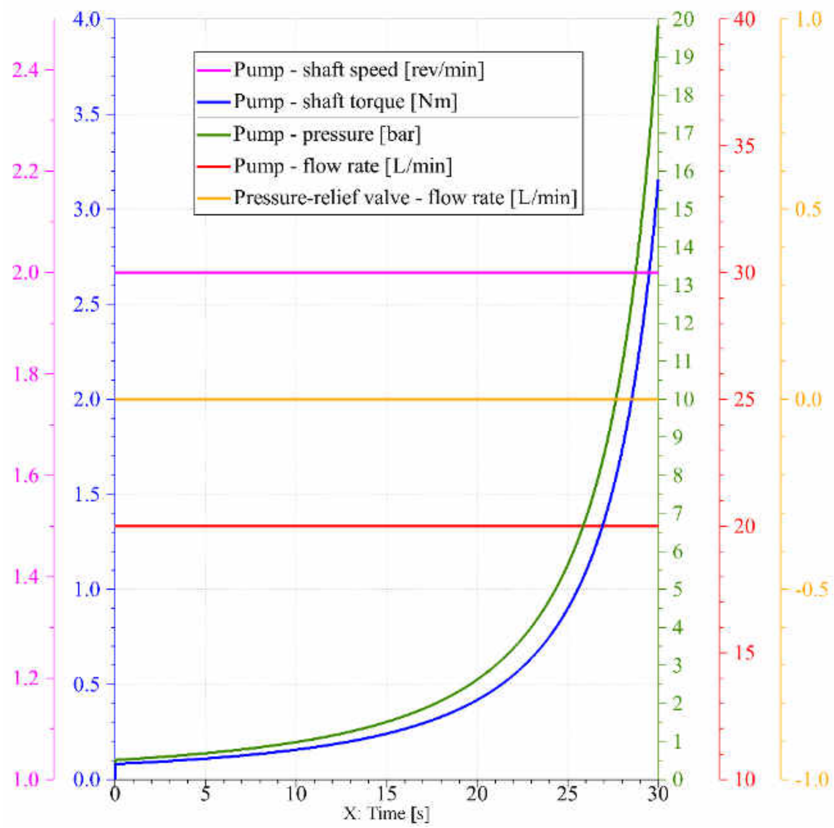

Fig. 5. Pump and pressure valve parameters.

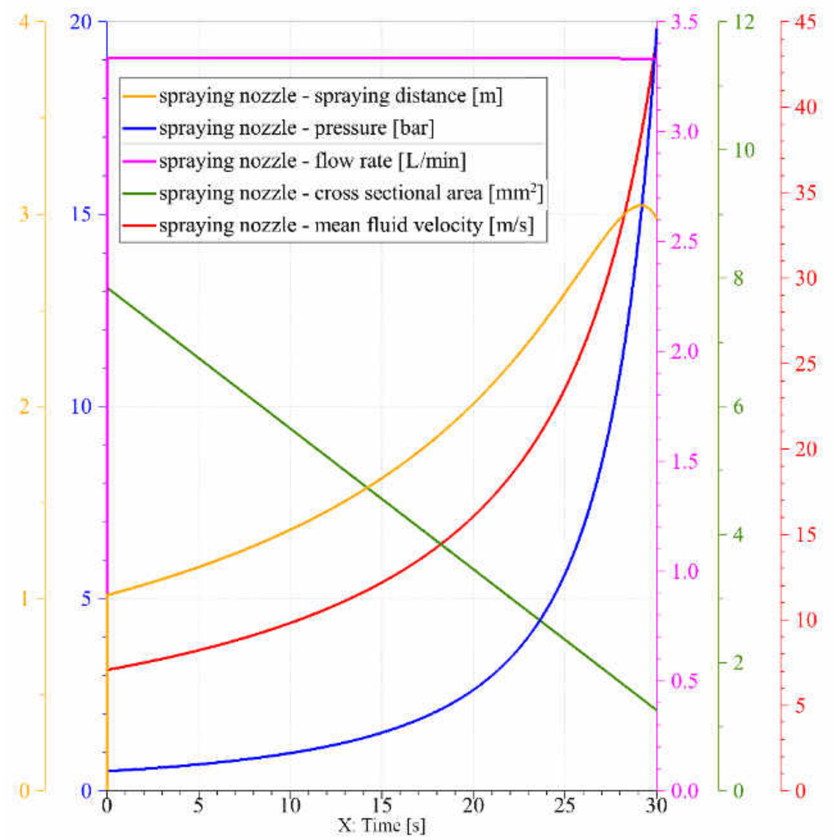

Fig. 6. Results of numerical simulation of nozzle parameters

This numerical simulation model allows optimization of the spraying process by choosing the nozzle dimensions correctly depending on the required performance. Figures 5 and 6 show the main parameters of the simulation, of interest being the variation in time of the spraying distance, which changes with the nozzle section variation.
The spraying distance can also be changed by adjusting the pressure by means of the pressure valve, but this adjustment is energy disadvantage because part of the flow will be transmitted to the tank passing through the pressure valve, resulting in a low energy efficiency.
In these graphs it can be seen that the constant parameters are: pump speed, pump flow rate, nozzle flow rate and flow through the pressure valve. The rest of the parameters vary over time because the diameter of the nozzle's changes from a maximum value to a minimum, which causes the values of the following parameters to increase: working pressure, fluid velocity, and last but not least the spraying distance ranging from 1 to 3 m. If the nozzle section decreases after a linear law, it can be noticed that the pressure increases exponentially and from a certain value of the nozzle section, the spraying distance is limited to a quasi-constant value. Lowering the section below this value should be avoided, as energy consumption increases substantially resulting in high energy consumption.

4. Brief presentation of the motorized agricultural platform

The conceptual model proposed for the motorized spraying platform is shown in Figure 7 below.

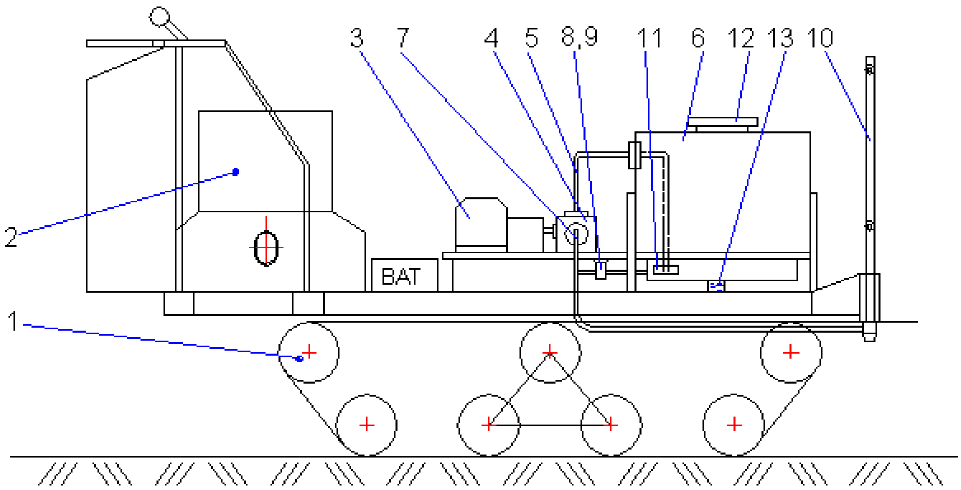

Fig. 7. Agricultural spraying platform

The conceptual model was conceived as a technical solution for long-distance spatial spraying, specific to crops and vines. The pattern is, in part, similar to the one above. It is also composed of a self-propelled platform on tracks (1), equipped with a thermal motor (2), which includes the fuel tank, the electric battery and a hydrostatic actuator, the thermal motor (3), the drive motor (4), the suction line (5), the liquid reservoir (6), the pressure relief pipe (7), the pressure limiting valve (8) and the return line (9) (10) whereby two spraying modes can be selected: spraying small plants when the dispenser arms are in the horizontal position or lateral spraying when the arms of the device are in the upright position. The machine is also provided at the end of the suction pipe with a corresponding filter (11), a visor cover (12) to the tank (6) and, of course, a drain plug (13) to the tank. As far as platform control is concerned, it is carried out manually as well as via distributors, and the levers can also be operated by means of servo-controls, which allow interfacing with the remote control / guidance system, which respond to the orders given by remote operator via a command console.

For the elaboration of the execution documentation, a 3D model was developed, as shown in Figure 8.

Fig. 8. The 3D model of the agricultural platform

The motorized agricultural platform has the possibility of spraying both the plants at the ground level as well as the trees or the vine, these can be achieved by placing the two spray arms vertically or horizontally, as shown in Figure 9.

Fig. 9. Physical realization of the agricultural platform

Technical characteristics and performance parameters of the agricultural platform:

- type of spraying: a) lateral, with vertical arms and b) horizontal;
- spraying distance .... max. 3 m;
- spray rate .... max.20 l / min;
- spraying pressure .... max. 20 bar;
- power of the spraying engine .... 1 kW;
- spraying capability .... 100 l;
- displacement motor power .... 5.2 kW / 1800 rpm;
- travel speed .... 0 - 7 km / h:

5. Experimenting and functional testing of the product

After the complete assembly of the experimental model of spraying platform was carried out, a series of house samples were carried out, in INOE 2000-IHP, samples which were designed to carry out the displacement and operation commands, according to the technical documentation, as such as gear shifts and change of travel direction. These are shown in Figure 10.

Fig. 10. Experimentation at the institute

Following these homemade samples, the experimental model of the motorized agricultural platform was declared complete, suitable for functional testing under real working conditions. In order to perform functional testing in real working conditions (shown in Figure 12), the product has to be transported to a field with a suitable culture.

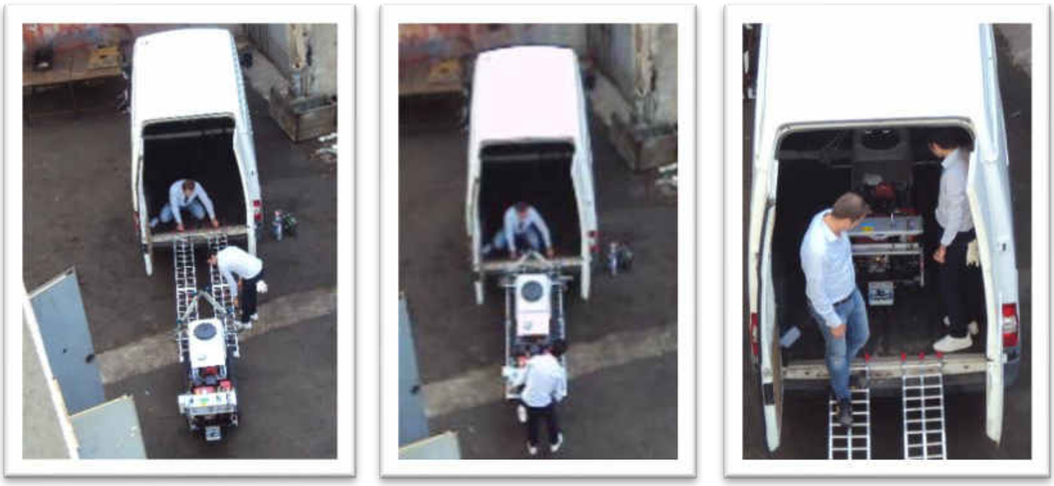

Fig. 11. Images from loading the product for transportation

Fig. 12. Functional testing in real working conditions

Functional testing of the experimental model of a spraying motorized agricultural platform was done under real working conditions on a land with a corresponding horticultural crop. Functional testing was done according to a procedure (scenario) established in the institute, in order to determine, experimentally, basic kinematic parameters and technological parameters.

The parameters to be determined are of two categories.
I. Kinematic (motion) parameters on 3 gears:
- the displacement speed, determined by integration of the acceleration;
- acceleration of the displacement, measured with the accelerometer;
- the distance travelled, determined by the integration of the speed and measured with the roulette.

II. Spraying technology parameters:
- workflow, measured with a flow-meter inserted on the tropics pump circuit.
- working pressure, adjusted to the valve and measured with an existing manometer;
- spraying distance, measured with roulette,

The following results were obtained after the functional test under the working conditions.
Measured kinematic parameters. When measuring the acceleration of movement with accelerometer and signal processing by simple integration for double speed and displacement was obtained graph in Figure 13.

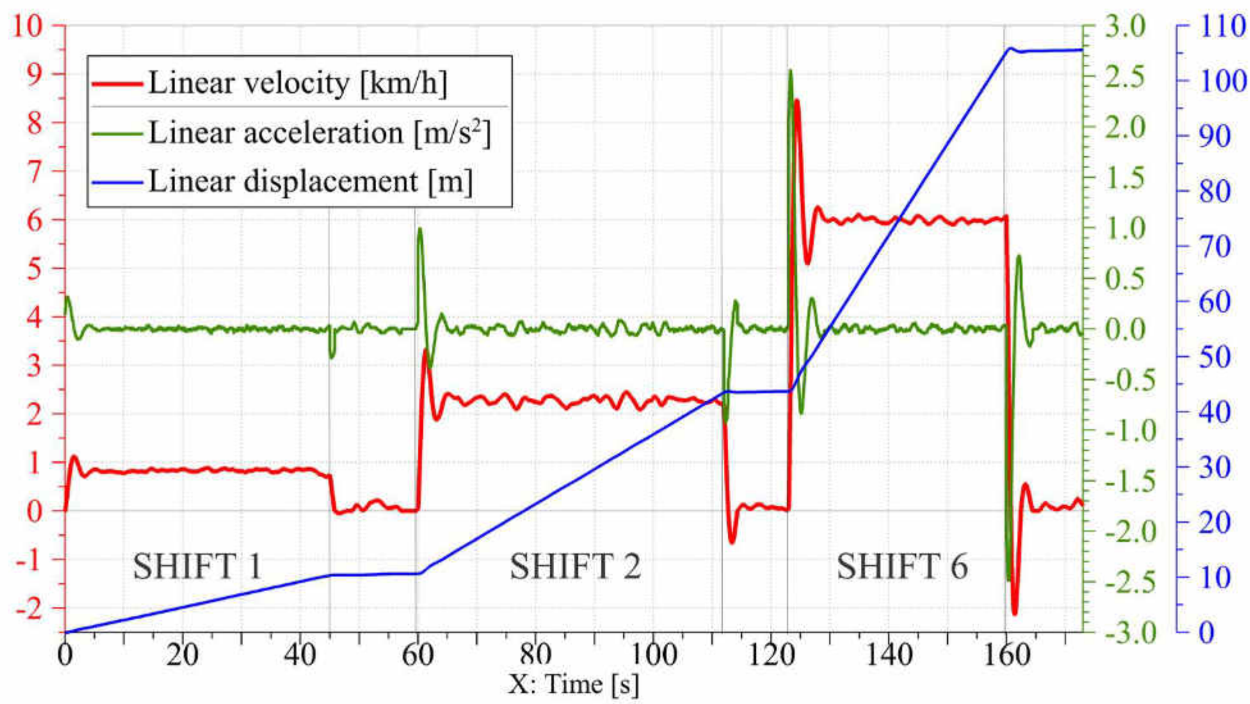

Fig. 13. Kinematic parameters

Table 1 below shows the measured spraying distances, as compared to numerical simulation, with the percentage differences being explicable and acceptable.

Table 1: Spraying technology parameters

Pressure [bar]	Flow [l/min]	Spraying distance [m]		Difference percentages [%]
		Numerical simulation	Measured	
5	20	1.0	0.8	25
10	20	2.0	1.8	11
20	20	Max. 3.2	3.0	7

6. Conclusions

Following the research project funded by the Innovation Checks Program, it can be concluded that this program is a generating program of progress, because these projects result in performing products with a high chance of being capitalized in the market economy.

Following technical documentation in the country and worldwide, on the achievements of machinery and equipment for spraying and / or spraying plants in the horticultural sector, the following conclusions were reached:

- Worldwide, modern wetting, spraying, spraying technologies have been developed to maintain, treat crops specific to the horticultural sector;

- In the world, a lot of types and sizes of spraying and spraying machines have developed;

- Such achievements are in the country, but in less diversity, but some are sold out;

- Following the documentation, two conceptual models were proposed, one with pneumatic spraying and one with hydraulic spraying, both mounted on track platforms.

- The experimental model of the motorized agricultural platform has both manual and remote controls and has undergone functional testing, both in the institute and in real field conditions, the technological results obtained being in full conformity with the technical documentation elaborated;

- The project was fully realized, all the activities and deliverables of the project being carried out in accordance with the project offer, all the status and progress indicators being achieved.

The project will be capitalized, following intensive marketing by the beneficiary SME, by developing a technical documentation for a prototype, in line with the concrete requirements of an interested customer in the market and then by introducing it into the manufacturing.
Although a conclusion may review the main points of the paper, do not replicate the abstract as the conclusion. A conclusion might elaborate on the importance of the work or suggest applications and extensions.

Acknowledgments

This paper has been developed in INOE2000-IHP, with the financial support of the Executive Unit for Financing Higher Education, Research, Development and Innovation (UEFISCDI), under PN III, Programme 2- Increasing the competitiveness of the Romanian economy through research, development and innovation, Sub-programme 2.1- Competitiveness through Research, Development and Innovation - Innovation Cheques, project title: "Development of a motorized agricultural platform used for spraying works with remote guiding automation system", Financial Agreement no. 259CI/2018.

References

[1] Dejeu, L., C. Petrescu, and A. Chira. *Horticultură şi protecţia mediului*. Bucureşti, Edit. Didactică şi Pedagogică R. A., 1997.
[2] Brumă, Ioan - Sebastian. *Tehnologii ecologice de întretinere a pomilor fructiferi*. Iași, Edit. Terra Nostra, 2004.
[3] Bălan, Viorica, L. Dejeu, A. Chira, and Ruxandra Ciofu. *Horticultura alternativă şi calitatea vieţii*. Bucureşti, Edit. G.N.P. Minischool, 2003.
[4] ***. "Tehnologii performante pentru tratamentele fitosanitare în vii și livezi." *Agro Business* (6 mai 2015). In: https://www.agro-business.ro/tehnologii-performante-pentru-tratamentele-fitosanitare-in-vii-si-livezi/2015/05/.
[5] Mecanica Fluidelor. Formule. In: http://www.e-formule.ro/wp-content/uploads/mecanica%20fluidelor.pdf.
[6] Anton, Viorica, Mircea Popoviciu, and Ioan Fitero. *Hidraulică şi Maşini hidraulice*. Bucureşti, Editura Didactică şi Pedagogică, 1978.

Optimizing Air Flow Instilled in an Aeration Pool

Prof.dr.eng. **Mariana PANAITESCU**[1], Prof.dr.eng. **Fănel-Viorel PANAITESCU**[2]

[1] Constanta Maritime University, panaitescumariana1@gmail.com

[2] Constanta Maritime University, viopanaitescu@yahoo.ro

Abstract: *The experiment is considering a case study for two municipal wastewater treatment plants that have been equipped with a new control system over a period of 10 months: 1) The experiment was carried out in parallel and the same conditions for water treatment on installation A and installation B, (experimental group) and 2) experiment on another pool with aeration controlled by the classic method (reference group). Both methods have been tested beforehand. Various cases have been studied during the experiment, corresponding to the main ways of controlling the aeration process. The values chosen for aeration control parameters are common values used in these cases.*

Keywords: *Flow, wastewater, treatment, plant, aeration, control, parameter, air, flow, algorithm.*

1. Introduction

The experiment has in mind a case study for two installations of municipal wastewater treatment plants which were equipped with a high-performance control system (experimental group) (Figure 1) [1]. The experiment was carried out over a period of 10 months, as follows:

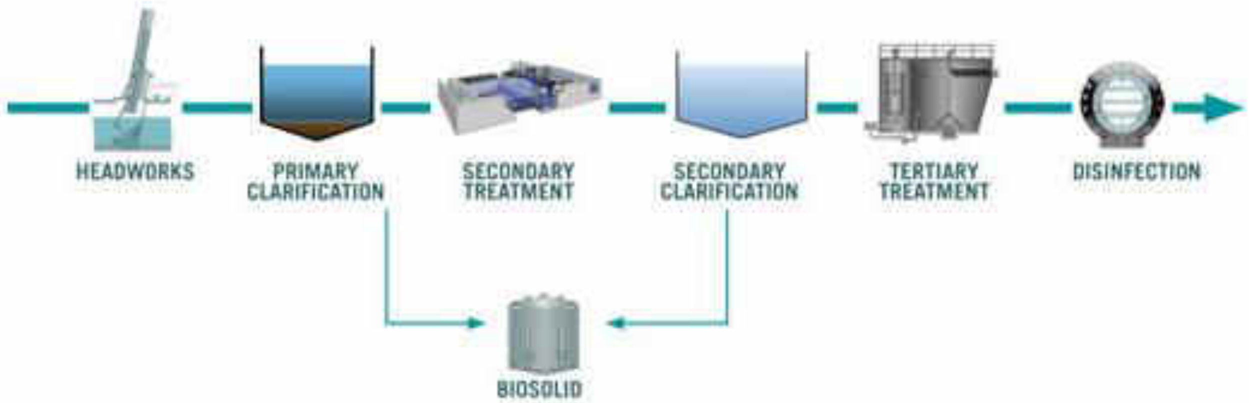

Fig. 1. The flux of municipal wastewater treatment plant [1]

- experiment was conducted in parallel and to the same conditions of water treatment plant, both on the aeration tank from wastewater plant A and on B using the process control system performance (experimental group) and
- experiment on another aeration tank with controlled aeration the classic method (reference group).
- both methods were tested (Figure 2).

Fig. 2. The experiment on the aeration tank

2. Material and methods

The equipment is composed of: electrodes are sensitive to ions (ISE) for ammonium nitrate (VARiONPlus 700 IQ WTW), a controller with programming logic (PLC-based on a patented algorithm aeration).
Doses of ammonium and nitrate were checked weekly to assess the estimated value of online sensors.
Energy consumption has been expressed through the "rate of electricity consumption (kWh)/day/treated water (m ³)/day.
The goal of the experiment is to shape the movement of air injected into the aeration basin with the possibility to optimize the air flow by adjusting the breathed it.

2.1 Injection of constant air flow versus variable air flow

Aeration can be carried out using air blowers equipped with a speed regulator. In this case, it is possible to adapt the air flow according to the amount of pollutants to be removed. In the present study, by adding a controller, decreases the amount of air provided by approximately 30%, leading to better air management required for operation (Figure 3).

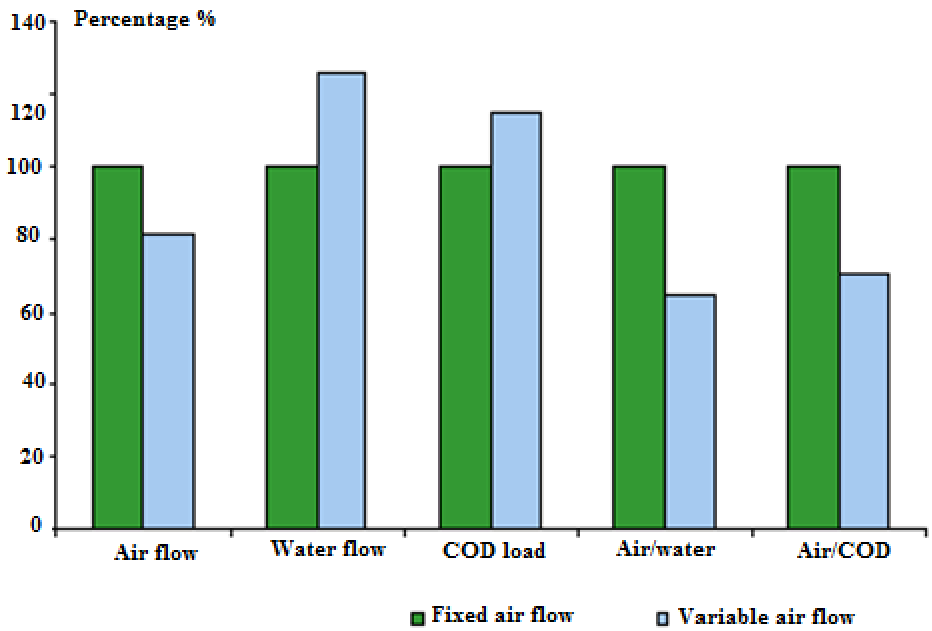

Fig. 3. Comparative power supply with constant and variable air flow [1])

2.2 Optimize air flow control through ammonium sensors/nitrates online

In this case, a group is controlled by a conventional programme in which the air flow is variable and the other is controlled by a programme [2], based on the monitoring of ammonium and nitrate samples.

The ratio between the required air flow and the treated water flow is used to compare the energy required in each group, considering that treated water has the same quality in both cases. This report shall be presented for the supply of constant air flow (Figure 4) and for the supply of variable air flow (Figure 5). In both cases, a 15% energy saving is achieved for the same qualities of purified water.

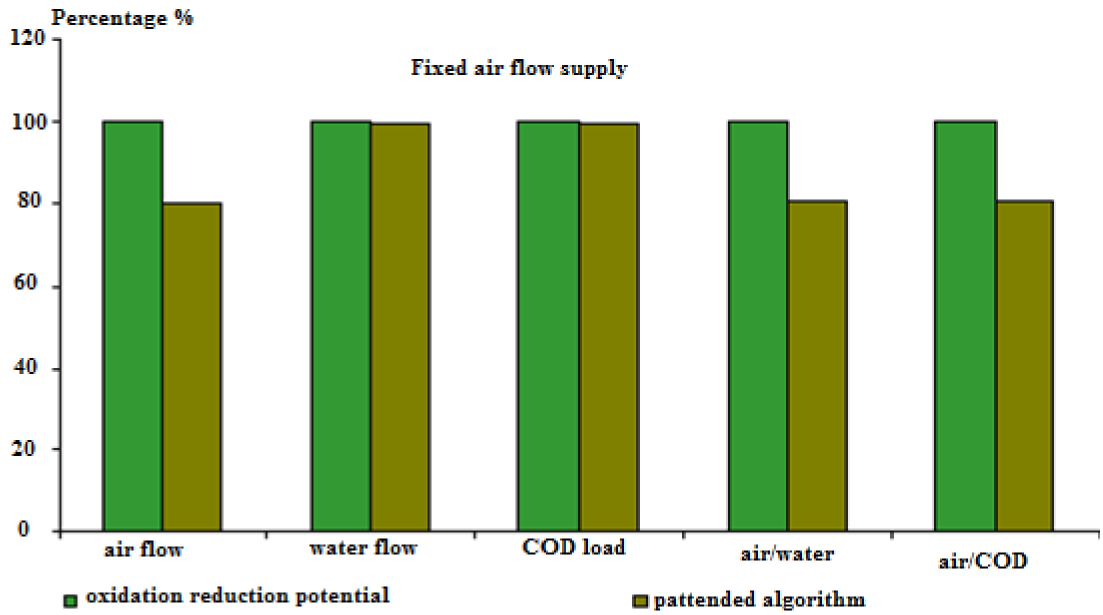

Fig. 4. Comparison between the controlled supply system with constant air flow and patented algorithm [2]

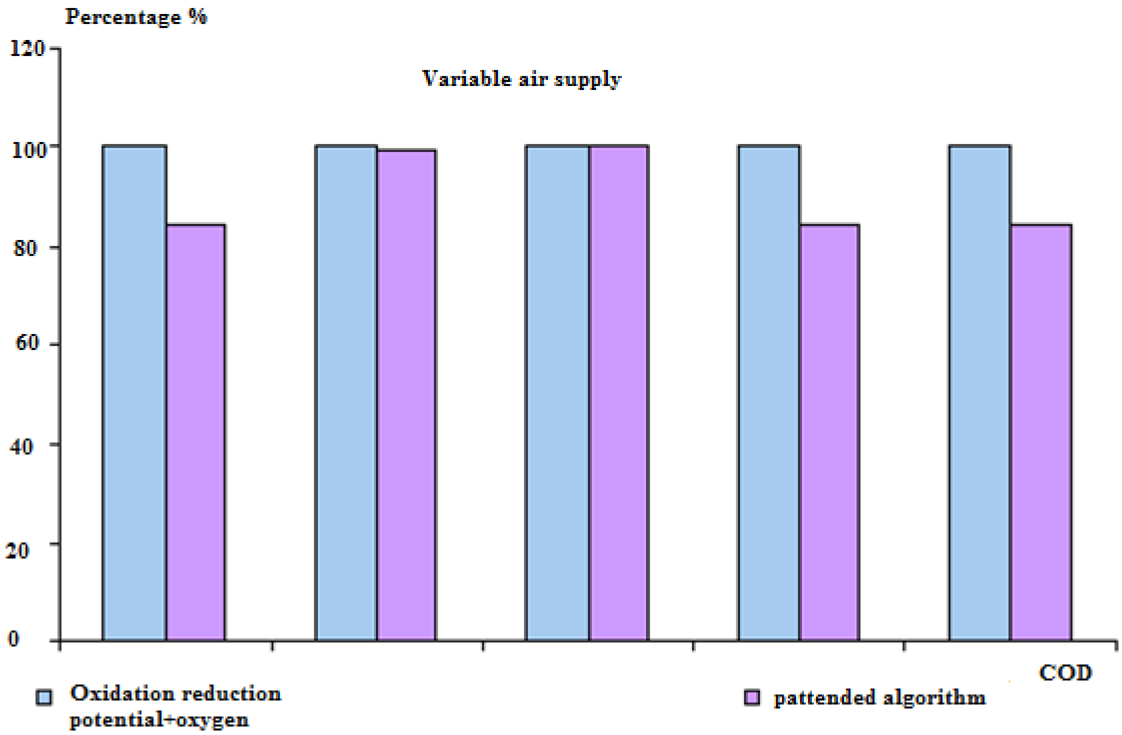

Fig. 5. Comparison between the controlled supply system with variable air flow and patented algorithm [2]

3. The study of biological parameters

Use oxygen is always delivered in excess in the aeration basin to ensure that the nutrients are removed under aerobic conditions. Lack of oxygen in that area favors sludge congestion and foam formation.

As shown in Figure 6, there are no significant differences in the speed of decantation in the classic and patented algorithm process.

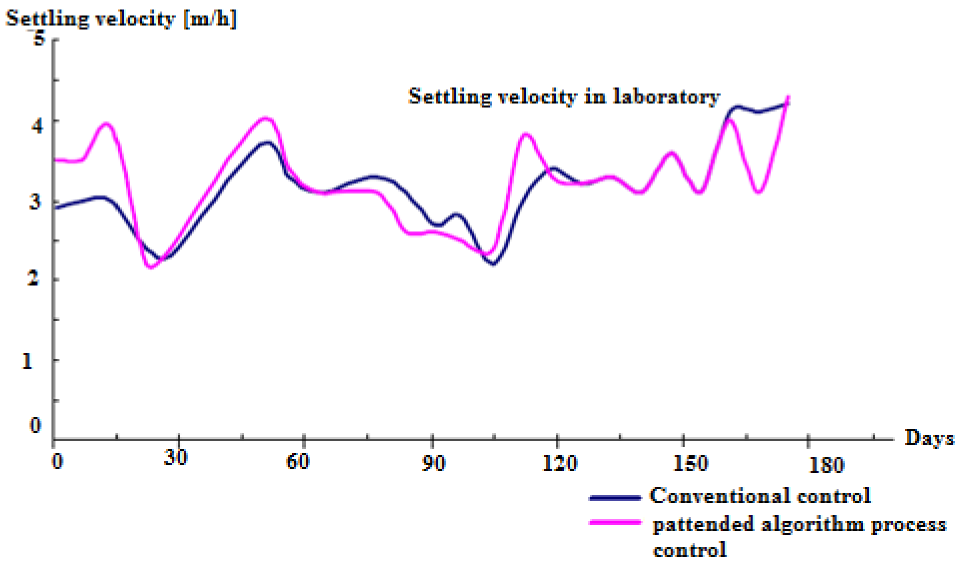

Fig. 6. Setting speed using the conventional controller and patented algorithm [2]

In the test on properties of sludge dehydration there were no differences in the consumption of polymers and the concentration of solid matter in suspension [3].

4. Conclusions

Advantages

Environment: A 10-15% decrease in energy consumption compared to traditional adjustment systems.

Performance: Can be adapted depending on the dimensions of each wastewater treatment plant a system that can easily be integrated into the logical diagram of the control and controls panels in most wastewater treatment plants.

Economy: By adjusting the air flow according to the needs of the treatment process, the energy costs are reduced.

References

[1] *** Degremont Technologies. "Treatment Solutions-Wastewater", November 9, 2018. Accessed November 9, 2018. http://www.degremont-technologies.com/-Wastewater.

[2] *** Degremont Technologies. "Biological treatment of effluents with high concentrations of ammonia ", November 9, 2018. Accessed November 9, 2018.http://www.degremont-technologies.com/Cleargreen-TM-Biological-treatment-of-effluents-with-high-concentrations-of-ammonia.

[3] Panaitescu, Ileana-Irina. *Operational management of wastewater treatment plants / Managementul operational al statiilor de epurare.* Bucharest, Politehnica Publishing House, 2014.

Hydraulic Stand for Research of the Correlation between Pellet Quality, Raw Material Quality and Physical-Mechanical Parameters of Manufacturing Equipment

PhD. Eng. **Gabriela MATACHE[1]**, PhD. Eng. **Gheorghe ȘOVĂIALĂ[1]**,
Dipl. Eng. **Valentin BARBU[1]**, PhD. Student Eng. **Adrian-Mihai ALEXE[1]**,
Dipl. Eng. **Mariana EPURE[2]**

[1] Hydraulics and Pneumatics Research Institute INOE 2000 – IHP Bucharest; fluidas@fluidas.ro

[2] National Institute of Research-Development for Machines and Installations Designed to Agriculture and Food Industry INMA Bucharest

Abstract: *The article has as a defining element the design and development of a hydraulic drive stand on which it is possible to investigate how some chemical-physical parameters of sawdust have influence on the production, and especially on the quality of the pellets. The stand is provided with control elements for moving a piston in the direction of passing the sawdust through one or more die holes. For the measurement of the force, movement and speed of movement, a pressure transducer and a positioning (displacement) transducer have been included as a whole. The stand has the facility to acquire and process the data that are gathered during the tests.*

Keywords: *Stand, pellets, forest sawdust, hydraulic drive, biomass*

1. Introduction

Many people believe that the type and amount of energy used by humanity, at a certain point, also determined the level of civilization of society. If at the beginning of history, the main energy resources were the sun and biomass, that is, direct heating or the use of heat obtained by combustion of wood, the use of hydro energy was also used over time. Significant changes have occurred with the use of fossil fuels such as coal, gas or oil. Since the fossil resources are not unlimited but not immediately exhaustible, the responsible people of the planet have gone to the serious study of the use of some forms of renewable energy on the short term, that is in several years. In the following analysis the authors will present a variant of using of wood biomass in the form of pellets.

There are many forms in which biomass is defined in literature. If we start from the idea that biomass is based on organic plant matter, animal metabolic residues and microorganisms, we find that there is great diversity of this resource and especially huge quantity available to humanity without demanding extra expense. Biomass resource that we consider is the forest biomass, primarily sawdust, primary and secondary material from the forestry and plantation of softwood and hardwood. Obviously, it is a rapidly renewable resource because otherwise even fossil fuels like coal and oil, although not considered biomass, neither in general nor in this material, originated in forest biomass of past ages, transformed substantially in geological time.

Biomass is biodegradable and renewable, but the energy obtained is not completely non-polluting. It is also to be said that although wood is extremely important in the field of energy obtained from biomass, it is found that exploitation that does not take into account the principles and criteria of sustainable development leads to aggressive deforestation, which also can be observed in Romania, that will create great ecological and economic problems in a not so far future. No matter how much energy the sun sends to earth, no matter how accurate and intense is the process of photosynthesis, no forest can regenerate if exploited in a chaotic, unscientific and uneconomic manner.

Forests offer a wide variety of biomass sources, including fast growing trees (poplar, willow, eucalyptus), fast growing herbaceous plants and various residues, such as wood from trimming of trees and from construction, scraps resulting from wood processing, but the main source of biomass and actually the most used in the history of humankind is wood.

The energy produced from forest biomass already represents a very large share of total energy consumption because there is a large amount of cellulosic matter abandoned today that will be transformed into energy products. The use of forest biomass for energy purposes leads to the production of solid or liquid fuels that could replace much of the current oil consumption once energy conversion technologies prove to be cost-effective.

2. Pellets from forest sawdust

2.1 The emergence of pellets from forest sawdust

Pellets obtained from forest sawdust have a fairly short history since the world oil crisis in the 1970s, when looking for alternative energy sources which had to be economical in terms not only of price but also of use. The first pellet factory was built in the mid-1970s in the American state of Oregon after potential users were convinced that forest residues could be used without too much expense and especially without significant efforts during the exploitation. The pellet market in Europe first developed in Scandinavia, especially Sweden and Denmark, which had a pioneering role in the development of pellet heating installations. In the early 90s, the pellets were used in most countries, first in large installations, and, as time went by, they were also used for household, for heat production in individual households.

Wood sawdust pellets are mostly made from residues that are a by-product of the wood processing industry. Wood pellets are a standardized fuel (in Germany DIN 51731 and DIN Plus, in Austria M7135, M7136, and M7137) and have a maximum content of 10% water, a density of 1 ton/m^3 and a strong structure with low dust and ash content. There is already, in the common language, a classification of pellets into superior and inferior depending on the surface quality, dust content and the density determined simply by the floating capacity.

2.2 Usefulness of wood pellets

Wood pellets are denser than burned wood and have a controlled degree of drying (10% -14%) that makes combustion efficient and uniform. The fact that the filling volume is superior to the wood burning, 95% to 70%, leads to increase in the time between re-supply up to 36 hours, which creates the prerequisites for automation of combustion systems. Due to the double density compared to natural wood and low moisture content, very little of the energy produced is needed to evaporate the water. This allows the pellet of biomass to be burned at high temperatures, with increased efficiency.

There are several elements that have facilitated the development of the use of pellet heating systems:

a) The first element to be considered is the price that for an individual becomes profitable with the passage of time as the pellet price and the maintenance of the equipment is superior to all other household heating systems.
b) The pellets are environmentally friendly, they are a renewable energy source and are extremely efficient during combustion and are based on a serious and steady technology.
c) Unlike wood or coal heating, the operation of pellet burning systems is easy, extremely clean and suitable for automation.

2.3 Manufacturing of wood pellets

Wood and sawdust pulp from wood sawing, sawdust or wood chips - all secondary products (other than bark) resulting from sawmills are the raw material for the production of wood pellets and can be processed in pellet manufacturing installations. The raw material used in the manufacture of wood pellets is a residual product from the wood processing industry and is therefore available at a convenient price.

The untreated sawdust is compressed under high pressure (160-240 bar) without the addition of chemical-synthetic adhesives. Since the quality of the sawdust used is important for a top-quality product, quality controls are carried out, starting with picking up the sawdust, preparing it and making pellets.

The well-pressed and compressed material is a homogeneous and natural fuel. When pelletizing the wood sawdust is pressed with rollers through a die. Here, it is essential that the press can process at any time a raw material with identical properties. Thus, a uniform size of the granules and uniform residual moisture of the sawdust must be ensured first. For this, before pressing, the sawdust is passed through a strip dryer; in addition, the type of wood should also be taken into account when pressing. The quality of the pellets depends also on the way of handling in the production hall, in the transport vehicle and all the way to the pellet store of the consumer.

Separating sawdust from impurities is an important step before introducing it into the pelleting process on pellet presses. The most common impurities in sawdust are: stones, plastics, metals and other harsh materials that can influence the working efficiency or even seriously wear the pellet press.

Stones and other non-metallic hard materials from sawdust can be removed by a sieve selector, while metallic impurities can be extracted with magnets.

The raw material with granulometric dimensions larger than those required by the pelletizing process is mechanically chopped into smaller pieces by means of hammer mills to better break down the lignin in the wood. Thus, all wood residues will have a unitary dimension (ideally four millimetres).

Drying. The preliminary condition of the pelletizing process is the drying of the material. For this, the water content of the wood residues should be reduced by means of a belt or drum dryer up to about 10%. As the final material is drier, the energy savings will be higher and costs of the production processes will be lower. The temporary storage of dry material in the silo is an intermediate step between drying and pelleting. The advantage is that if a technological sequence is stopped before or after drying, it is not necessary to stop the process, thus ensuring the economic and technical efficiency of the installation.

Conditioning. To fluidize the lignin, which joins the components of the pelletized material, the sawdust contained in the conditioning device is treated with hot steam. Some manufacturers improve the binding properties by adding amylose (concentration below 2). Thus, pellet quality, press yield and die reliability increase, and energy expenditure decreases.

Pellet heating is an ecological solution. Not only is biomass regarded as a renewable fuel, but heating on pellets contributes to the recovery of wood waste (forestry, wood-sawdust, bark, tree remains), vegetable waste from technological processes in agriculture (secondary production of straw, stems, seeds, kernels, shells), energy crops (herbaceous and woody plant - elephant grass, willow, poplar) considered neutral in terms of greenhouse emissions.

In addition, by pelletizing, the calorific power of the combustible materials is increased, being higher than the usual wood. And that's not all of it: burning pellets generates very little smoke and noxious emissions, transport costs are low, there is an improved logistics for storage and automated use. The resulting ash, which represents less than 1.5% of the burning mass, is an excellent natural fertilizer.

Pellets are a **standardized fuel**. Each manufacturer must meet certain requirements to allow for appropriate and energy-efficient heating. The **European standard EN 14961-2** [1] established the quality requirements for pellets for awarding the **EN Plus** certificate, table 1.

ENplus certifies quality at the manufacturer, but also checks for merchandising and logistics. This ensures a continuous quality check and transparency from the manufacturer to the final consumer. For consumers, the new system ensures strict values of the burning process parameters.

Thus, for the pellets there are 3 classes of quality: A1, A2 and B classes. These classes are mainly distinguished by dimensions (maximum length 40 mm), the maximum percentage of powders or elements with a length of less than 3.15 mm (less than 1% of the packed quantity), combustion ash (≤ 0.7% for class A1 and ≤1.5% for class A2), full combustion temperature (≥ 1200 °C for class A1, and respectively ≥1100 °C for class A2).

Quality class A1 (also called premium quality) is the most commonly used, being consumed especially in the residential sector for burning in stoves and individual boilers, producing the lowest amount of ash and most importantly having the highest calorific power.

Quality class A2 is used for burning in large plants and produces a higher amount of ash.

Quality class B, also called the "industrial" class, produces the highest amount of ash, can even contain impurities (sand, etc.) with a significantly lower calorific value than that of the A2 class. For this quality class, EN Plus certification is not required.

Depending on the use of stoves or boilers (residential or industrial), manufacturers and installers strongly recommend the use of EN Plus certified pellets.

Table 1: Quality requirements for pellets, for awarding the EN Plus certificate

Parametru	U.M.	ENplus-A1	ENplus-A2	EN-B
Diametru	mm	6 (± 1) oder 8 (± 1)[2]	6 (± 1) oder 8 (± 1)[2]	6 (± 1) oder 8 (± 1)[2]
Lungime	mm	3,15 ≤ L ≤ 40 [3]	3,15 ≤ L ≤ 40 [3]	3,15 ≤ L ≤ 40 [3]
Densitate în vrac	kg/m³	≥ 600	≥ 600	≥ 600
Putere calorică	MJ/kg	16,5 ≤ Q ≤ 19	16,3 ≤ Q ≤ 19	16,0 ≤ Q ≤ 19
Umiditate	Ma.-%	≤ 10	≤ 10	≤ 10
Particule fine (< 3,15 mm)	Ma.-%	≤ 1	≤ 1	≤ 1
Durabilitate mecanică	Ma.-%	≥ 97,5 [4]	≥ 97,5 [4]	≥ 96,5
Conținut cenușă	Ma.-% [1]	≤ 0,7	≤ 1,5	≤ 3,0
Temperatura de topire a cenușii	(DT) °C	≥ 1200	≥ 1100	≥ 1100
Conținut de Clor	Ma.-% [1]	≤ 0,02	≤ 0,02	≤ 0,03
Conținut de Sulf	Ma.-% [1]	≤ 0,03	≤ 0,03	≤ 0,04
Conținut de Azot	Ma.-% [1]	≤ 0,3	≤ 0,5	≤ 1,0
Conținut de Cupru	mg/kg [1]	≤ 10	≤ 10	≤ 10
Conținut de Crom	mg/kg [1]	≤ 10	≤ 10	≤ 10
Conținut de Arsen	mg/kg [1]	≤ 1	≤ 1	≤ 1
Conținut de Cadmiu	mg/kg [1]	≤ 0,5	≤ 0,5	≤ 0,5
Conținut de Mercur	mg/kg [1]	≤ 0,1	≤ 0,1	≤ 0,1
Conținut de Plumb	mg/kg [1]	≤ 10	≤ 10	≤ 10
Conținut de Nichel	mg/kg [1]	≤ 10	≤ 10	≤ 10
Conținut de Zinc	mg/kg [1]	≤ 100	≤ 100	≤ 100

[1] în stare anhidră (wf)

[2] diametrul trebuie să fie specificat

[3] maxim 1% din peleți pot să fie mai lungi de 40 mm, lungime maximă 45 mm

[4] La măsurători cu Lignotester (control intern) se aplică limita de ≥ 97,7 Ma.-%

3. Factors that influence the quality of pellets [2]

3.1 Influence of granulation of raw material and chemical composition on pellet quality

Particle sizes, shape and distribution are factors that greatly influence the mechanism of intermolecular bonding creation in the biomass densification process by pressing. The value of intermolecular links is dependent on several factors, among which the most important are:
- the atoms' ability to combine, that is the number of electrons with which the atom participates in forming of chemical bonds (valence electrons);
- hydrogen bonds or hydrogen bridge;
- *van der Waals* forces, which are the forces of attraction between neutral molecules.

Generally, intermolecular bonds are inversely proportional to particle size, because smaller particles form a larger contact surface in densification. However, when the particles are very small, the finished product loses fibre consistency and does not bind in the densification phase.
Particle sizes have some influence on the characteristics of the pellets, more pronounced in the case of pelletizing at low and medium pressures.
Also, there is obvious the dependence of the compressive strength of the pellets on the particle size, dependence reflected in the quality of the pellets.

Carbon, oxygen and hydrogen are absorbed by the plant in the form of CO_2, O_2, H_2O or HCO_3. These components make up all the plant biomass compounds. Chemical compounds of biomass can be distinguished into two major classes: carbohydrates (about 2/3 of the total volume of synthesized substances) and organic nitrogen-containing substances.
The most important carbohydrates are cellulosic molecules (C6 polymer), surrounded by hemicellulose (C5 polymers predominantly, with inclusions of C6) and lignin, which is deposited between the fibres. The content of these three types of biopolymers in the total biomass mass is approx. 95%. The remaining proportion is made up of a number of associated materials, called extractive substances in the form of resins, fats, tannins, starch, sugar, proteins and minerals.
The content of cellulose, hemicellulose and lignin in plant biomass is different and as a result, the energy potential of different types of biomass is quite varied. At the same time, because the content of the main chemical elements, which are carbon (C), hydrogen (H) and oxygen (O), does not differ significantly from one type of biomass to another, it results that the biomass burning power is in the most part influenced by the relationship between these elements.
The lower the O / C and H / C ratios, the higher the calorific value. Thus, the higher the C content of the biomass, the higher the combustion power.
Since lignin contains most C, lignin's thermal energy is higher and represents approx. 5500 - 6500 kcal / kg in the dry state, and the one of cellulose and hemicellulose, which are lower in carbon, is lower (4000 - 4500 kcal / kg in absolute dry state).
The calorific value of wood biomass is higher because it has a higher percentage of lignin, compared to biomass from agricultural residues and herbaceous energy crops, which have a lower percentage of lignin.
Lignin is also the main binder in the formation of solid biofuels.
Lignin, which has a major weight in the biomass composition (in some cases up to 25%), binds the cellulosic molecules between them and has an important effect on pelleting technology, as it eliminates the need for binders or other dangerous substances.
A full assessment of the biomass characteristics used for the production of solid biofuels requires detailed knowledge of the chemical composition, in particular the elements that influence the combustion process, the reliability of the manufacturing equipment and the combustion equipment, as well as those that directly or indirectly impact on the environment.
Plant biomass used for pellet production contains up to 2% nitrogen, 1.8% chlorine and approx. 7% sulphur. It should be noted that the ENPlus rules limit the nitrogen content to 0.3% (ENPlus-A1), 0.5% (ENPlus-A2), 1% (ENPlus-B), sulphur content to 0.03% (ENPlus-A1), 0.03% (ENPlus-A2), 0.04% (ENPlus-B), and chlorine content to 0.02% (ENPlus-A1), 0.02% (ENPlus-A2), 0.03% (ENPlus-B).
The requirements regarding the content of major and minor elements are quite severe. For example, the content of semi-metal must not exceed 1 mg per kg of pellets, the cadmium content, which is a very toxic metal, cannot exceed 0.5 mg / kg, and the mercury content is even more limited – no more than 0.1 mg / kg of pellets.

3.2 The role of temperature in biomass pelleting

The temperature required for pelletization to a large extent is generated as a result of the tribological processes that take place inside the biomass and at the contact boundary between the biomass and the die walls. In some cases, the biomass is further heated by steam or other methods to provide better densification conditions.
As a rule, in the process of industrial pelletization, the temperature is not a controllable parameter, although it is estimated indirectly, being dependent on the nature, moisture content and granulation of the feedstock, the rotational speed of the roller presses of the pelleting press, the value of the gap between them and the die.
Regarding the dependence of temperature in the working area on the raw material, it is believed that the temperature is conditioned by the lignin content, which in the vegetal biomass varies between 15-35% and its melting temperature is approx. 90^{o}C.
Among the first researches on the effects of temperature on the densification of biomass, there are those of Smith et al. They studied the dependence of the density of straw briquettes depending on the variation in the temperature applied in the range 60-140^{o}C. Research has shown that the

biomass density increases as the temperature increases to 90°C, after which the density remains constant.
Ivin and Gluhovskij, on the contrary, considered that the temperature of 90°C is the minimum temperature the die may have, because pellets formed at temperatures below 90°C, although stiff, are not "glued" and, as a rule, they form cracks at the boundaries of biomass particles. At the same time, they pointed out that when pellets are formed at temperatures above 100°C, if biomass contains a higher percentage of moisture, it passes into steam, which, through explosions, forms microcavities between biomass molecules or even can destroy it.
In order to obtain high quality pellets, the compression ratio of the die, which is calculated according to the formula R = G / D, must be between 14 and 20, where: R = compression ratio; G = die thickness, in mm; D = die hole diameter, in mm.
If the compression ratio is too high, a very good quality of the pellets will result, the main disadvantage being the premature wear of the die.
If the compression ratio is too low, the lifetime of the die will increase quite a lot, but the main disadvantage will be the poor quality of the pellets, which will result in their fraying.
For normal operating conditions, the lifetime of the die is at least 1,500 hours, reaching up to 5,000 hours of operation. The lifespan of the press rollers is minimum 800 hours of operation.
Regarding the granulation of the material to be pelletised, it is recommended that the diameter of the sieve holes in a hammer mill should be up to 1.0 mm smaller than the diameter of the die holes.
The recommended extrusion speed of the biomass through the die for 8 mm diameter holes is 127 mm/min [3].

4. Hydraulic stand for research of the correlation between physical-mechanical parameters of manufacturing presses, saw dust quality and pellets quality

The stand, fig. 1, fig. 2, comprises a rigid frame, integral with the liner of hydraulic drive cylinder *5*, a cross-bar that can move on two columns and can be fixed in the desired working position, a pressing device *3*, which is integral with the hydraulic cylinder rod.
On the cross-bar, there are mounted the force transducer 1 and the piston which is pressing the extruded material in the die.
The hole in the die and the pressing piston are perfectly coaxial, so as to avoid the occurrence of some torque generated by possible offsetting.
Pressing the material is done by moving the presser vertically to the pressing piston.
Between the presser (mobile) and the cross-bar which, by bolting on the columns, closes the frame of the test chamber *4* in the upper part, there is mounted a resistive motion transducer *2*.
The hydraulic power supply of the actuating cylinder is made from a hydraulic group consisting of an oil reservoir, an electropump *12*, a return filter *11*, a safety valve *10*. The gauge *9* mounted on the pumping group discharge circuit indicates the value of the hydraulic oil pressure at the input of the distribution devices. Servovalve *8* allows very precise control of the flow / pressure values for the execution element (hydraulic cylinder), by increasing the size of the electrical signal; through their values, the flow and pressure rates adjusted by the servovalve determine the values of speeds and forces of the cylinder rod, required by the tests conducted on the stand.
The pressure transducer *6*, mounted on the hydraulic cylinder piston supply circuit, provides information on the pressure value during the biomass compression process.
The hydro-pneumatic accumulators *7* have the function of pulsating attenuation and maintaining constant pressure value in the rod / piston chambers of the hydraulic cylinder during the working phases of compression of the material to be extruded in the die / piston retraction.
The technical parameters of the extrusion process (compression force, friction forces) are determined on a set of single-hole dies of various diameters, shapes, depths.
The data subject to experimentation are acquired using a data acquisition system.

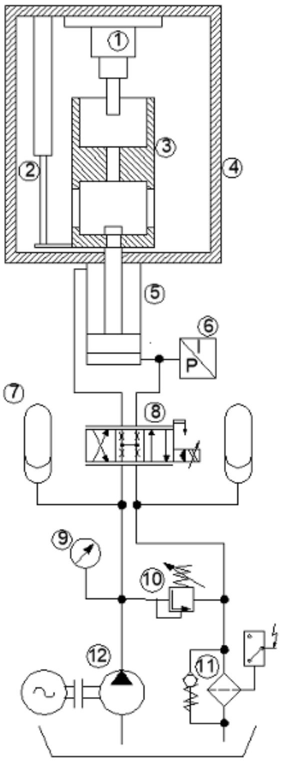

Fig. 1. Hydraulic drive diagram of the pellet stand
1-force transducer; 2-position transducer; 3-press device; 4-metallic frame; 5-hydraulic cylinder; 6-pressure transducer; 7-hydropneumatic accumulator; 8-servovalve; 9-manometer; 10-safety valve; 11-return filter; 12-electropump

Fig. 2. Physical realization of the research stand

4.1.1 Block diagram of the pellet stand

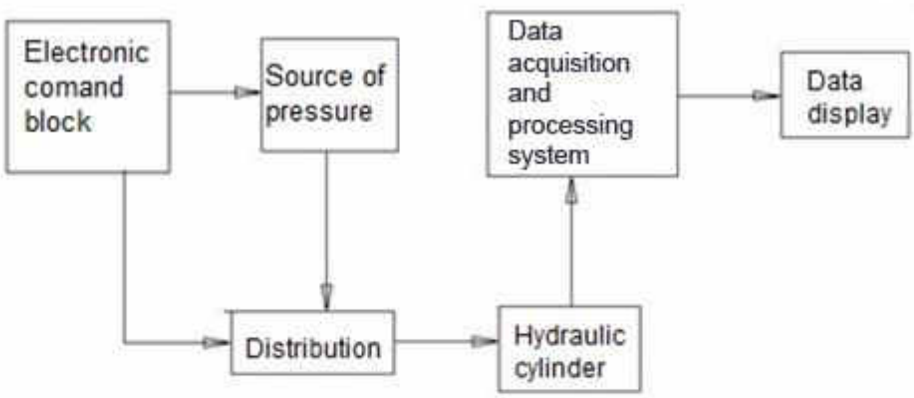

Fig. 3. Block diagram of the pellet stand

From the electronic control unit there are set the values of the electric signals (current or voltage) for driving the distribution devices (servovalve), depending on the flow / pressure generating velocity / pre-set forces to the rod of the hydraulic cylinder.
Information on the strength and speed of biomass compression in the die are collected from the force and displacement transducers, displayed in real time or transmitted to a data acquisition system.

5. Conclusions

- The biomass pellet optimization for thermal energy generation is an alternative to the use of fossil fuels, biomass being considered as a neutral energy source in terms of pollutant emissions.
- Obtaining thermal energy from pellets has reached technical and economical maturity, with advanced technologies and equipment for pellet production and burning, with a high degree of automation.
- The raw material, derived from forest exploitations, woodworking units, agriculture (secondary production - straw, stems, vines, wastes from the main agricultural products - kernels, shells - processing factories), is a renewable, cheap and good quality energy source; by densification, biomass transformed into pellets achieves a calorific value comparable to that of wood.
- The stand proposed and developed by IHP is useful for determining the constructive parameters of the extrusion dies (diameter, shape, depth of the holes, quality of materials and machining), compression and friction forces that lead to the production of quality pellets for types of biomass differing in terms of structure, granulometry, humidity, temperature.

Acknowledgments

This paper has been developed in INOE 2000-IHP, with the financial support of the Executive Unit for Financing Higher Education, Research, Development and Innovation (UEFISCDI), under PN III, Programme 2- Increasing the competitiveness of the Romanian economy through research, development and innovation, Sub-programme 2.1- Competitiveness through Research, Development and Innovation - Innovation Cheques, project title: “Technological stand for the determination of the die’s geometry used in biomass pellet making equipment”, Financial Agreement no. 264 CI/2018.

References

[1] European Standard (EN 14961) for Wood Chips
On: https://www.researchgate.net/.../268403209_EUROPEAN_STANDARD_EN_14961.
[2] Gudîma, Andrei, Marian Grigore, and Andrei Pavlenco. “Stadiul actual al cercetărilor cu privire la influența variabilelor de producție asupra calității biocombustibililor densificați în formă de peleți.” *Meridian Ingineresc*, no. 1 (2017): 51-60.
[3] Nielsen, Niels Peter K., Douglas J. Gardner, Torben Poulsen, and Claus Felby. “Importance of temperature, moisture content, and species for the conversion process of wood residues into fuel pellets.” *Wood and Fiber Science* 41, no. 4 (October 2009): 414-425.

ISSN 1453 – 7303 **"HIDRAULICA" (No. 4/2018)**
Magazine *of Hydraulics, Pneumatics, Tribology, Ecology, Sensorics, Mechatronics*

Argumentation of the Optimal Hydrodynamic Profile of Blades of the Flow Microhydrostation Rotor's

Academician **Ion BOSTAN**[1], Prof. PhD. Dr.Sc. **Viorel BOSTAN**[1],
Prof. PhD. Dr.Sc. **Valeriu DULGHERU**[1], Assoc. Prof. PhD. Eng. **Oleg CIOBANU**[1],
Assoc. Prof. PhD. Eng. **Radu CIOBANU**[1], Ph.D Student Eng. **Polifron CHIRIȚĂ**[2]

[1] Technical University of Moldova; valeriudulgheru@yahoo.com

[2] Hydraulics and Pneumatics Research Institute INOE 2000-IHP, Bucharest, Romania; chirita.ihp@fluidas.ro

Abstract: *Insistent searches of authors have led to the design and licensing of some advanced technical solutions for outflow micro hydroelectric power plants. They are based on the hydrodynamic effect, generated by the hydrodynamic profile of blades and by the optimal blades' orientation towards water streams with account of energy conversion at each rotation phase of the turbine rotor. The selection of the optimal blades hydrodynamic profile is very important for functional optimization of micro hydro power plants. It will allow increasing the conversion factor (Betz coefficient) due to the hydrodynamic buoyant force. Due to the fact that the relative velocity of blades concerning the water currents is twice bigger, practically, at their motion against the water currents, the hydrodynamic lift force is relatively big, and the generated torque is commensurable to the one generated by the water pressure.*

Keywords*: Micro hydroelectric power plant, hydrodynamic profile*

1. Introduction

The inevitable increase of global energy consumption and the risk of a major environmental impact and climate change as a result of burning fossil fuels opens wide prospects for the exploitation of renewable energies. Hydropower, as a renewable energy source, will have an important role in the future. International research confirms that the emission of greenhouse gases is substantially lower in the case of hydropower compared to that generated by burning fossil fuels. From the economical point of view, the utilisation of half of the feasible potential can reduce the emission of greenhouse gases by about 13%; also, it can substantially reduce emissions of sulphur dioxide (main cause of acid rains) and nitrogen oxides.
Hydraulic energy is the oldest form of renewable energy used by man and has become one of the most currently used renewable energy sources, being also one of the best, cheap and clean energy sources. Hydraulic energy as a renewable energy source can be captured in two extra power forms:

– potential energy (of the natural water fall);
– kinetic energy (of the water stream running).

Both extra power forms can be captured at different dimensional scales.

2. Conceptual diagrams

To avoid the construction of dams, it is possible to use the river kinetic energy by utilizing water flow turbines. This type of turbines can be mounted easily and are simple in operation. Their maintenance costs are rather convenient. The stream velocity of 1m/s represents an energy density of 500W/m^2 of the flow passage. Still, only part of this energy can be extracted and converted into useful electrical or mechanical energy, depending on the type of rotor and blades. Velocity is important, in particular, because the doubling of water velocity leads to an 8 times increase of the energy density. The section of Prut River is equivalent to 60 m^2 and its mean velocity in the zones of exploration is (1-1,3) m/s, which is equivalent to approximately (30-65) kW of theoretical energy. Taking into account the fact that the turbine can occupy only a part of the riverbed, the generated energy could be much smaller. There are various conceptual solutions, but the issue of increasing the conversion efficiency of the water kinetic energy stands in the attention of the researchers. The analysis of the constructive diversion of micro hydroelectric power plants, examined previously, does not satisfy completely from the point of view of water kinetic energy conversion efficiency. The maximum depth of blade's immersion is about 2/3 of the blade height *h* in a classical hydraulic wheel with horizontal axle (Figure 1). Thus, only this surface of the blade participates at the transformation of water kinetic energy into mechanical one. As well, the preceding blade covers approximately 2/3 of the blade surface plunged into the water to the utmost *(h"≈ 2/3h')*, that reduces sensitively the water stream pressure on the blade. The blade, following the one that is plunged into the water to its utmost, is covered completely by it and practically does not participate in the water kinetic energy conversion. Therefore, the efficiency of such hydraulic wheels is small.

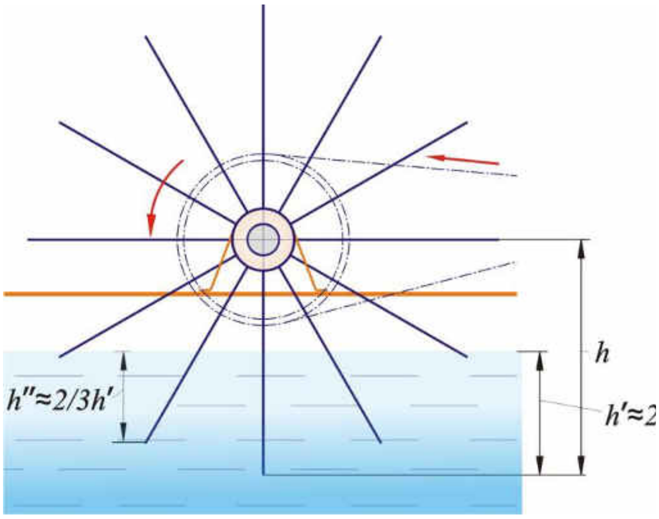

Fig. 1. Conceptual diagram of the water wheel with rectilinear profile of blades.

Insistent searches of authors have led to the design and licensing of some advanced technical solutions for outflow micro hydroelectric power plants. They are based on the hydrodynamic effect, generated by the hydrodynamic profile of blades and by the optimal blades' orientation towards water streams with account of energy conversion at each rotation phase of the turbine rotor (Figure 2). To achieve this, it was necessary to carry out considerable multicriteria theoretical research on the selection of the optimal hydrodynamic profile of blades and the design of the orientation mechanism of blades towards the water streams.

The main advantages of these types of micro hydroelectric power plants are:

- reduced impact on the environment;
- civil engineering works are not necessary;
- the river does not change its natural stream;
- possibility to produce floating turbines by utilizing local knowledge.

Another important advantage is the fact that it is possible to install a series of micro hydro power plants at small distances (about 30-50 m) along the river course. The influence of turbulence caused by the neighbouring plants is excluded.

The results of investigations conducted by the authors (on the water flow velocity in the selected location for micro hydro power plant mounting, on the geological prospects of the river banks in the location of installing the anchor foundation and on the energy demands of the potential consumer) represent the initial data for the conceptual development of the micro hydro power plants and the working element.

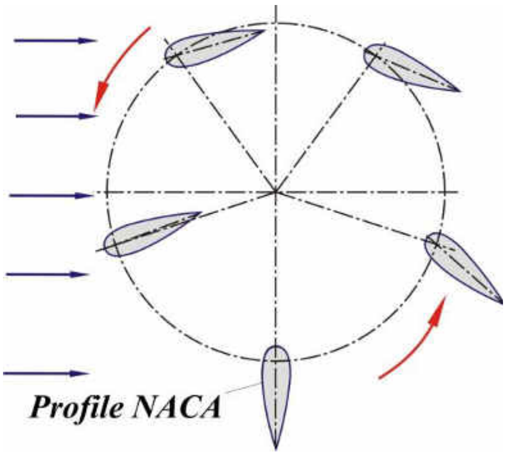

Fig. 2. Conceptual diagram of the water rotor with hydrodynamic profile of blades with its orientation towards the water streams.

The conceptual development of the plant structures with hydrodynamic profile of the blades was performed on the basis of three conceptual diagrams:

- Micro hydropower plant with pintle and blades fixed on the vertical axles anchored by steel structure;
- floatable micro hydro power plant with pintle and blades fixed on the vertical axles;
- floatable micro hydro power plant with horizontal axis and blades fixed on the horizontal axles.

In order to increase the conversion factor of water kinetic energy (Betz coefficient), a number of structural diagrams of floatable micro hydro power plants has been developed and patented [1-3]. The micro hydropower plants comprise a rotor with vertical axis and vertical blades with hydrodynamic profile in normal section. The blades are connected by an orientation mechanism towards the water streams direction. The rotational motion of the rotor with vertical axis is multiplied by a mechanical transmissions system and is transmitted to an electric generator or to a hydraulic pump. The mentioned nodes are fixed on a platform installed on floating bodies. The platform is connected to the shore by a hinged metal truss and by a stress relieving cable.

3.Theoretical justification of the hydrodynamic profile selection of the blade in normal section

Let consider the symmetrical profile of the blade placed in a fluid stream that moves uniformly at velocity $\vec{V}_\infty$ (Figure 3 [1]). In the fixing point *O′* of the symmetrical blade with lever *OO′* let consider two coordinate systems, that is: the system *O′xy* with axis *O′y* oriented in the direction of the velocity vector $\vec{V}_\infty$, and axis *O′x* - normal for this direction; and the system *O′x′y′* with axis *O′y′* oriented to the lever direction *O′O,* and axis *O′x′* - normal for this direction. Point *A* corresponds to the rear edge, and point *B* corresponds to the entering edge. The entering angle α is the angle between the chord *AB* of the profile and the direction of the velocity vector $\vec{V}_\infty$, and the positioning angle *φ* is the angle formed by the velocity vector direction and lever *O′O.*

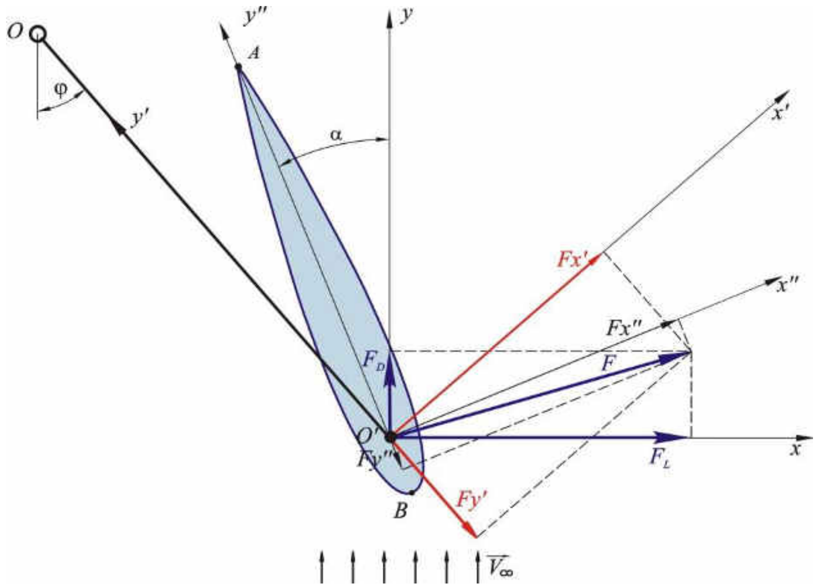

Fig. 3. Hydrodynamic profile blade.

The components of the hydrodynamic force $\vec{F}$ in the directions *O′x* and *O′y* are named the lift force and the resistance force:

$$F_L = \frac{1}{2} C_L \rho V_\infty^2 S_p, \tag{1}$$

$$F_D = \frac{1}{2} C_D \rho V_\infty^2 S_p, \tag{2}$$

where *ρ* is fluid density, V_∞ is flow velocity, S_p=*ch* (*c* is the length of chord *AB*, and *h* is the blade height) represents the area of the blade lateral surface, and C_L and C_D are hydrodynamic dimensionless coefficients, called the lift coefficient and drag coefficient. The hydrodynamic coefficients C_L and C_D are functions of the entering angle *α* , Reynolds number Re and the hydrodynamic shape of the blade profile. The components of the hydrodynamic force in the coordinate system *O′x′y′* are:

$$\begin{aligned} F_{x'} &= -F_L \sin\varphi + F_D \cos\varphi, \\ F_{y'} &= F_L \cos\varphi + F_D \sin\varphi. \end{aligned} \tag{3}$$

The torque moment of the rotor spindle *OO′* developed by blade *i* is

$$T_{r,i} = F_{x'} \cdot |OO'|, \tag{4}$$

and the summary torque moment developed by blades is

$$T_{r\Sigma} = \sum_{i=1}^{Npal} T_{ri}, \tag{5}$$

where N_{pal} is the number of rotor blades.

Generally, the hydrodynamic force has no point of application in the origin of the blade axes system *O'* so as it produces a resulting moment. The produced moment is determined by comparing it to a certain point of reference. The point situated at distance ¼ of the chord from the entering edge *B* will be considered as point of reference. The moment, also called the pitching moment, is calculated according to formula

$$M = \frac{1}{2} C_M \rho V_\infty^2 c S_p, \tag{6}$$

where C_M is the profile number of turns.

4. Optimisation of NACA 0016 hydrodynamic profile

In order to maximize the moment of torsion produced by the micro hydro power plant rotor, the optimization of the hydrodynamic profile will be considered [4]. The moment of torsion depends on the lift and drag hydrodynamic forces given by formulas (7) and (8). The hydrodynamic forces through the hydrodynamic coefficients depend on the entering angle α, Re number and the shape of the hydrodynamic profile. The hydrodynamic shape of the profile was selected from the NACA library having as parameters (with account of the profile symmetry) only the maximal thickness. The entering angle constitutes the second parameter. The optimization aims at maximizing the lift force and, at the same time, does not allow the pitching moment and the resistance force to take very big values. The following issue of optimization should be considered:

Maximize $C_L = C_L(\theta, \alpha)$
with constraints imposed to the coefficients C_D and C_M, (7)

where θ is the maximum thickness and α is the entering angle.
The values of the inferior and superior borders are determined, as follows: the negative maximum value for the pitching coefficient will correspond to the solution for the entering angle 0. The maximum value for the resistance coefficient will correspond to the solution for the entering angle *α = 18˚*. Also, restrictions have been added to the optimization parameters $10\% \le \theta \le 20\%$ and $0^o \le \alpha \le 20^o$. To find the optimal values of function $f = f(x_1, \ldots, x_n)$ an iterative method is used:
As long as the demanded accuracy is not reached the solution will be,

$$B_i s_i = -\nabla f(x_i),$$
$$x_{i+1} = x_i + \alpha_i s_i, \tag{8}$$

where α_i are the multipliers and B_i are the definite positive approximations of the Hessian function f. The partial derivation of function f related to the component i is approximated with the help of the finite difference formulas:

$$\frac{\partial f}{\partial x_i}(x) = \frac{f(x + he_i) - f(x - he_i)}{2h}, \tag{9}$$

where e_i is the basis vector.
The optimization is done by the MATLAB optimization soft: *"Sequential quadratic programming algorithm with a line search and a BFGS Hessian update".* The quadratic sub-tasks are solved by modified projection method. The gradient of function $C_L = C_L(\theta, \alpha)$ is calculated by the finite difference formulas with the constant pitch $h = 10^{-4}$. NACA 0016 profile was considered as the initial profile (Figure 4). The result of optimization is presented in Figure 5.

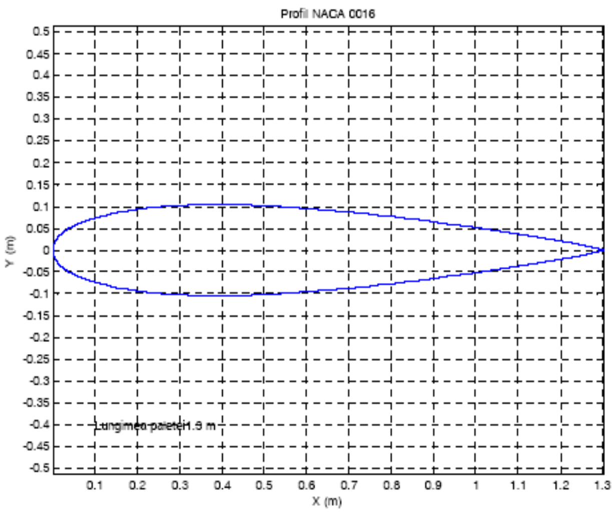

Fig. 4. NACA 0016 hydrodynamic rack profile standard.

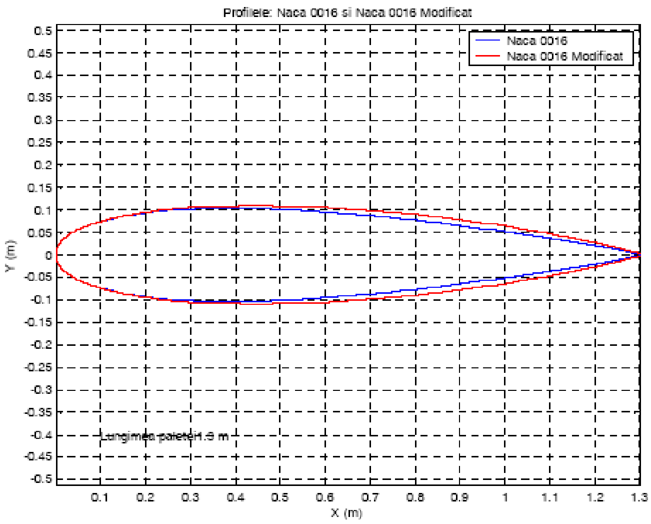

Fig. 5. NACA 0016 hydrodynamic rack profile standard and the optimised profile.

5. Argumentation of the optimal hydrodynamic profile of blades

The selection of the optimal blades hydrodynamic profile is very important for functional optimization of micro hydro power plants. It will allow increasing the conversion factor (Betz coefficient) due to the hydrodynamic buoyant force. As well, conversion increase is achieved by ensuring the optimal position of blades towards the water streams at various phases of rotor revolution, employing an orientation mechanism of blades. Thus, practically all blades (even those blades which move against the water currents) participate in the generation of the summary torque. Moving in the water currents direction, for torque generation the blades use both the hydrodynamic forces and the water pressure exercised on the blade surfaces. Moving against the water currents direction the blades use only the hydrodynamic lift force for torque generation (figure 6). Due to the fact that the relative velocity of blades concerning the water currents is twice bigger, practically, at their motion against the water currents, the hydrodynamic lift force is relatively big, and the generated torque is commensurable to the one generated by the water pressure.

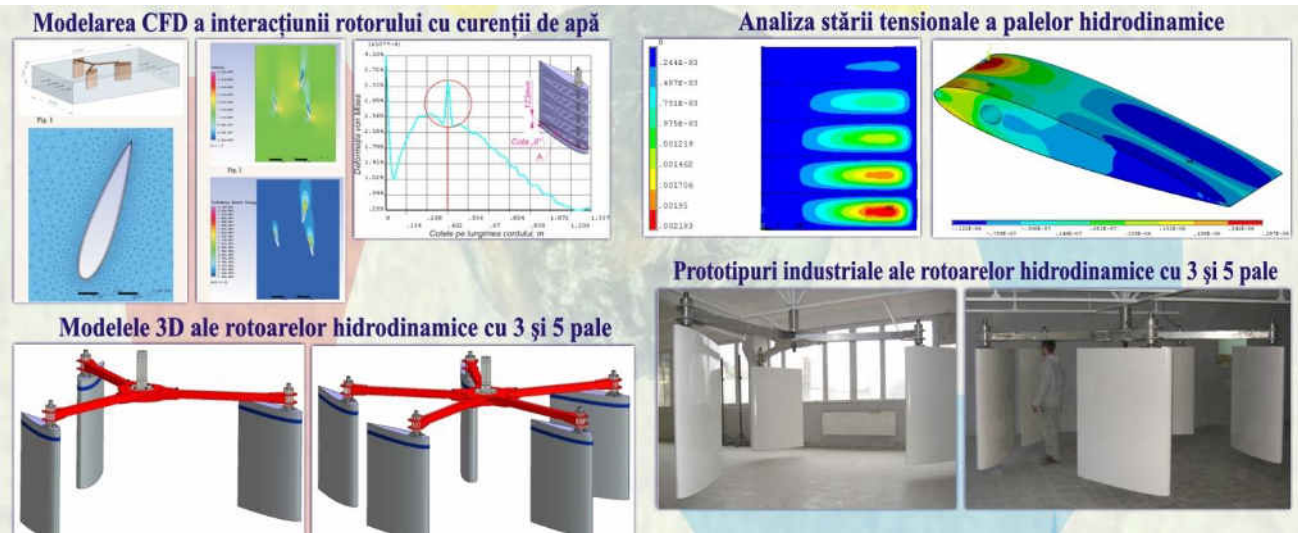

Fig. 6. Argumentation of the optimal hydrodynamic profile of blades.

This effect makes the basis of all patented technical solutions. The technical solutions of micro hydro power plants comprise various basic nodes and conversion principles that have been patented. These technical solutions allow essential increasing of the river water kinetic energy conversion coefficient. Full description of the most representative technical solutions and brief description of the conceptual diagrams of micro hydro power plants properties are given below.

4. Conclusion

Hydrodynamic rotors provide kinetic energy conversion of river water into mechanical or electrical energy without building barrages. Increased efficiency is provided by blades aerodynamic profile and their optimum position for efficient conversion of water kinetic energy.
To ensure the floating stability of the micro hydro power plants the rotor is mounted on the main structure with displacement *e* against the water stream. Thus, the micro hydro power plants designed to be anchored on the left bank cannot be anchored on the right bank.

Acknowledgments

This paper has been developed as part of a project co-financed by the Romanian government, project title: nr. 00055003. Autonomous integrated irrigation systems based on wind turbines, small hydro and photovoltaic installations.

References

[1] Bostan, I., A. Gheorghe, V. Dulgheru, I. Sobor, V. Bostan, and A. Sochirean. *Resilient Energy Systems. Renewables: Wind, Solar, Hydro.* Ed. Springer, VIII, 507 p., 2013, ISBN 978-94-007-4188-1.
[2] Bostan, Ion, Valeriu Dulgheru, Ion Sobor, Viorel Bostan, and Anatol Sochireanu. *Renewable Energy Conversion Systems* / *Sisteme de conversie a energiilor regenerabile*. Chișinău, Ed. "Tehnica Info", 592 p., 2007, ISBN 978-995-63-076-4.
[3] Bostan, I., V. Dulgheru, V. Bostan, and R. Ciupercă. Patent No. 2981 (MD), CIB B63 B 35/44: E02 B 17/00. Hydraulic Plant / U.T.M. – No.2005 0274; Decl. 15. 09. 2005; Publ. BOPI 2006.- No.2.
[4] Bostan, I., A. Gheorghe, V. Dulgheru, V. Bostan, A. Sochireanu, O. Ciobanu, and R. Ciobanu. Patent 3846 (MD), CIB F 03 B 13/00; F 03 B 7/00; F 03 B 13/18; F 03 B 13/22; F 03 B 17/06. Hydraulic station with horizontal axle / U.T.M. Publ. BOPI – 2009. - Nr. 2.

Comparative Study of a 1D and 2D Numerical Analysis Modelling a Water Flow at a River Confluence under Accidental High Waters

Lect.dr.eng. **Şerban-Vlad NICOARĂ**[1], Assoc.prof.dr.eng. **Gheorghe LAZĂR**[2], Lect.dr.eng. **Albert Titus CONSTANTIN**[3]

[1] POLITEHNICA University Timişoara, serban.nicoara@upt.ro

[2,3] POLITEHNICA University Timişoara

Abstract: *There are presented two numerical simulations – 1D and 2D – regarding the water flow on Timiş River in the Town of Caransebeş, Romania, at the confluence with its tributary Sebeş River. There was considered an accidental high waters wave following the synthetical configuration of a given significant hydrograph that happened from 4th to 11th of April 2000. The flow simulation by the two numerical models analysed by the help of HEC-RAS package aim to estimate the flow configuration, the velocities and levels developments, on a confluence river sector with specific bridge and protection structures. The analysis looks to establish some additional technical aspects regarding the flood defence of the urbanised major river plain or the streambed and framing embankments erosion protection.*

Keywords: *River model, 1D / 2D numerical modelling, flow modelling, river levels development, water velocity development.*

1. General considerations

The developed numerical modelling regarding the studied site emerged from a specialized technical expertise [1] upon implications from the accomplishment of a three-storey official building in the immediate flooding plain of Timiș River in the Town of Caransebeş, Romania. There was also considered the procedure engaged for a former 1D numerical simulation [2] generated by the help of HEC-GeoRAS 4.3, an ArcGIS 9.3 implemented version able to generate a 3D type ground surface [3]. The building site is in the crossroads area of Teiuşului and Dâlmei Streets (figure 1), aside of the access ramp to the road bridge over Timiș River (figure 2). As about Dâlmei Street, since it lies on the immediate major river plain, it is high water protected by a concrete parapet of about 0.90m height.

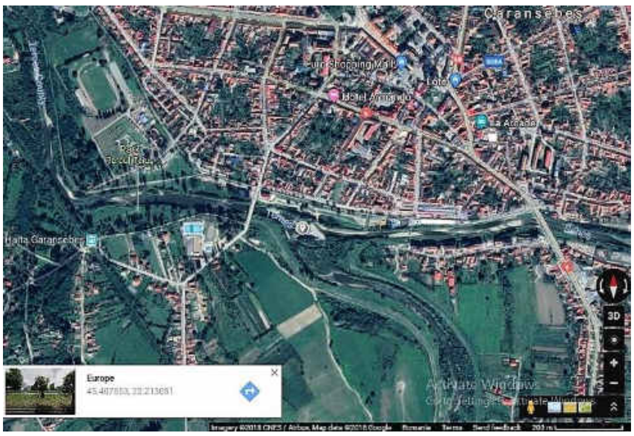

Fig. 1. General plan view of the analysed Timiş - Sebeş confluence river sector in the Town of Caransebeş

Fig. 2. Streambed view towards the crossing road bridge and the left bank of Timiş River downstream the confluence point

About one hundred meters upstream from the road bridge, the Timiș River gets a right-side tributary – the Sebeş River – that besides the natural flow brings the outgoing discharge from Zerveşti tail reservoir of Ruieni Hydropower high head Station. This flow has usual fluctuations between 3 and 54.5 m^3/s and so the present performed analysis follows the accidental situation given by a dysfunctional tail reservoir that would allow the passage of the entire maximum turbinated discharge 2x27.25 = 54.5 m^3/s. As the plan view shows, the confluence comes on the outside of Timiș River bend and its general flow path tends towards the right bank, meaning against the site of the mentioned built area.

The streambed geometry was modelled by considering three connected river sectors: the upstream 1330m sector on Timiş River, the downstream 2270m sector on Timiş River and the upstream 1490m sector on Sebeş River [2]. The spatial streambed configuration (figure 3) was developed by numerical 3D graphic processing [2] of a standard Stereo 70 topographical database consisting from the x,y,z ground points coordinates [1].

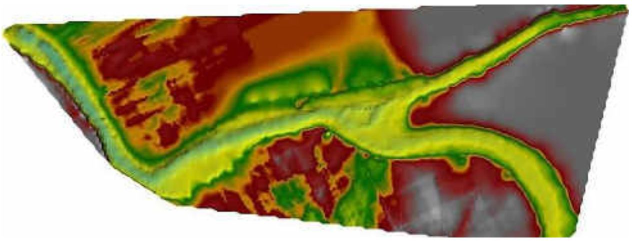

Fig. 3. 3D configuration of Timiş - Sebeş river confluence considering the existing crossing bridge and protection embankment

A 3D ground surface graphical representation can be achieved by the help of a satellite view as supplied by Earth Explorer. Still, as it is limited to a meshing net of 30x30m, the available graphic representation would be quite coarse for a satisfying model. Lazăr et.al. [2] employs a convenient graphical processing method working with supplied topographical measurements. The method engages a 2D graphical interpolation topography software which generates a 3D shape type surface as an .shx file. This surface is further on uploaded by ArcMAP 9.3 where can be divided by discrete triangular elements resulting in a 3D final shape type TIN (Triangulated Irregular Network). In order to be afterwards accepted by RAS Mapper graphic processor module in HEC-RAS 5.05 [4], the spatial shape needs to be converted in an accessible grid file type DTM (Digital Terrain Model). There is to be mentioned that such a satellite type of 3D representation results as usually based on rather poor topographical measurements (relatively reduced number of topographic points) so it can not generate specific configurations – framing flood protection structures or the ground shape in the riverbed – with a proper accuracy. The inconvenient needed to be solved in the HEC-RAS 5.05 model by rectifying the river cross-sections.

2. Development of the 1D river numerical model

The TIN ground representation converted in a DTM raster graphic type file was transformed in a file of .FLT extension (FLoaTing point raster file) that was so uploaded to the RAS Mapper module in HEC-RAS 5.05 (figure 4).

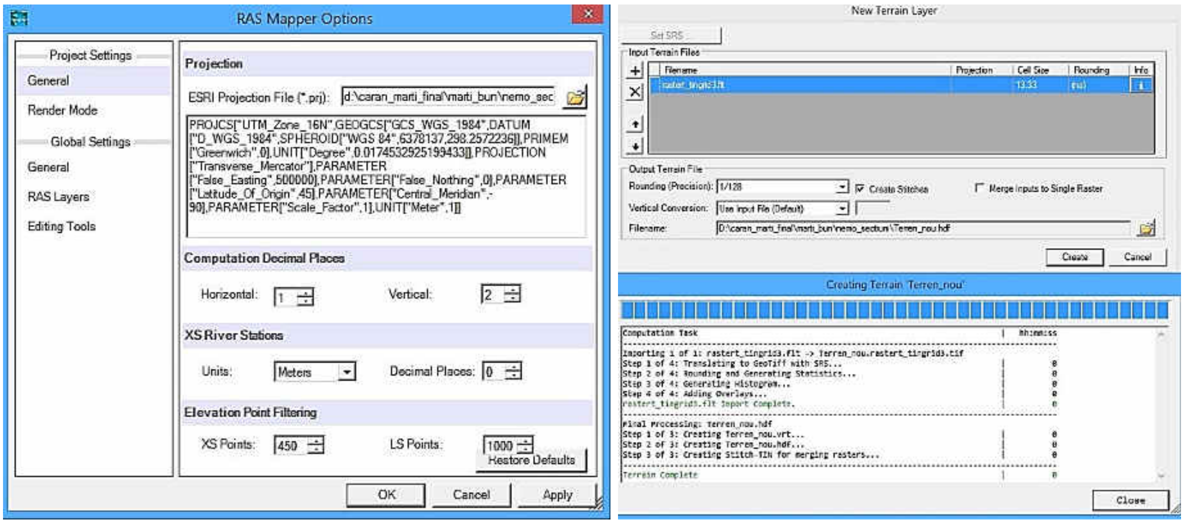

Fig. 4. Uploading the 3D graphic model of the Timiş - Sebeş river confluence sector

The generated ground becomes available only if added in Terrain facility. As already defined in RAS Mapper as a 1D model, the options River and Cross Sections are selected as background map characteristics and shall be available for a 2D model also. By selecting River in the explorer type window and then opting for Edit Geometry, one can perform to draw the river thalweg in the graphic area over the background map (figure 5). The Timiş River path is split at the confluence point and then the three river sectors are merged. The flow paths and the banks lines are to be also defined and saved. After leaving the edit operations, the Compute command must be considered in order to associate all the defined attributes and at the end all the initiated entities are saved (figure 6) [3,5].

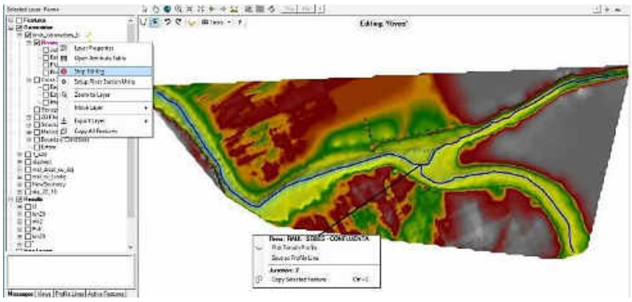

Fig. 5. Graphic digitalization of Timiș and Sebeș Rivers sectors in the confluence area

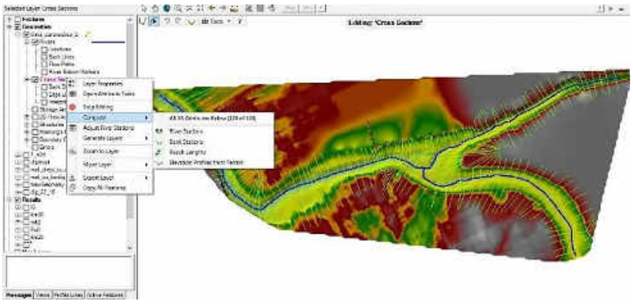

Fig. 6. Graphic digitalization of cross-sections on Timiș and Sebeș Rivers sectors with geometric database development

The two crossing structures – one bridge downstream of the confluence (see figure 1) and the other on the Sebeş River sector – in the RAS Mapper modelled area were considered by adjusting the associated specific cross-sections (figure 7), operation that can be subsequently resumed by addressing to the Geometric Data command in the main menu. Each bridge structure geometry is defined by two predetermined consecutive cross-sections.

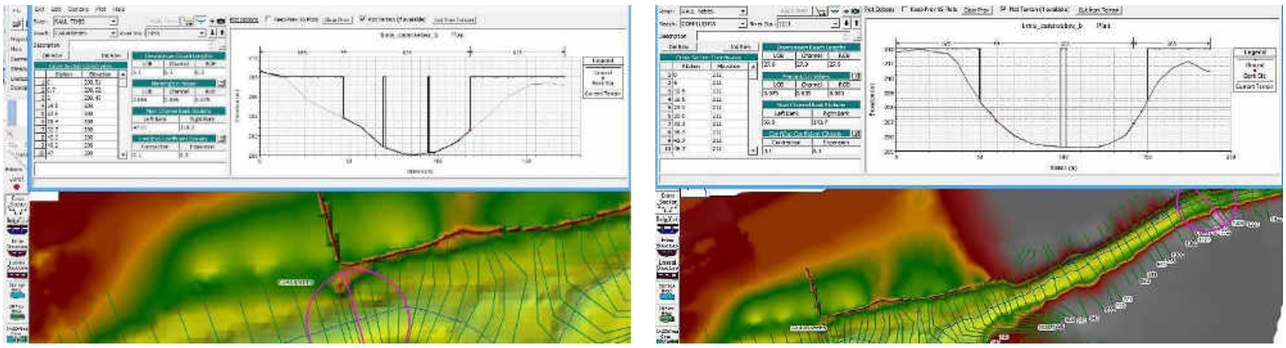

Fig. 7. Adjusting the crossing sections according to the two bridges geometry in the modelled river sector

The surface roughness coefficients in the customary cross-section of the modelled area is considered to vary in the range of 0.075…0.065 for the immediate major plain to 0.035 for the streambed (as recommended by specialized literature and confirmed by previous study [2]).
The relative distances of the upstream and downstream cross-sections edging the modelled Timiș-Sebeș river sector were specified as geometry data with respect to the confluence point and there was also selected the hydraulic facility to be employed by analysis – the impulse method and the energy balance method.

2.1 Initial and boundary conditions

As usual [7], the boundary conditions for a 1D path are assumed as the transited flow (of a given occurrence probability) attached to the upstream cross-sections and the hydrodynamic slope attached to the outgoing downstream cross-section. As for the developed model [1], the water flows were assigned as synthetic high-waters hydrographs to the sections identified by "1487" on

Sebeş River and "3692" on Timiş River, while the given hydrodynamic slope was assigned to the final section on Timiş River identified as "26". The initial flow condition for the 1D model was considered at the value of 15.5 m^3/s for each of the two entering cross-sections, so that their summation on the cross-section "2249" immediately downstream of the joining point to be 31 m^3/s. The maximum level of the enforced hydrograph on Timiş River is 784.82 m^3/s (as proved along a special event that occurred on the spring of 2000), while for the Sebeş River is 54.50 m^3/s (as an accidental coincidence determined by the upstream hydropower arrangement).
The actual river flow numerical simulation is to be developed over a given period of time, as it specifically occurred from the 4th to 11th of April 2000. The running analysis goes for a time step of 20 seconds, while the final results storing is set for each 10 minutes.

2.2 Numerical analysis and results presentation

The common time dependent parameters – water levels, flow and velocity developments – were estimate for all cross-sections by running the numerical analysis for the 1D model. Following the postprocessing operations, the numerical results are stored in distinct files that can be afterwards visualized in the usual RAS Mapper area or by accessing the HEC-RAS main menu, graphical and as spreadsheets.
The following figure 8 brings the graphic representation of the confluence streamlines progress by the RAS-Mapper area and the velocity distribution in the road bridge cross-section as revealed by the help of HEC-RAS menu, both at several moments along the modelled time period: 20:00 on April 5th, 04:00 on April 6th and 08:00 on April 8th, 2000.

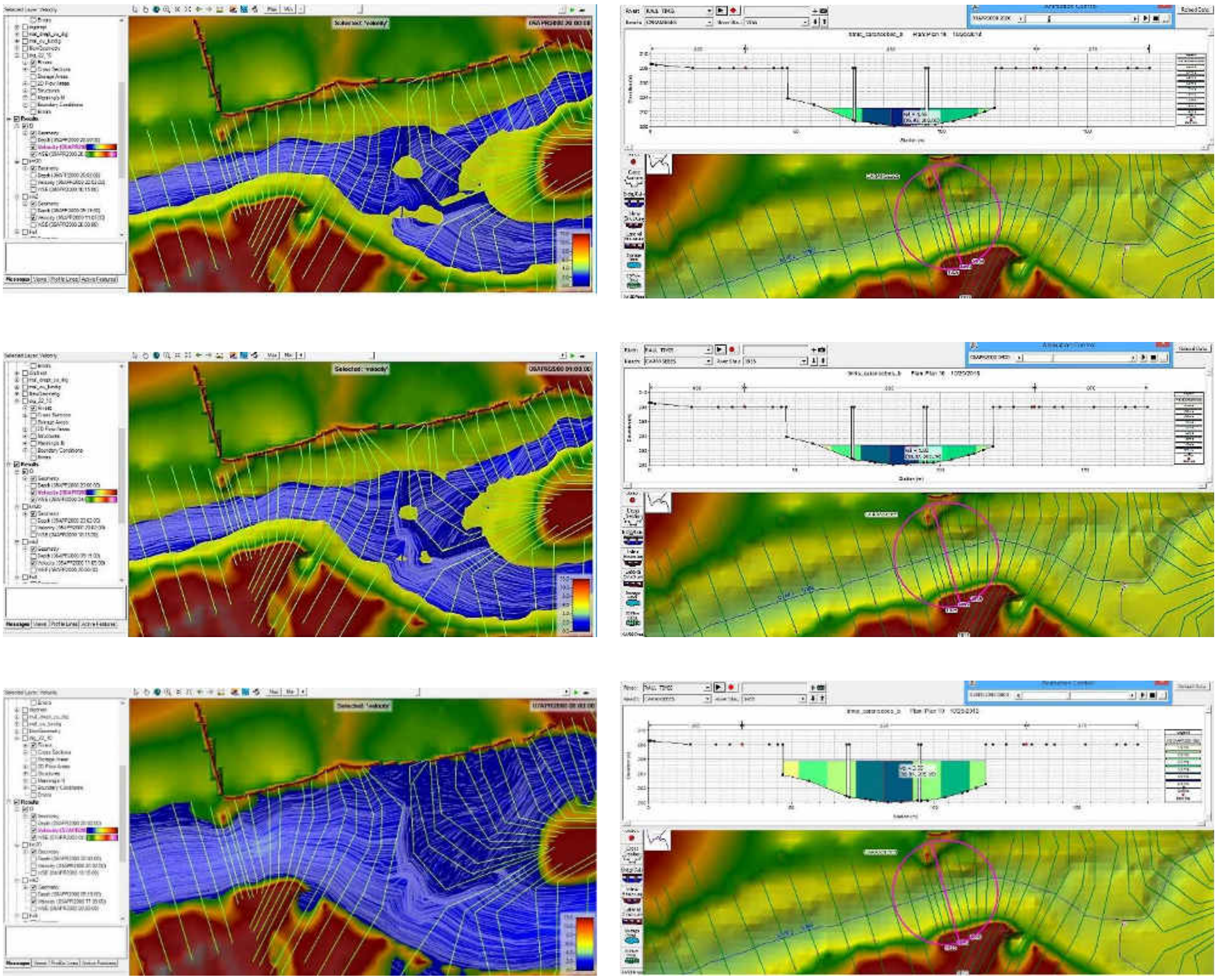

Fig. 8. Streamlines in the confluence area and velocity distribution in the cross-section attached to the downstream road bridge for the 1D river model at several specific moments: 20:00 on April 5th, 04:00 on April 6th and 08:00 on April 7th, 2000

As one can notice from the processed images in figure 8, the streamlines paths bend rather by relatively rough angles and not smoothly as in real natural flow. As about the water flow velocity maximum values in the considered narrowed cross-section at the specific consecutive moments along the hydrograph increasing side, they are 1.69 m/s, 1.82 m/s and 3.55 m/s.

3. Development of the 2D river numerical model

The 3D model built by bi-dimensional interpolation was altered in HEC-RAS 5.05 by the help of the facility that allows placing a fictitious water course, which in this case will model the flood defence embankment on Timiș River right bank in the proximity of the crossing road bridge [8].
The 2D surface domain is generated over the initial ground model. The analysis 2D domain contour is accomplished by the help of 2D Flow Areas facility from the explorer type window. The associated points and their corresponding properties were generated on the area meshed by a 15x15 m grid. Similarly, the embankment axel route was defined and saved. The cross-section of the embankment upper part was then defined by the help of Geometry Data main menu (figure 9), the shape being so attached to each inflection cross-section along the river path. The model's cross-sections are in the end automatically thickened at a maximum in-between distance of 20 m (figure 10).

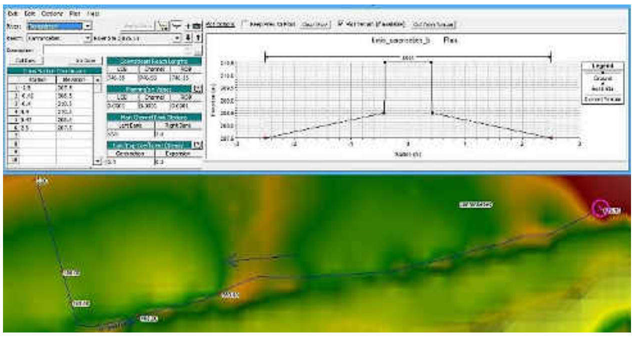

Fig. 9. Geometry data defining the embankment cross-section

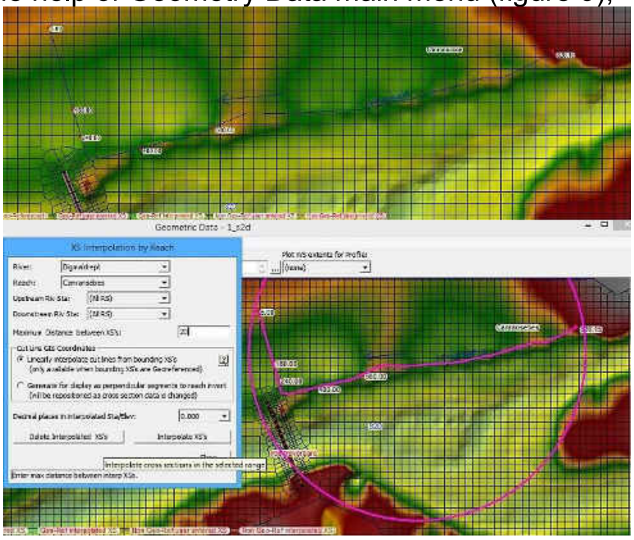

Fig. 10. Cross-sections development along the flood defending embankment route

The Interpolation Surface option is selected in Cross Sections menu in RAS Mapper window. The embankment geometry is exported by the help of Export Layer facility in the explorer type window, by selecting the Create Terrain GeoTiff from XS's option (figure 11).
The modelling of the cross-sections corresponding to the bridges downstream (on Timiș River) and upstream (on the tributary Sebeş River) from the confluence point was performed by breaking the surface lines by associated perimetric domains. The engaged facilities and data corresponding to the confluence downstream bridge are presented in figure 12.

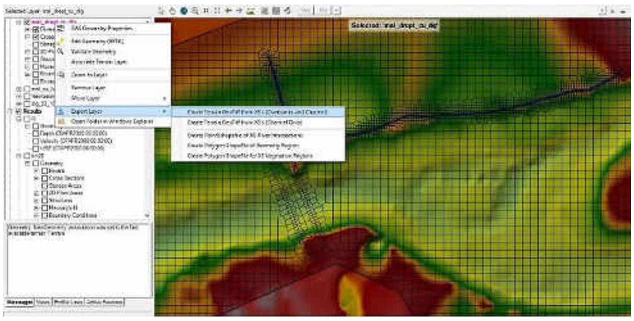

Fig. 11. Options engagement for exporting the protection embankment interpolation area

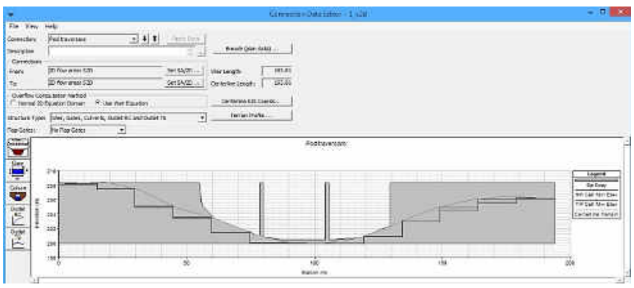

Fig. 12. Facilities and data engaged to define the confluence downstream road bridge

3.1 Initial and boundary conditions

Obviously, the boundary conditions attached to the 2D model, are identical as numerical development (but not as initial levels) to the ones engaged for the 1D model.
The 2D model requires the definition of the three paths as Boundary Conditions Lines by the help of SA/2D Area Conn option. There were defined two upstream paths – BC_S2D_11 on Timiș River and BC_S2D_22 on Sebeș River – and one downstream path as BC_S2D_33 on Timiș River (figure 13).

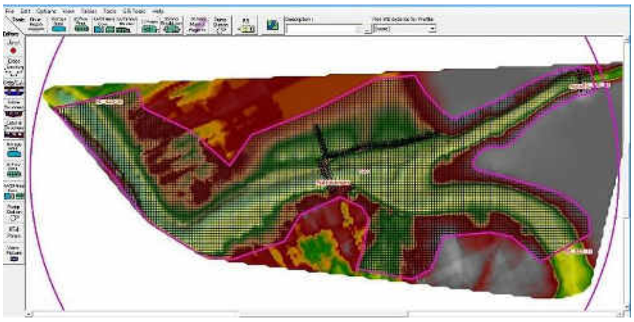

Fig. 13. Locations of upstream and downstream boundary conditions for the 2D analysis model

The high waters flow hydrograph on Timiș River following to reach the 784.82 m^3/s maximum value and the hydrodynamic slope of 0.000475 are attached (upstream / downstream) to path BC_S2D_11. By engaging the energy slope option, the model will deal out the entrance flow distribution upon the boundary line. In the same way, the high waters flow hydrograph on Sebeș River reaching the 54.50 m^3/s maximum value and the hydrodynamic slope of 0.000375 are attached to path BC_S2D_22. The hydrodynamic slope of 0.000375 was attached to the downstream boundary of path BC_S2D_33.
The actual numerical analysis of the water flow transition goes over the known period of time starting from 10:00 on April 4th and ending at 04:00 on April 11th, 2000. The analysis runs at an execution time step of 20 seconds, while the output storage is set for a time step of 10 minutes.

3.2 Numerical analysis and results presentation

The constant or time depending parameters regarding water levels, flows and velocities on each grid cell of the 2D model were reached by running the numerical simulation. Following the postprocessing operations, the numerical results are stored in specific files that can be afterwards accessed to be visualized in any grid cell or along specific routes defined by the user in the 2D domain by engaging the options offered by RAS Mapper area.
There were selected here some significant options that would allow the comparation with the results offered by the previous 1D model, specifically the streamlines progress in the confluence area and the velocity distribution in the downstream road bridge cross-section at the three consecutive moments along the modelled time period: 20:00 on April 5th, 04:00 on April 6th and 08:00 on April 8th, 2000 (figure 14).
One can notice that the streamlines develop by smooth natural like bends. In the same time, by selecting an about middle cell in the cross-section the maximum velocity value is revealed: 1.477 m/s for a water level of 202.46 mSL at the first considered moment, 1.558 m/s for 202.69 mSL and 2.751 m/s for 205.85 mSL respectively.

4. Conclusions

As considering the water velocity development in the narrowed cross-section corresponding to the road bridge downstream the Timiș - Sebeș Rivers confluence, its reached maximum values at three equally consecutive moments along the ascending side of the flow hydrograph for the two 1D and 2D numerical models are relatively presented in table number 1.
By comparing the corresponding velocity values, it rises up that the 1D analysis leads to noticeably increased estimations – with about 12 to 18 % – than the 2D situation, meaning that a one-dimensional modelling overestimates the hydraulic parameters. As about the water levels comparison in the studied cross-section, it results that for relatively low water flow values – as about the initial values of the hydrograph corresponding to the common river flow – one can accept that the proven difference is situated under the error limit of ± 0.06m adopted for the 2D analysis.

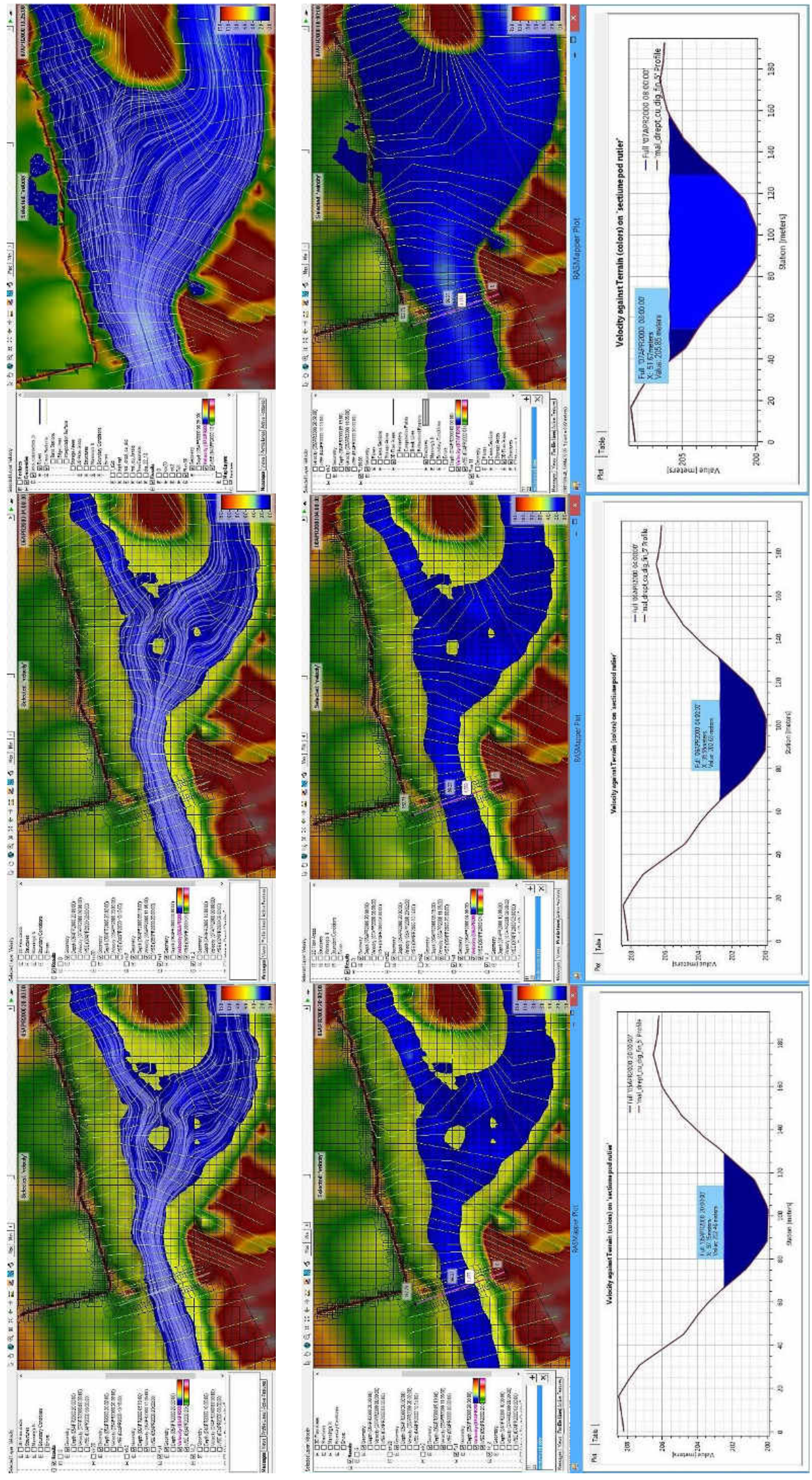

Fig. 14. Streamlines in the confluence area and velocity distribution in the cross-section attached to the downstream road bridge for the 2D river model at the three specific moments: 20:00 on April 5th, 04:00 on April 6th and 08:00 on April 7th, 2000

Table 1: Maximum values on road bridge cross-section

Crt. no.	parameter	1D model day/hour			2D model day/hour			Δ (1D)-(2D)
		5/20	6/04	7/08	5/20	6/04	7/08	
1.	Velocity [m/s]	1.690			1.477			0.213 (-12.6%)
	Level [mSL]	202.06			202.46			-0.40
2.	Velocity [m/s]		1.820			1.558		0.262 (-14.4%)
	Level [mSL]		202.39			202.69		-0.30
3.	Velocity [m/s]			3.550			2.751	0.799 (-22.5%)
	Level [mSL]			205.16			205.85	-0.69

Further on, at special situation of lowest occurrence probability (but never the less requested to be considered by the analysis) that would go up to the maximum summated flow value (784.82 + 54.50 = 839.32 m^3/s) the water level difference soon becomes really significant for the crossing structure and the framing embankments as the 1D model underestimates this parameter.

The revealed differences are understandable since the 2D analysis employs the full Saint Venant motion equations, turbulence and Coriolis effects too. In the same time, the 1D analysis as a simplified approach of the flow phenomenon accepts geometry and hydraulic data as estimated by the user, which is not anymore the case for the 2D approach. Besides, the confluence area of the 1D model is developed by a rough geometry. Even by considering a ring area as an improved modelling for the 1D confluence development, the deficiency would not be eliminated since this would assume to introduce two junction points instead of one. A more reliable and still affordable solution for the 1D model would be to intercalate a 2D local confluence model connected to the corresponding cross-sections of the general 1D model.

By considering the fluent / gentle bending streamlines along the modelled river sector and the slightly undulated cross-section water surface revealed by the 2D analysis, one can accept this approach reveals an artificial numerical phenomenon development much closer to the natural one.

Regarding the extreme values reached by the 2D analysis – the maximum velocity of about 2.75 m/s corresponding to the maximum water level of about 205.9 mSL (still in the range of the structures safety levels) for the narrowed road bridge cross-section – there is advisable to closely monitor the streambed erosion process development and so to ensure the crossing and flood protection structures stability by specific proper measures.

References

[1] Ion, M., and Gh.I. Lazăr. *Expertiză privind implicaţiile rezultate din amplasarea noii clădiri a Parchetului Caransebeş în albia majoră a râului Timiş asupra fenomenului scurgerii apelor mari în zona respectivă, / Technical valuation regarding implications of developing the Caransebeş Courthouse building in the immediate major Timiş River plain upon the high waters flow phenomenon*, Beneficiary: S.C. Tehnoproiect Ltd. Bucharest, Politehnica University Timişoara, Contract no.768/2007.

[2] Ghiţescu, M.A., Gh.I. Lazăr, A.I. Popescu-Buşan, A.T. Constantin, and Ş.V. Nicoară. "Numerical modelling of high water flow transit for a specific river reach." *Scientific Journal of Politehnica University Timişoara, Transactions on Hydrotechnics* 60(74), no. 2: 29-36, 2015.

[3] ∗∗∗. *HEC–GeoRAS GIS Tools for Support of HEC-RAS using ArcGIS User's Manual, Version 4.3.93*., US Army Corps of Engineers Institute for Water Resources Hydrologic Engineering Center, February 2011.

[4] Brunner, G.W. *HEC–RAS 5.05*. June 2018, US Army Corps of Engineers.

[5] ∗∗∗. *HEC-RAS River Analysis System, Supplemental to HEC- RAS Version 5.0 User's Manual Version 5.0.4*. April 2018, US Army Corps of Engineers.

[6] Brunner, G.W. *HEC–RAS 4.1, River Analysis System Hydraulic Reference Manual*. US Army Corps of Engineers, November 2002.

[7] Brunner, G.W. *Combined 1D and 2D Modelling with HEC–RAS*. October, vers.5 2016, US Army Corps of Engineers.

[8] Kiers, G. *Lifting Terrain in HEC-RAS 5.0*, VIZITERV Consult Kft., Hungary, Copyright © The RAS Solution and Gerrit Kiers 2015.

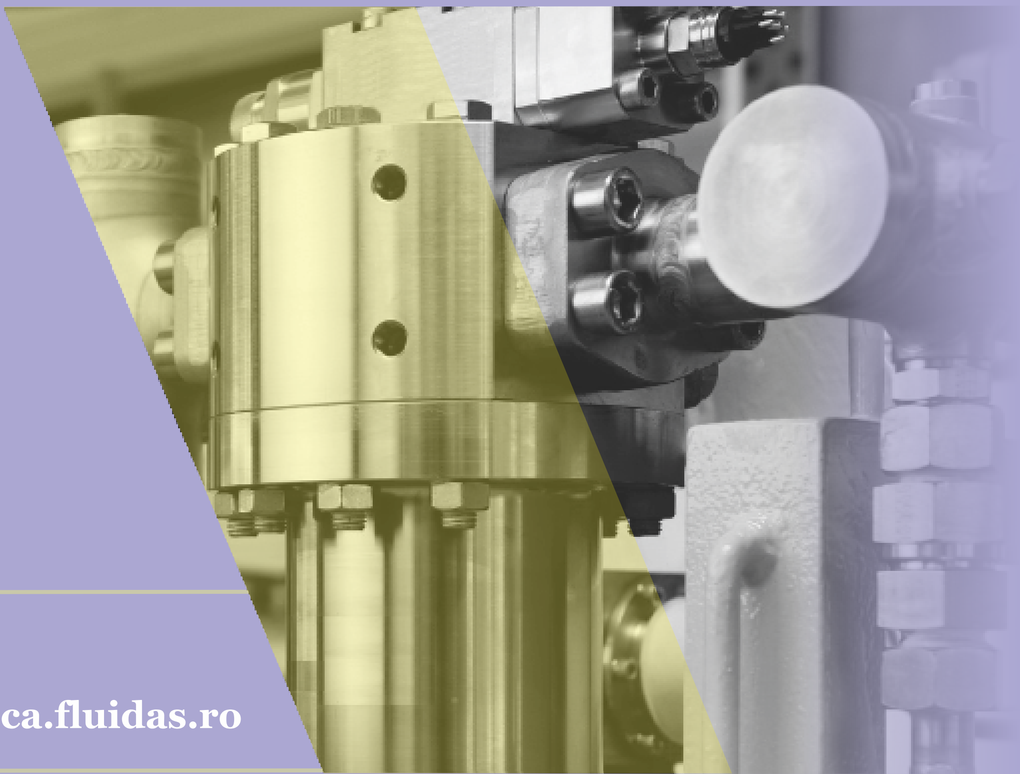

http://hidraulica.fluidas.ro